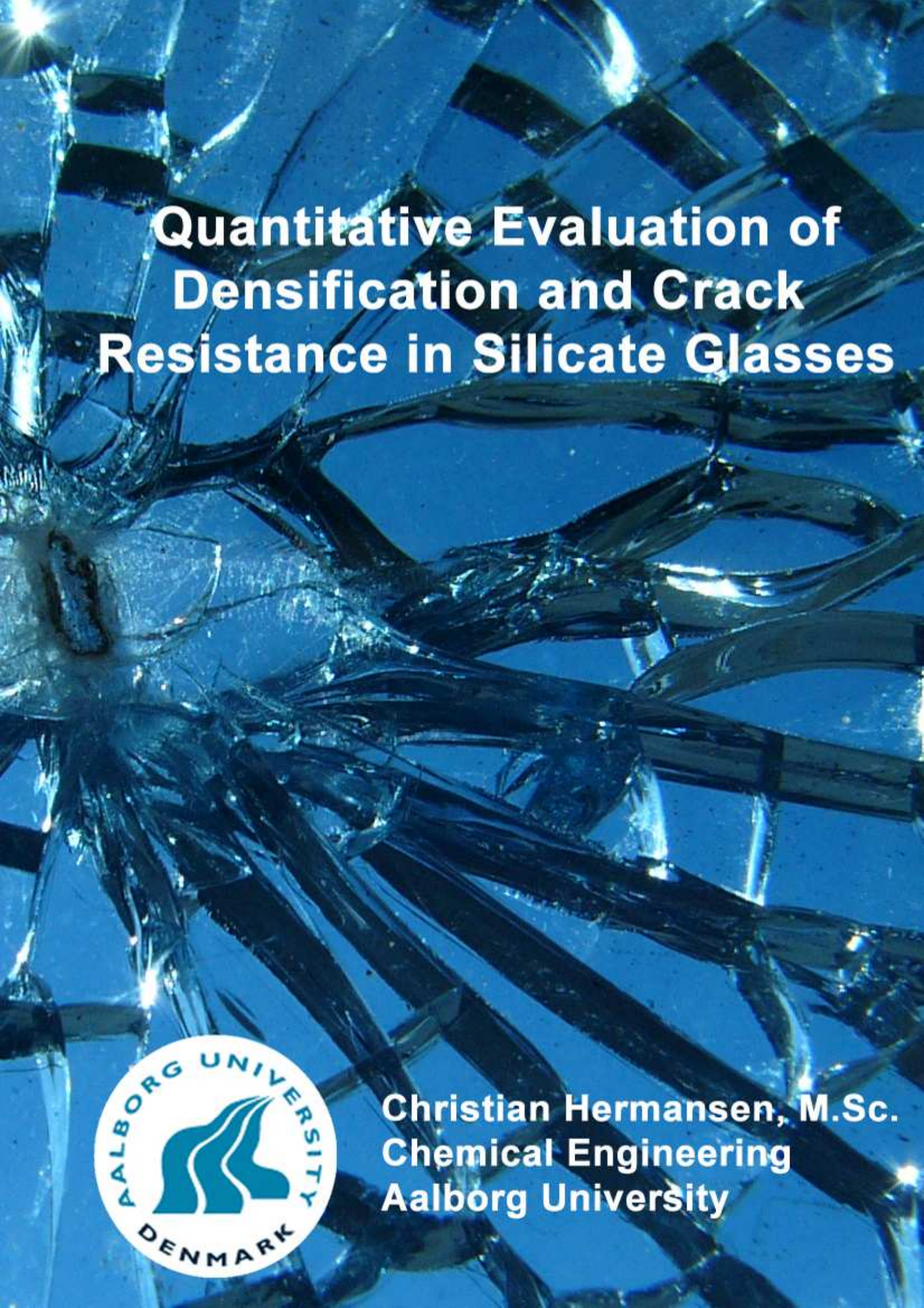

Quantitative Evaluation of Densification and Crack Resistance in Silicate Glasses

Christian Hermansen, M.Sc.
Chemical Engineering
Aalborg University

QUANTITATIVE EVALUATION OF DENSIFICATION AND CRACK RESISTANCE IN SILICATE GLASSES

By

Christian Hermansen

A Project Submitted to the

Faculty of Aalborg University

in Partial Fulfillment of the

Requirements for the Degree of

MASTER OF SCIENCE

Major Subject: CHEMICAL ENGINEERING

Approved:

Prof. Yuanzheng Yue, Aalborg University, Denmark, Project Adviser

Prof. Jun Matsuoka, The University of Shiga Prefecture, Japan, Project Adviser

Aalborg University
Aalborg, Denmark

July 5th 2011
(For Graduation July 2011)

CONTENTS

LIST OF TABLES

LIST OF FIGURES

ACKNOWLEDGMENT

This master project has been a joint venture between Aalborg University, Denmark, and the University of Shiga Prefecture, Japan, with financial, experimental, and intellectual support by Nippon Electric Glass Company, Japan. I would like to express my sincere thanks to these institutions, and the people who make them. Especially the following people deserve my heartfelt thanks:

Nippon Electric Glass

- Director & Senior Vicepresident Shigeru Yamamoto, for kindly offering his collaboration and support.
- Vicepresident Hiroki Yamazaki, for his cultural and academic guidance.
- Dr. Yoshinari Kato, for many inspiring conversations.
- Senior Manager Kazuyoshi Shindo, for helping arranging many practical things.
- Senior Engineer Noriyuki Yoshida, for measuring the helium solubility.
- Takahiro Kawaguchi, for teaching many things about Japanese culture.
- Masataka Kawaguchi, for delicious Japanese cuisine.
- Tetsuya Murata, for making life easier in the dormitory.

The University of Shiga Prefecture

- Professor Jun Matsuoka, for accepting me into his laboratory.
- Associate Professor Satoshi Yoshida, for much academic guidance.

Aalborg University

- Professor Yuanzheng Yue, for making everything possible.

ABSTRACT IN ENGLISH

The Vickers hardness and the indentation induced densified and plastic flow volumes were determined in simple silicate glasses by atomic force microscopy by measuring before and after annealing at $0.9 \times T_g$ *for two hours.*

It was found that the densified volume decreases linearly with the measured bulk modulus, and the plastic flow volume with the silica molar fraction (becoming zero close to 80%) of the glass. Hardness was related to the elastic properties, in particular the shear modulus, but it was not possible to develop an improved model for hardness prediction given the discovered relations to the deformation volumes.

The relative contribution of densification to plastic flow was attempted to be related to measures of the free volume, such as Poisson's ratio and the helium solubility. However there is no clear relationship with these properties, instead the results being described accurately by the ratio of the resistances described above.

For some glasses the loads for crack initiation were measured and the residual stresses at these loads estimated from the extrapolated plastic flow volumes. The estimated stresses range from $110 - 470 MPa$ *(*$\pm 70 MPa$*,) and thus it does not seem a single stress for crack initiation exists, even in simple silicates.*

ABSTRACT IN DANISH

Vickers hårdhedstallet, den indentations-inducerede højdensitets og plastisk deformations volumen i silikatglas er blevet kvantificeret med atomic force mikroskopi ved at måle før og efter varmebehandling ved $0.9 \times T_g$ *i to timer.*

Resultaterne viser at volumenet med høj densitet bliver mindre i lige proportioner med glassets kompressibilitetsmodul, og det plastic deformerede volumen med mol fraktionen af SiO_2*, og bliver nul omkring en mol fraktionen på*80%*. Hårdheden kunne relateres til de elastiske egenskaber, især forskydningsmodulet, men det var ikke muligt at fremstille en forbedret model til at forudsige hårdheden af glas udfra de fundne relationer til de irreversible deformerede volumener.*

Det blev forsøgt at relatere den relative mængde af høj densitets til plastisk deformation til det frie volumen, f.eks. igennem Poissons tal og helium opløseligheden. Det var ikke muligt at finde nogen klar sammenhæng med disse parametre, men forholdet imellem de ovennævnte modstande til permanent deformation beskrev resultaterne godt.

For nogle af de producerede glasprøver blev modstanden mod fraktur målt og den residuale mekaniske spænding estimeret med ekstrapolation fra de målte plastiske deformations volumener. De estimerede residuale spændinger ligger imellem $110 - 470MPa$ *(*$\pm 70MPa$*,) og derfor lader der ikke til at være en enkelt spænding ved den målte nødvendige kraft til at initiere fraktur i silikatglas.*

1. INTRODUCTION

It has been more than sixty years since Taylor startlingly reported a permanent microindentation impression in glass [1]. Since then, hardness testing of glasses has proven an easy method of evaluating the surface strength [2,3] (i.e. "scratchability",) crack resistance [4–9], fracture toughness [10–17], and with newer nanoindentation equipment even elastic properties [18–27]. However, despite the immense amount of papers written in the field, the processes occurring during indentation of glasses are still poorly understood. In metals and crystals, there is no doubt that volume conservative plastic shear deformation occurs by breaking and reformation of low-energy bonds [28]. The theoretical framework used to describe this, the Burger's dislocation vector, at first glance seems inapplicable to glasses as they lack a periodic structure, although some authors argue that there is no fundamental difference [28]. Despite the controversy, it is known that some form of plastic deformation does indeed occur, along with a deformation unique to glasses, a non-volume conservative densification [28]. Indeed, for amorphous silica there seems to be little or no plastic flow, only densification [29].

Given this state of affairs, and the inherent spread of indentation data, it is not surprising that sixty years of research have led to relatively little predictive power of indentation related properties. Determination of elastic properties from nanoindentation is usually done by the Oliver-Pharr method [18, 19], which goes to great lengths to minimise the plastic deformation, nevertheless pile-up due to plastic flow is a significant problem [22]. The indentation fracture toughness is so named because the fracture toughness values obtained by indentation do not correspond well with those determined by other methods. The crack resistance is an attempt of quantification of the susceptibility of glasses to surface cracking, which is the cause of the actual strength of glasses being some fifty times lower than the theoretical value [30–32]. Indentation cracking is thought by *Tomozawa and Gross* [8] to be caused by stress mismatch with origin in a fictive temperature induced change of mechanical properties during indentation (including a dilation of normal glasses,)

while *Kato et al.* [33] find the densificative contribution at the load for crack initiation is paramount. As for the most important property measured by indentation, the hardness itself, the most successful attempt at linking the hardness to other mechanical properties - and through them composition - was arguably by *Yamane & Mackenzie* [34]. Notably they argued the hardness as being the total resistance of each deformation mechanism; elastic, plastic, and densification. Despite having very little data on the relative contributions of the various deformation mechanisms, this semi-empirical model accurately describes hardness of a wide range of glasses, and immediately led to the development of some of the highest hardness glasses measured at the time [35].

This thesis will attempt to shed light onto the compositional dependence of the plastic and densificative deformation mechanisms in glass, and illustrate the importance of understanding these properties for predicting indentation derived parameters such as hardness and the load for crack initiation.

2. REVIEW OF STATE OF THE ART

2.1 Hardness Testing

A wide variety of testing methods and scales of hardness have been employed in the industry to quantify this rather intuitive, yet elusive property of materials. The very first implementation was due to *Brinell* [36] whom assessed the hardness of steel by placing a hardened steel ball between two plates, squeezing them together in a vice, then measuring the size of the resulting dent. The modern version applies a hardened steel ball with normal force to a material, i.e. microindentation with a Brinell indenter. Many other indenter geometries exist, for example: Vickers, Berkovich, Knoop, and Rockwell, each with their own hardness scale, as the values do not agree well [36].

The Vickers indentation method will be used extensively in this work, which is why this is taken as the basis for further description. This indenter is a square-based pyramid with an angle, θ, of 136° between opposite pyramid faces and is usually made of diamond. The hardness in a microindentation test is usually evaluated as the force over the projected surface area of the indent, which for a Vickers indenter is:

$$H_V = \frac{2P\sin\theta}{L_{ci}^2} = 1.8544\frac{P}{L_{ci}^2} \tag{2.1}$$

where H_V is the Vickers hardness, P the load, and L_{ci} the indentation diagonal. The hardness determined from equation 2.2 (or the likes of it) is sometimes referred to as the Meyer hardness. This is due to the hardness usually not being constant with load and indentation size, an effect dubbed the indentation size effect (ISE.) Generally a decrease of hardness with size is found, which can be fitted reasonably well by the empirical Meyer's law.

$$P = C_M \cdot L_{ci}^{n_M} \tag{2.2}$$

where both C_M and n_M are fitting parameters.

The origin of hardness is still under debate, and has been interpreted in a

variety of ways over the years, such as: As a yield strength measured under non-uniform loading [19, 37], the energy required to create the indentation volume [38], or a yield pressure for densification [39]. For this reason the origin of the ISE is a popular research topic. The ISE occurs for crystalline materials [36], polymers [40], ceramics [41, 42], and glasses [43]. Many plausible origins have been argued, and odds are that most of them are at least qualitatively correct. For example, the following material or measurement specific causes have all been proposed as possible causes of the ISE: The presence of a surface film, surface roughness, surface energy, composition variation, crystal anisotropy, fracture, rounding of the indenter tip, misalignment of indenter and surface, friction, and loading conditions [40, 44, 45]. Others believe that the ISE is an inherent property of the material, arguing for intrinsic effects like strain hardening and increased surface energy due to cracking [40].

2.2 Composition Dependence of Hardness

Quite a few attempts [46] have been made at correlating the glass hardness to structure before the seminal paper by *Yamane and Mackenzie* [34] in the seventies, but the latter is the first major contribution. They broke down the hardness into a variety of resistances caused by the three deformation mechanisms known to occur; elastic, plastic, and densification. Semi-empirically they derived a reasonable expression for each based on the elastic constants,

$$R_E \propto K \tag{2.3}$$

$$R_P \propto \alpha G \tag{2.4}$$

$$R_D \propto \sqrt{\alpha G K} \tag{2.5}$$

$$R_T = (R_E R_P R_D)^{1/3} = \sqrt{\alpha G K} \tag{2.6}$$

where R_E, R_P, R_D and R_T are the respective elastic, plastic, densificative and total resistances, and α, K and G the average bond strength, bulk and shear modulus. The total resistance is taken as the geometrical mean, and fitted to the calculated value to the hardness of amorphous silica. The final equation is:

$$H_V = C_{YM} \cdot R_T = C_{YM} \cdot \sqrt{\alpha G K} \tag{2.7}$$

H_V being the Vickers Hardness and C_{YM} the proportionatility constant determined empirically from the hardness of amorphous silica in the *Yamane & MacKenzie* model. As the elastic properties can be fairly accurately calculated from composition [47–49], this equation can predict hardness from scratch, and indeed accurately so across a wide variety of glass forming systems, as seen in figure 2.2.1 [34].

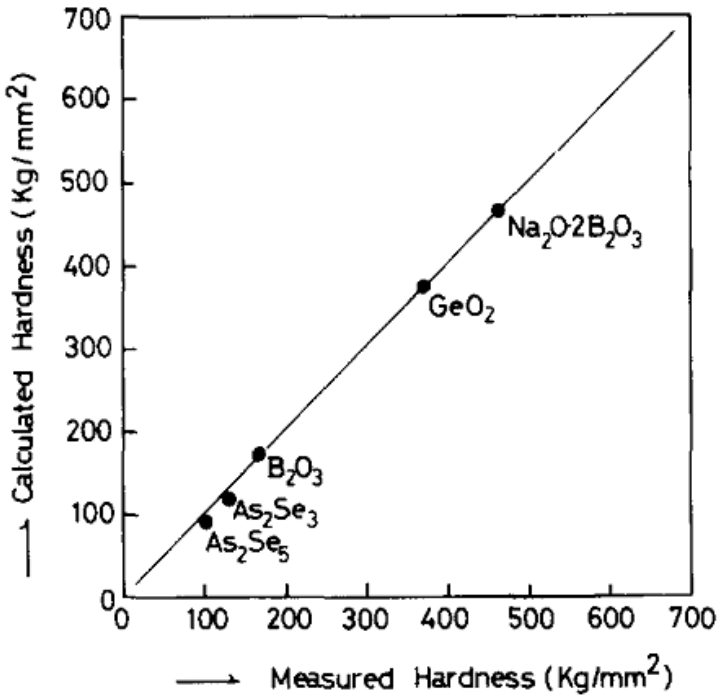

Figure 2.2.1: Calculated values of Vickers Hardness, H_V, with application of equation 2.7 plotted agaist the experimental values for some non-silicate glasses.

A newer approach based on hardness theories of metals and crystals is that of

Calleja et al. [37]. For metals it is empirically found [50] that,

$$\frac{H_V}{\sigma_y} \cong 3 \tag{2.8}$$

where σ_y is the yield strength of the metal. This was later theoretically confirmed under the assumption of an expanding spherical cavity in an elastic-plastic material [51] giving,

$$\frac{H}{\sigma_y} = \frac{2}{3}\left[1 + ln\left(\frac{E}{3(1-2\nu)\sigma_y}\right)\right] \tag{2.9}$$

where E is the Young's modulus and ν Poisson's ratio, which is the ratio of strain in the tranverse direction to the strain in the direction of applied force in a linear tension or compression experiment. Standard values of these elastic constants for metals give approximately the relationship in equation 2.8. A similar empirical relation exists for glassy polymers, given as,

$$\frac{H_V}{\sigma_y} \cong 1.9 \tag{2.10}$$

However using an unmodified equation 2.9 yields very poor correlation to results for inorganic glasses and glassy polymers. Replacing the factor 2/3 by an empirical constant c, found to be around 1/2 gives a reasonable fit [37].

Another related approach takes the maximum in the internal pressure, the change in internal energy during isothermal volume change, as a measure of yield strength of a material [37]. The internal pressure P_i is defined as,

$$P_i = \left(\frac{\partial U}{\partial V}\right)_T \tag{2.11}$$

where U and V is the internal energy and volume, respectively. Simplifying the problem to a one-dimensional extension in the elastic regime, P_i is simply the applied stress relative to the strain by Hooke's law,

$$P_i = E \cdot \frac{\Delta r}{r_0} \tag{2.12}$$

where r_0 is the equilibrium value of interparticle distance and Δr the change due

to strain. Of course there will be a limit to elastic response, and at some point the lattice anharmonicity will set in, as illustrated in figure 2.2.2. This onset of

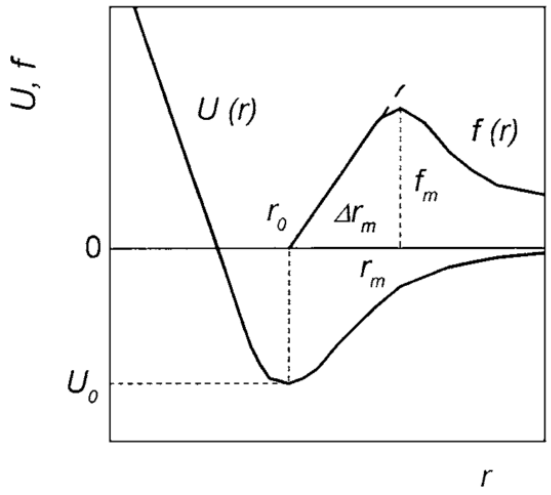

Figure 2.2.2: Schematic representation of the potential energy, $U(r)$, and the interparticle interactions force, $f(r)$, vs. the interparticle distance, r.

lattice anharmonicity is basically a yield strength, as it also marks the maximum of the interparticle interaction force at the maximum strain r_m. What is needed to assess r_m is then an evaluation of this interparticle interaction force as a function of interparticle separation. A Taylor series expansion of the potential energy as a function of interparticle distance truncated after the fourth term coupled with the use of the Grüneisen parameter used in thermal expansion theories can be used in combination with equation 2.12 to yield,

$$P_m = \left(\frac{1}{6\gamma}E\right) \cong A\left(\frac{1-2\nu}{6(1+\nu)}\right)E \tag{2.13}$$

where P_m is the maximum internal pressure, γ is the Grüneisen parameter, and A defined as,

$$A = \frac{9}{2\ln\left(1/V_f\right)} \tag{2.14}$$

where V_f is the free volume fraction of the glass, and will be discussed further in section 2.4. In practice the A variable is taken as constant due to the difficulty of measuring the free volume of glasses [37].

2.3 The Deformation Processes of Indentation

It is generally accepted that at least three processes occur during indentation: Elasticity, densification, and plastic flow [29]. For now it will suffice to say that densification involves a non-volume conservative flow, or collapse of the network structure, during indentation. This has been found [52] to be the major process occuring for glasses with open structures (low Poisson's ratio.) A seemingly volume conservative plastic flow displacing matter to the surface however becomes increasingly important in densely packed glassy structures (high Poisson's ratio.)An overview of these processes can be seen in figure 2.3.1 [53] and will be discussed further in the following.

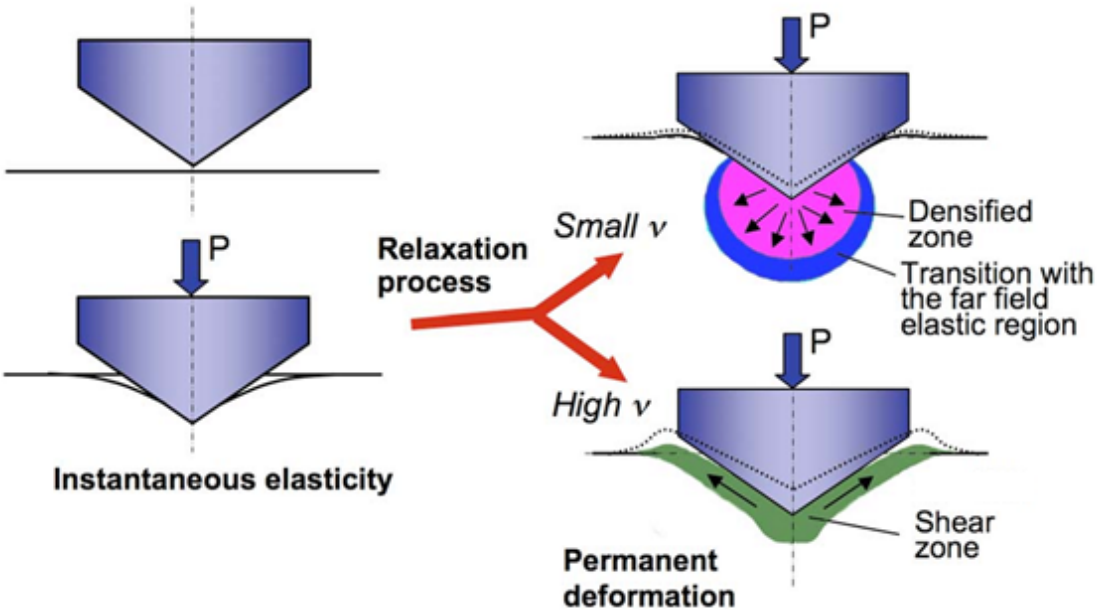

Figure 2.3.1: An overview of the processes occuring during sharp indentation on glass.

2.3.1 Elasticity

Although released upon unloading, the elastic response during indentation cannot be disregarded, indeed it is paramount to any proper understanding of the hardness concept. This is emphasised by the empirically found correlation that hardness is roughly proportional to the elastic properties of the glass, namely Young's modulus and shear modulus [54]. Indeed, the search for very hard materials is often

undertaken through the shear modulus, as it can be predicted from first principles, while hardness in itself is poorly understood [54]. As seen in figure 2.3.2 [25] the

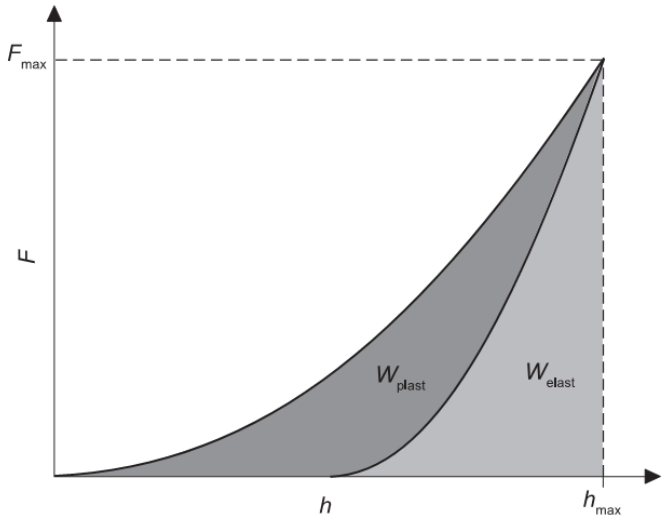

Figure 2.3.2: A typical glass nanoindentation load-displacement curve. The work of elastic (W_{elast}) and plastic deformation (W_{plast}) corresponds to the respective integrals.

elastic work during nanoindentation constitutes a major fraction of the total, for amorphous silica around 70% [55], given credence to the above relation. Also evident is that the penetration depth during loading is very different from that seen after unloading. This is mainly caused by surface deflection, i.e. a sinking-in of the surface outside the surface region in actual contact with the indenter, and the problem has been adequately solved theoretically [18, 19]. Generally elastic shrinkage of the diagonal is neglectable, but for some glasses, e.g. amorphous silica, this gives rise to some error.

2.3.2 Densification

Densification in silicates occurs through a reduction in Si-O-Si bond angles, as measured by Raman spectroscopy in the center of a Vickers indentation [52]. This densified region can be relaxed by annealing far below the glass transition temperature (e.g. $0.9 \times T_g$ (K)) with activation energies reported as 35-55kJ/mol for amorphous silica [56,57], and thus comparable to that of densification induced by hydrostatic pressure [58]. The degree of shear induced under otherwise hydrostatic

conditions has qualitively been linked to greatly increased degree of densification. New evidence suggests that under good hydrostaticity a maximum densification is reached at pressures above $20GPa$ for a soda-lime-silicate glass, the density slightly higher than that of crystallised quartz [39]. Thus one might imagine the process as a collapse of the open structure into the free volume as compared to the crystal structure.

Most of the quantative data of densification in glass was made by *Yoshida et al.* [52, 59], including silicates, sodium borates, oxy-nitride, and bulk metallic glasses by measuring the volume of indents and pile-up before and after annealing. The influence of time and temperature of this annealing process to recover the densified volume has previously been researched by the same authors, and found to be saturated for $0.9 \times T_g$ (K) for 2 hours, while no evidence of viscous flow being evident [60]. *Kato et al.* [9, 61] also report quantative data for boro-silicate glasses, however including only the depth recovery, not the volume. *Yoshida et al.* [52] find a monotonic decrease of the determined volume recovery ratio with Poisson's ratio, as seen in figure 2.3.3.

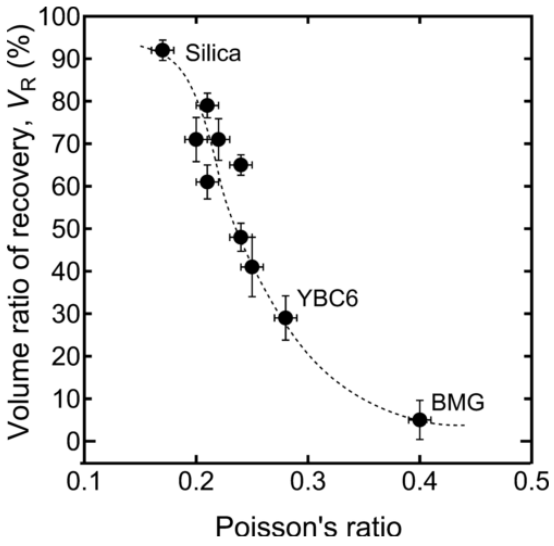

Figure 2.3.3: The volume recovery of densification, V_R, as a function of Poisson's ratio, ν, for a variety of silicates, silica, oxy-nitride, and a bulk metallic glass. The data can be found in appendix B. Error bars indicate ± 1 standard deviation. The line is a guide for the eyes.

It is recognised that the Poisson's ratio is closely related to the compactness

of structure of a material. By definition a Poisson's ratio of zero means the material is perfectly compressible; compression or expansion in one direction does not elicit a response in the other. This is closely related to the presence of voids in the material, which can either expand in the direction of strain, or the material can be compressed into. Cork and sponges are generally the materials which are close to this ideal. On the other hand a value of one half corresponds to ideal incompressibility, i.e. perfect conservation of volume under strain. This is generally approximately true for liquids and very compact solids. Figure 2.3.4 [62] shows the evolution of Poisson's ratio for a variety of inorganic glasses, plotted with the maximum relative density change under high pressure treatment, emphasising it as a measure of the degree of structural openness.

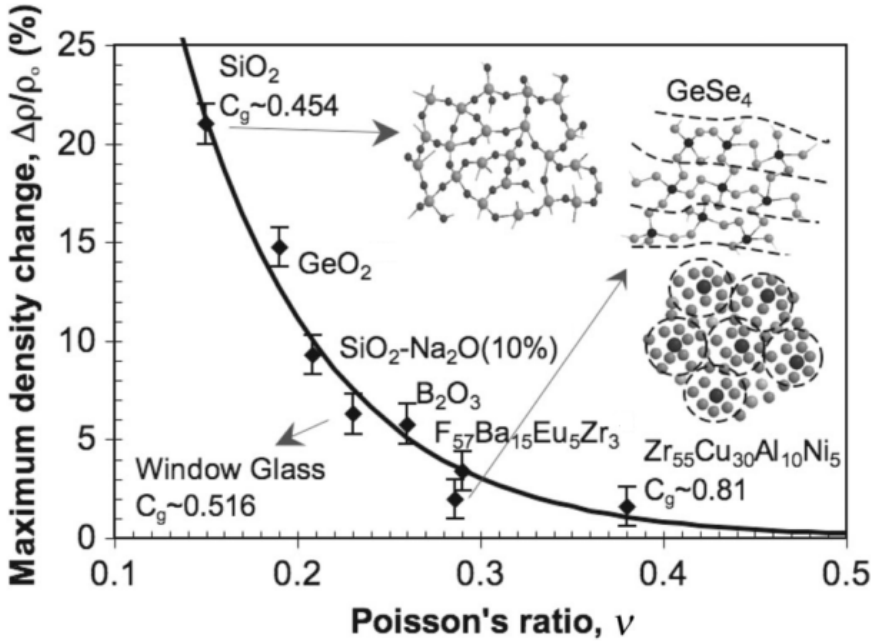

Figure 2.3.4: The maximum density change, $\Delta\rho/\rho_0$, under high hydrostatic pressure treatment (up to 25GPa) as a function of Poisson's ratio, ν, for some inorganic glasses. The trend of ionic volume fraction, C_g, and network dimensionality is also illustrated. Error bars indicate ± 1 standard deviation. The line is a guide for the eyes.

The ionic volume fraction, C_g seen in figure 2.3.4 is the ratio of molar volume of the constituent ions to molar volume of a material. A related measure is the

space ratio, V_{SR}, defined as the remaining volume, or mathematically,

$$V_{SR} = 1 - C_g = 1 - \frac{\rho}{M}\frac{4\pi}{3}\sum_i (n_i r_i) \tag{2.15}$$

where ρ and M are the density and molar weight of the glass, while n and r are the moles and radius of the ith constituent ion. Using only the composition, density, coordination numbers (e.g. from *Sun*'s table [63],) and ionic radii equation (e.g. from *Shannon*'s table [64]) 2.15 can give an estimate of the openness, or free volume, of the glass structure. Indeed, the empirical determination of Poisson's ratio of glasses from the the ionic volume fraction has been suggested. *Yoshida et al.* [59] have subsequently found a relationship between ionic volume fraction and the volume recovery ratio for silicates, but no clear relation for sodium borates, as seen in figure 2.3.5. The authors [59] argue that the mechanism of densification is fundamentally

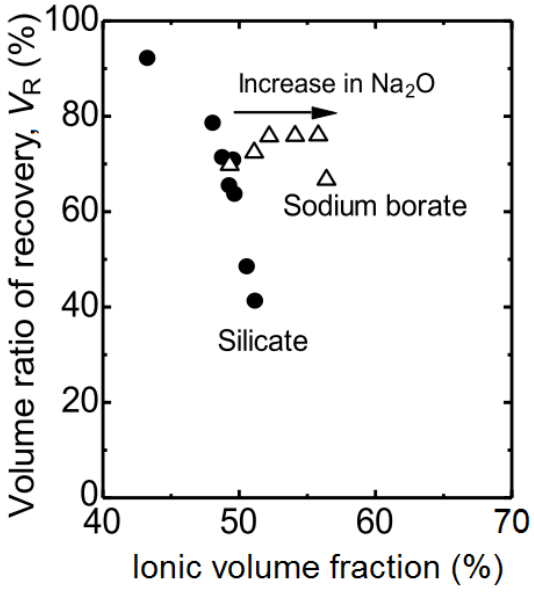

Figure 2.3.5: Volume ratio of recovery, V_R, as a function of ionic volume fraction, C_g, for silicate and sodium borate glasses.

different from silicates - the aforementioned narrowing of bond angles - while for sodium borates there is little change in bond angle, however a significant change in ring statistics is found. As for the volume recovery ratio trend across the sodium borate series, showing a distinct maximum near the maximum of four-coordinated

boron at a molar modifier fraction of one third [65], it is thought that irreversible shear flow can occur by two different mechanisms: Slipping between three-membered planar boroxol rings (predominant at modifier fractions lower than one third,) and redistribution of non-bonding oxygen (present only above modifier fractions of about one third.)

2.3.3 Plastic Flow

It was *Marsh* [31] that convincingly brought attention to the numerous theoretical discrepancies between experiment and the assumption of perfect brittleness - i.e. non-plasticity - of glass. Especially using sharp indentation of a relatively soft material significant ridges, or pile-up, along the edges of the indent are evidence of plastic flow. First, let us inspect figure 2.3.6 [29] and see how this pile-up region actually looks for a sharp indentation of glass. Given the distribution of pile-up at

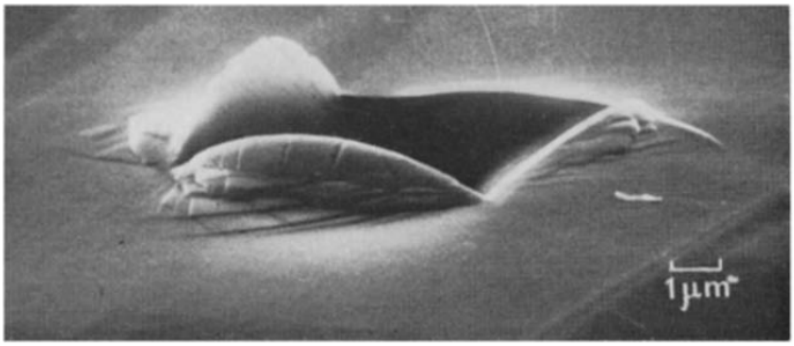

Figure 2.3.6: Scanning Electron Micrograph of a plate glass indent made with 70° pyramid.

the indentation edges, decreasing towards the corners, the driving force is likely the large shear stresses occuring at these locations during loading. The same is found for metals and crystals, where the mechanism is established to be slipping along dislocation lines in the crystalline lattice [66]. Indeed for many crystals it is found that the hardness shows excellent correlation with the bond modulus, taken as the energy gap (i.e. bond strength) divided by the dislocation volume [67,68]. However, given the lack of periodicity in amorphous solids and as a result also dislocation lines, despite the superficial similarities most researchers do not want to invoke this explanation. An exception is the work by *Gilman* on metallic glasses, who does not

hesitate to argue for moving dislocations in glasses nucleating at weaknesses in the network; for metallic glasses perhaps a region with low packing density [28]. A yield stress is thought to be associated with the creation of a locally expanded structure which spreads in the shear plane, with concurrent dilation of the structure facilitating slip. In regards to oxide glasses *Peter* [29] also envisions slipping between planes in the structure, but instead thinks of modifier rich regions as the likely place of origin. This interpretation is fueled by the increasing importance of plastic flow with higher modifier content in silicates.

Such a slipping between dislocation planes agrees with another important finding; that the flow in glasses is accompanied by formation of regularly spaced shear bands. These have been evidenced by serration in nano-indentation load-displacement curves of bulk metallic glasses [69–71] and microscopic imaging techniques [71–73], a representative example shown in figure 2.3.7.

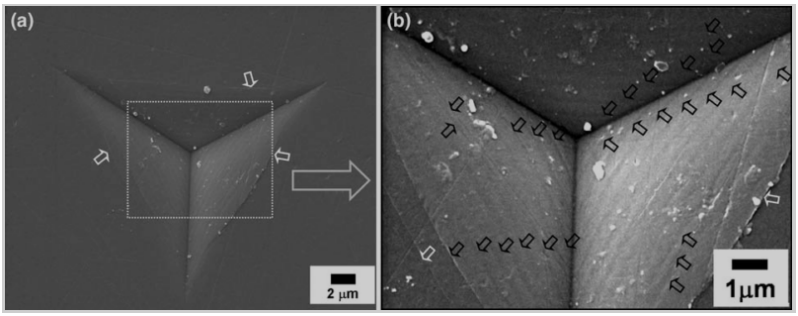

Figure 2.3.7: Scanning Electron Microscopy photomicrographs of Berkovich nanoindents made with 1000mN applied load at 1mN/s loading rate on a soda-lime-silica glass. Black and white hollow arrows indicate the shear bands inside and around the nanoindentation cavity, respectively: (a) lower magnification (times 4.5K) view and (b) higher magnification (times 13K) view of (a).

The previously mentioned theories both intrinsically assume that actual shear flow in glasses at room temperature is neglectable due to the extremely large viscosity. Yet it is known that glasses exhibit a large viscosity drop at large stress or strain-rate levels, this is known as shear-thinning [53,74,75]. Moreover the generally accepted mechanism of shear-thinning is an orientation of the liquid structure under stress, thus reducing the resistance to deformation. Molecular dynamics simulation has found exactly this kind of a layered structure of a glass melt under shear by par-

allel plates, and the results agree very well with experiments for soda-lime-silicate and rubidium-silicate glasses [76].

2.4 Free Volume of Glass

The free volume of a glass can be defined in many ways. A very simple one is as the additional volume present in the glassy structure as compared to the corresponding crystal, and is a direct consequence of the structural entropy present in glasses. With this definition the free volume can be calculated as,

$$V_f = \frac{V_g - V_c}{V_g} = 1 - \frac{\rho_g}{\rho_c} \tag{2.16}$$

where V is volume, and subscribts f, g, and c indicate free, glass, and crystal, respectively. The rightmost expression of equation 2.16 is derived by taking the masses of the glass and corresponding crystal as the same, since their compositions are identical. Using this equation on amorphous silica ($\rho_g = 2.2\text{g/cm}^3$) and cristobalite crystal ($\rho_c = 2.32\text{g/cm}^3$) gives a free volume fraction of approximately 5%. This is however an extreme example, and the density of most glasses will be approximately 1% less than that of the corresponding crystal, giving a relative free volume of the same magnitude. The major problem with equation 2.16 is that very rarely will there be a crystal corresponding to a given glass composition, which is why the free volume has for a long time been a quantity known to exist, but ill-quantified.

The free volume has been utilised in many theories attempting to describe the property of glasses, most notably the glass transition phenomenon [77–79], but has fallen out of favour, first to the residual entropy theory by *Adam & Gibbs* [80, 81], then the energy landscape theory by *Goldstein* [82–85].

As mentioned previously, the free volume is invoked in the maximum internal pressure model of the compositional dependence of hardness, and currently a free volume model of the densification process of silicate glasses is favoured [59, 62], yet based only on indirect measures of the free volume: Poisson's ratio and the theoretically derived atomic packing density defined in equation 2.15. For this reason, it is very much of practical interest to know whether these parameters truly reflect

the free volume of a glass, and as such if the free volume can be invoked as an explanation of the results.

One method that is thought to give a more direct measure of the free volume in glasses is that of physical solubility of gases [86]. In the theory developed by *Doremus* [87,88], the physical solubility of glasses is due to two effects, the interaction between solute gas and the glassy matrix, and the free volume of the structure. From equilibrium thermodynamics and assuming that the gas retains all degrees of freedom when dissolved, the following is derived,

$$\ln\left(\frac{C_d}{C_{atm}}\right) = \left(\frac{E_i - P\widehat{V}_m}{RT}\right) + \ln V_f \tag{2.17}$$

where C_d is the concentration of gas dissolved in the glass, and C_{atm} that of the surrounding atmosphere (equal to the molecular density,) E_i is the potential energy of the gas-matrix interaction, P the pressure, $\widehat{V}_m$ the partial molar volume of the solute gas, and V_f the partial free volume as experienced by the given gas. The ratio of concentration of gas dissolved in the glass to that of the surrounding atmosphere is termed the Ostwald solubility, and is used to eliminate an artifical temperature dependence of solubility due to the ideal gas law. It is seen from equation 2.17 that studying the temperature dependence of the Ostwald solubility can separate gas-matrix interaction from the free volume. In general however, both E_i (the interaction energy) and $\widehat{V}_m$ (the volume change of glass upon solution) are very small, and the gas solubility will be almost temperature independent across a large temperature range [89]. The validity of this measure of free volume was checked by the solubility of various gasses in amorphous silica. It was found that for inert gas atoms and molecules with diameters below 0.3nm not only are the Ostwald solubilities similar, but so is also the relative free volume of $V_f = 3\%$, while the values for larger gas atoms or molecules drop rapidly [87–93]. This indicates a pore size (or rather interstitial size) of about 0.3nm. Results on crystalline tridymite ($\rho_c = 2.28\text{g/cm}^3$) gives a very similar value, while that of cristobalite ($\rho_c = 2.32\text{g/cm}^3$) is about two-thirds, casting doubt on the reliance of equation 2.16 to assess the free volume in practice [87, 94].

As for the compositional variation of gas solubility it is found that generally it decreases approximately linearly with modifier fraction in silicates. For binary alkali silicates the helium solubilities are similar within experimental error for sodium, potassium, rubidium, and cesium containing glasses, excepting the phase-separated sodium silicate glasses with soda contents above approximately 25mol%, as seen in figure 2.4.1 [86]. It is also seen that the helium solubility is higher for the soda-lime-silica glasses, indicating either a change in gas-matrix interaction, or a higher free volume.

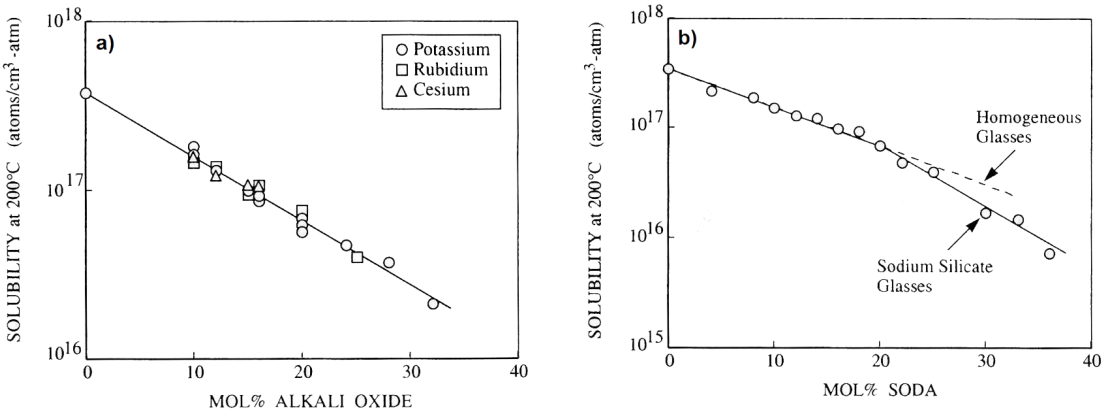

Figure 2.4.1: (a) The helium solubility in homogenous alkali silicate glasses. (b) The helium solubility of sodium silicate glasses, which are homogenous up to approximately 25mol% soda content.

2.5 Load for Crack Initiation

The load for crack initiation as measured by indentation is a rather new field of research, with only a few research groups providing significant contributions. Here we will focus on the theories proposed by three groups: *Sehgal & Ito* [6, 95], *Gross & Tomozawa* [7, 8], and *Kato et al.* [9, 33, 61]. The concept sounds intuitively simple; the load at which cracks are formed during indentation. However, things get complicated because there exist a variety of crack types [8], a time dependence on their emergence, a strong influence of atmosphere [8], surface condition [96], and temperature [97]. Generally the first type of crack to emerge is the edge crack seen in figure 2.5.1b along the faces of the indent. However, in the method developed

by *Wada et al.* [98] and employed by *Kato et al.* [9, 61] only the number of radial cracks (see figure 2.5.1a [8]) emerging from corners of a Vickers indentation are considered, and a crack resistance (CR) defined as the load where the average number of radial cracks per indentation is two, *i.e.* half of the maximum possible. *Gross and Tomozawa* [7, 8] expand on this definition, taking also the conical cracks (see figure 2.5.1c [8]) - commonly found for anomalous glasses - connecting corners into account; one conical corner in a quadrant equalling one crack. The data is plotted

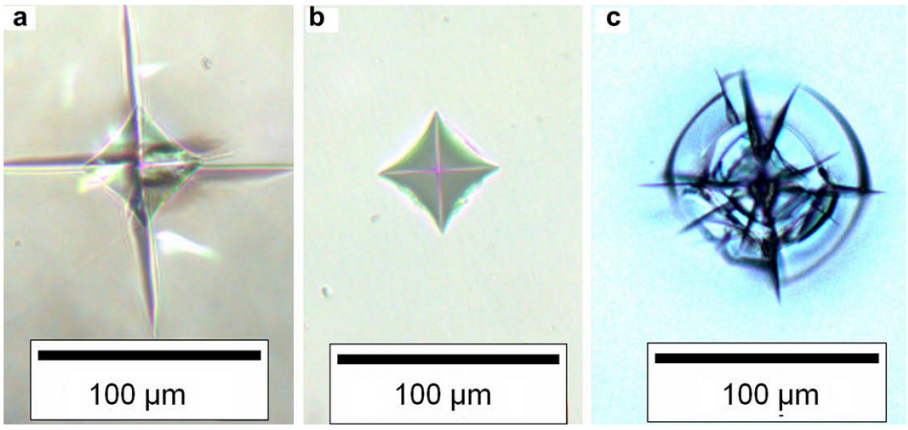

Figure 2.5.1: Cracking behaviour of representative glasses under a 1kg force load with a Vickers indenter. (a) 60% SiO_2 20% Al_2O_3 20% CaO; (b) 80% SiO_2 10% Al_2O_3 10% CaO; (c) 100% SiO_2.

as number of cracks against applied load, and generally takes on a sigmoidal shape as illustrated by figure 2.5.2 [33]. *Gross and Tomozawa* [7, 8] utilise a sigmoidal fit to this plot in order to predict the CR.

The three groups have taken widely different approaches in an attempt to explain the large differences seen in CR values of different glass compositions.

2.5.1 Brittleness

For ceramics the macroscopic fracture behaviour is commonly assessed through the fracture toughness, K_{Ic}. Basically the fracture toughness is a measure of the materials resistance to brittle fracture in the presence of a crack. However, in glasses the fracture toughness fall in a rather narrow range and apparently has little effect on crack initiation, and as such crack resistance [11, 95]. *Lawn & Marshall* [99] realised that all materials seem to show deformation in small scale loading, and

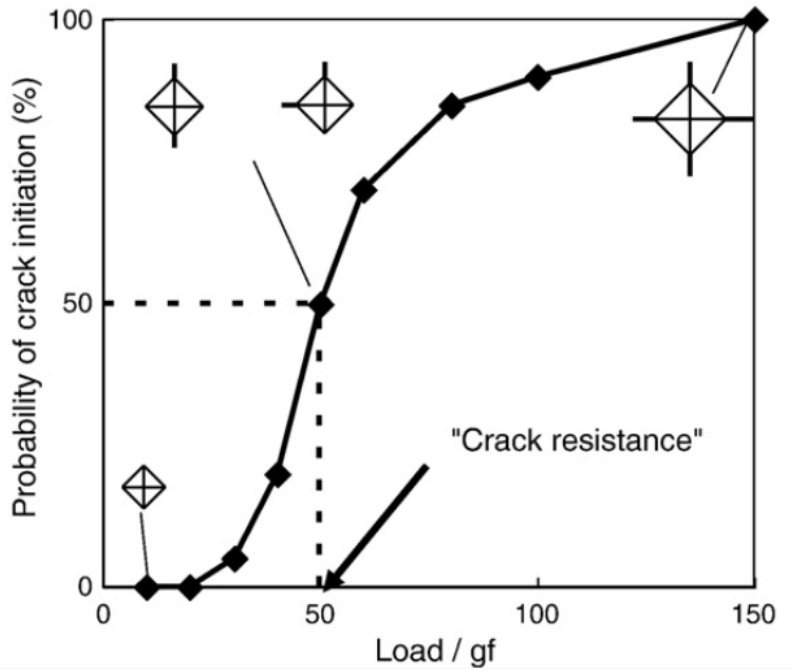

Figure 2.5.2: The number of radial cracks initiated in a Vickers indent divided by four plotted against the indenter load, P.The crack resistance, CR, is the load for which on average half the corners contain a crack.

fracture on larger scale. They proposed a normalisation of these two characteristic dimensions as a measure of brittleness.

$$B = \frac{H}{K_{Ic}} \tag{2.18}$$

where B is the brittleness. Several methods have been proposed to evaluate fracture toughness, and hence brittleness, from the length of radial cracks formed in an indentation measurement at high load [11, 99, 100], but generally do not agree well with those measured by e.g. the single edge notched beam method, said to give self-consistent values close to the intrinsic ones [10].

The brittleness, as seen in equation 2.18, is basically the ratio of resistance to microscopic deformation - through elasticity, densification, and plastic flow - and resistance to macroscopic failure in the presence of a crack [11]. It is found that low brittleness, i.e. low hardness and high fracture toughness, yields high resistance to crack initiation in a wide variety of glasses, as seen in figure 2.5.3 [6]. However,

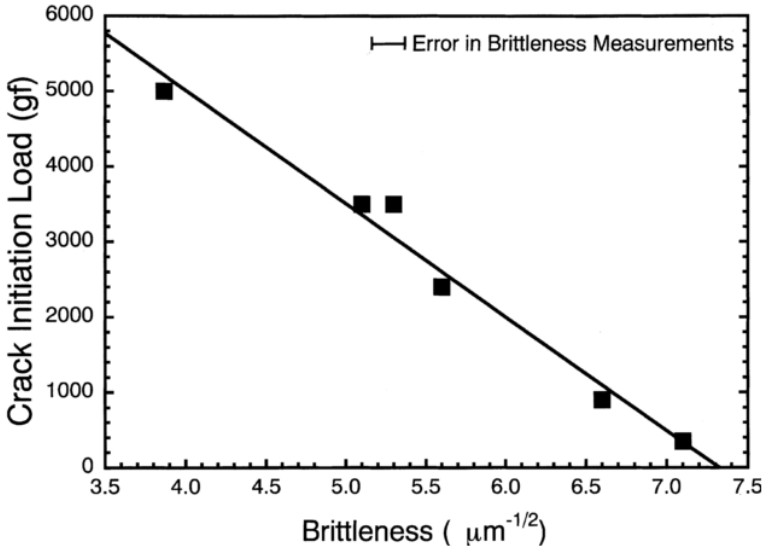

Figure 2.5.3: The load for crack initiation, CR, as a function of brittleness of variety of glasses containing very different amounts of the following components: SiO_2-Al_2O_3-Na_2O-K_2O-CaO-MgO-B_2O_3.

Kato et al. [33] finds brittleness to be only weakly correlated to CR, especially when the molar fraction of boron changes across compositions.

2.5.2 Elastic-plastic Stress Mismatch

Gross and Tomozawa argue for a fictive temperature increase during indentation [101], which change the mechanical properties [8], ultimately leading to fracture due to stress mismatch. In their trail of reasoning it is implicit that also the density of normal glass decreases on indentation, as the measured fictive temperature increases. This agrees with the results by IR reflection measurements on indented glasses by *Koike & Tomozawa* [102], but is directly contradictory to the theory of densification of glass during indentation as discussed in section 2.3.2. *Gross and Tomozawa* do find a relation between the minimum load dependence of hardness, or the ISE, with the load for crack initiation [103]. This is more along the route which *Kato et al.* works.

2.5.3 Plastically Induced Stress

In simple silicates very generally the crack resistance tends to decrease with modifier fraction, as observed by 1kgf crack-free indentations being possible in water-free amorphous silica in inert atmosphere [7]. This caused *Kato et al.* [33] to try and correlate the crack resistance to the plastic deformation volume. This was evaluated indirectly by the depth recovery of crack-free Vickers indent when annealed at $0.9 \times T_g$ (K) for two hours; the same procedure as used by *Yoshida et al.* [57] to measure the densified volume under an indent. Establishing first that the fracture toughness and brittleness indeed does not adequately describe the results, they find approximately linear relationship between crack resistance and recovery of indentation depth. They conclude that densification is probably the determining property for the large differences in crack resistance found in glasses, but there must also be other factors involved to describe the data.

Later work expanded on the idea of densification being a major influence, arguing that only the plastically deformed volume induces stress into the glass, this residual stress being the origin of crack formation. They attempted to calculate the residual stress by a cavity model based on that of *Lawn et al.* [104], who also assumed plastic deformation as the origin of residual stress, however the difference being that these authors did not take densification into account. The residual stress according to *Lawn et al.* [104] is calculated as,

$$\sigma_{rs} = K\frac{\Delta V_{pz}}{V_{pz}} \tag{2.19}$$

where σ_{rs} is the residual stress, ΔV_{pz} the change in plastic zone volume (taken as the post-annealing volume,) and V_{pz} the volume of the plastic zone. Of course this raises the question: What is the size of the plastic zone? *Yoffe* [105] assumed that the plastic zone is hemispherically shaped with a diameter of the indentation diagonal,

$$V_{pz} = \frac{1}{16} \cdot \frac{4}{3}\pi \cdot L_{ci}^3 = 0.262 L_{ci}^3 \tag{2.20}$$

Note that the assumptions of hemispherical shape of the plastic zone is generally accepted in the literature, as seen in theory [51,106], modelling [107], and experiment

[108]. This implies that the size most likely does scale with the cube of the diagonal, and any error will only be relative. The relationship found by *Kato et al.* [33] and the calculated residual stress is shown in figure 2.5.4.

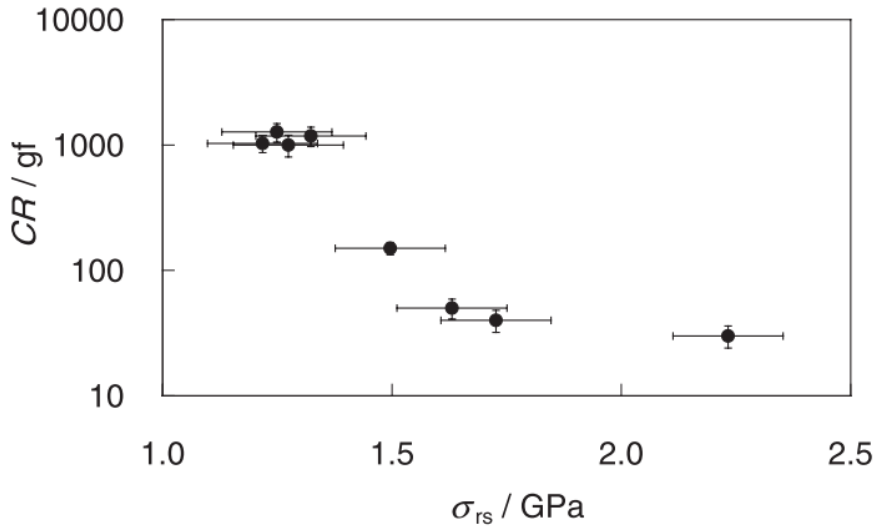

Figure 2.5.4: Crack resistance, CR, as a function of residual stress, σ_{rs}, under a 100gf Vickers indentation in a variety of commercial silica-based glasses as calculated by equation 2.19.

These results are basically just a different representation of the crack resistance vs. recovery of indentation depth ones, and other parameters still seem to have an effect on the crack resistance. However, framing the problem in this manner, it is emphasised that the residual stress initiates cracking, or more precisely, the residual stress *at the load for crack initiation initiates cracking.* It becomes apparent that if there exists a load dependence of densification, like the hardness ISE, this will influence the relationship shown in figure 2.5.4, as these estimated residual stresses are at 100gf. Indeed, such a relationship might explain the results of *Gross & Tomozawa* [103], finding a maximum in crack resistance in compositions exhibiting a low degree of ISE. That the hardness ISE is probably at least in part related to a change in the relative contribution of the deformation processes was indicated by *Chakraborty et al.* [109]. They measured the nanoindentation hardness as a function of load and loading rate on a soda-lime-silica glass. Increasing the loading rate increased the plastic deformation energy up to a certain maximum, and this maxi-

mum was then linked to the increase of nanoindentation hardness with loading rate. *Kato et al.* [61] therefore undertook a study of the load dependence of densification (figure 2.5.5), and the estimated residual stress, with three of the glasses previously examined, choosing ones with widely varying crack resistances.

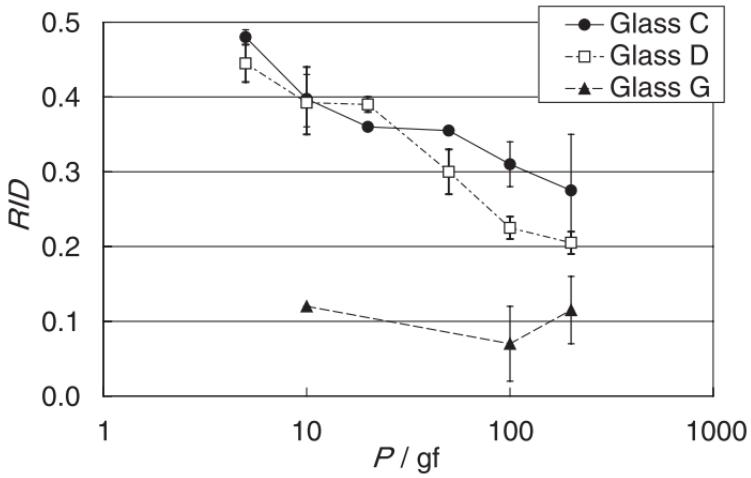

Figure 2.5.5: The recovery of indentation depth, RID, as a function of Vickers indenter load, P, for a variety of commercial silica-based glasses.

It is found that there is indeed a load dependence of densification with decreasing densification with decreasing load, as was previously reported by *Ji et al.* [39]. But why is this so? There is not yet a clear answer, but some related research is of interest. *Rouxel et al.* [53] find that glass hydrostatically densified at 25GPa exhibits more pile-up upon Vickers indentation as compared to normal density samples. There is even significant pile-up in densified amorphous silica ($\rho = 2.674$g/mL,) which has not been observed under any other circumstances for this glass. Since indentation is a dynamic process, one might envision that increasing the load corresponds to snuggly forcing the indenter into an indentation previously done at a lower load. However the glass beneath the indent is no longer that of the pristine surface, but densified, the depth of the densified zone being significant larger than that of the indent, proven by refractive index measurements [110]. As per the previously mentioned results on hydrostatically densified glass, one would suspect a larger contribution of plastic flow, and hence a decreasing densificative contribution with load. This view is supported by the fact that the pile-up region is indeed densified,

i.e. the material is first densified, then plastically flows to the surface. The analogy does however fail in one major aspect; judging from the high activation energy, shear flow probably occurs in the initial stages of indentation when the shear stress is the highest.

The load dependence of estimated residual stress found by *Kato et al.* [61] is shown in figure 2.5.6. We learn from figure 2.5.6 that the estimated residual stress

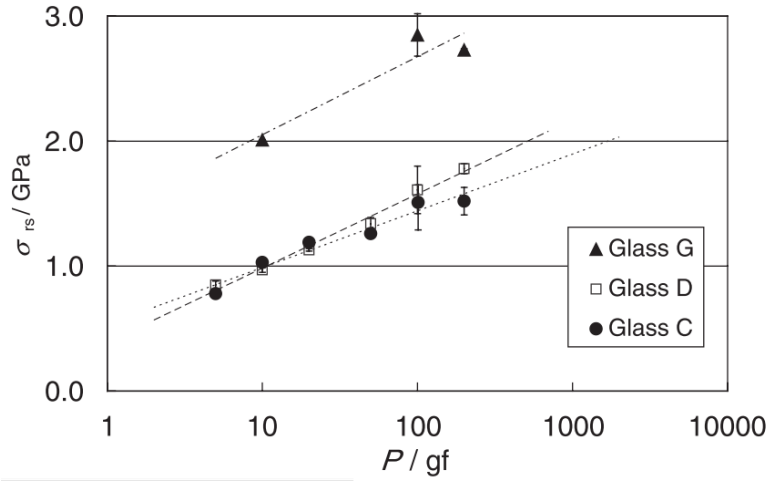

Figure 2.5.6: The estimated residual stress, ρ_{rs}, as a function of applied Vickers indenter load, P, for three commercial silica-based glasses. The crack resistances of the glasses are CR(C) = 1200gf, CR(D) = 150gf, and CR(G) = 30gf.

varies logarithmically with applied load, and that it seems similar for each of the three compositions (around 1.7-1.9GPa) at their respective loads for crack initiation. Despite the scarcity of data, *Kato et al.* [61] took this as evidende for the existence of an universal yield stress for radial crack formation in silicates, at least within experimental error.

3. PROBLEM STATEMENT

The problems to be solved in this Master Thesis can be summarised as:

1. How does densification and plastic flow in silicate glasses under sharp indentation quantitatively depend on composition and load?
2. What kind of model with predictive power can explain the above dependence?
3. What is the compositional dependence of the crack resistance, and how can it be predicted?

3.1 Problem 1: Quantification of Densification and Plastic Flow

The previous work on compositional dependence was reviewed in section 2.3.2, most of the work performed by *Yoshida et al.* [52,59] and *Kato et al.* [9,61]. However it has been very difficult to derive a compositional relationship; the strongest being that with Poisson's ratio shown in figure 2.3.3, which does not work for sodium borates. This relation with Poisson's ratio for silicates was interpreted as densification occuring by a collapse of the structure into the free volume, where free volume increases with lower Poisson's ratio. Yet, there is little evidence for this theory, as many other factors than merely the free volume varies with composition. The compositions tested so far have been a rather broad selection, encompassing a variety of silicate, borate, oxy-nitride, and bulk metallic glasses. Certainly this has been helpful in qualitatively evaluating the densification process; however for quantification using simple and systematically varying compositions is a must given that the mechanism is unclear.

As for the load dependence of these processes there exists very little useful quantitative data, only three compositions measured by *Kato et. al* [61], two by *Ji et al.* [39] with only a total of five loads tested, and one by *Yoshida et al.* [111]. The data by *Kato* [61] has better resolution, but measures only the depth recovery,

which cannot accurately predict the volume recovery [59]. Therefore, as fundamental a question as how the densified and plastic flow volume quantitatively varies with indentation load is barely answered, and the compositional dependence wholly unknown.

3.2 Problem 2: Modelling the Densified and Plastic Flow Volume

It has been shown through the work of *Yamane & MacKenzie* [34] that a more quantitative understanding of the processes occuring during indentation is an approach to predicting the hardness of glass from composition alone. Such prediction is an extremely powerful tool for development of new materials, and indeed the development of the hardest glasses known at the time was a direct result of their work. However as quantitative measurements were practically non-existant at the time, it is wholly unknown whether the relations (equation 2.3 to 2.6) derived for the resistance of each individual deformation mechanism reflect any kind of scientific truth, or the total resistance related to hardness alone has some merit. Even the derivation of this total resistance from the individual ones seems suspect, as it is taken as the geometrical mean, while surely some combination of serial and parallel connections would be more grounded in theory. Also, the presence of the average bond strength seems difficult to understand given what else is known of the processes. During densification bonds are not broken, so why should the average bond strength have any effect on the densified volume? Perhaps the average bond strength captures some truth about the difference in indentation behaviour of different glass-forming families, yet the meaning within the silicate system seems unclear.

Moreover, from the work of *Kato et al.* [9,33,61] it seems that the plastic flow volume, and its load dependence, might just be key to understanding another key glass property, the crack resistance. Modelling the quantitative measurements of various compositions would be necessary to see if it can be related to the results of crack resistance measurements. These measurements might also shed light on another indentation related problem, the generally found increase of hardness with decreasing load, dubbed the indentation size effect (or ISE.) The change in relative

contribution of the processes occurring during indentation most likely has an effect on the ISE [109], although other effects are also known to contribute.

3.3 Problem 3: Compositional Dependence of Crack Resistance

Two promising models have been proposed to quantify crack resistance without actually performing the time consuming experiements needed: The brittleness concept by *Lawn & Marshall* [99], and later used for glasses by *Sehgal & Ito* [6] gives good correlation across a wide variety of compositions, however the data by *Kato et al.* [33] is not well described by this approach. Another problem is that since the compositional dependence of fracture toughness is unknown, this approach cannot be used to predict which compositions will have low brittleness, and as such high crack resistance. However the estimated residual stress approach by *Kato et al.* [33] is through the plastic flow volume, which is why this route thus reduces more or less to Problem 1 - the lack of data. Although these measurements of densificative and plastic flow contributions to indentation are even more time consuming than measurements of crack resistance - especially if the load dependence is to be determined - the possibility of prediction from composition seems within reach. But first a question of great importance must be answered about the method suggested by *Kato et al.* [61]: Is there a single stress value for radial crack nucleation in silicate glasses under given conditions? If this turns out not to be the case, there is a strong need for evaluating the actual stress distribution around the indentation in order to proceed further, and answering this question is therefore the primary goal of Problem 3.

3.4 Glass Composition Selection

Selection of the compositions to be studied is of paramount importance in solving the above problems. To reduce the number of variables and maximise the usefulness of the results rather simple compositions with practical importance are preferable, why our attention is turned to the ternary soda-lime-silicate system. As the amount of plastic flow is suspected to increase with the modifier fraction

present in the glass, this is an important factor that must be varied. It was chosen to focus on a series of soda-lime-silica (SLS) glasses based on $3SiO_2{\cdot}Na_2O$ where calcia is systematically added until reaching a composition of $3SiO_2{\cdot}Na_2O{\cdot}CaO$. This systematically changes not only the modifier fraction but also the elastic properties greatly through addition of calcia. As hardness is know to vary approximately linearly with elastic constants such as Young's modulus and shear modulus, these compositions are thought to be simple, practical, and contain a large variation in the properties of interest.

Another factor that is thought to influence densification behaviour is the free volume, why a series of glasses with the same modifier fraction yet thought to have highly varying free volumes will be made. From a base composition of $75SiO_2$ $15Na_2O$ 10CaO the modifiers were substituted to potassium and barium respectively, in all four possible combinations. As the sizes of the modifiers vary widely, it is thought that the free volume of the glasses will show large variation in this modifier substituted (MS) series of glasses.

4. EXPERIMENTAL

4.1 Glass Making

The compositions used in this work are listed in table 4.1.1, and the reagents used were all carbonates (except silicon dioxide) of reagent grade from Sigma-Aldrich. The glasses in the SLS series except $80SiO_2$ have linearly varying molar fractions of soda, lime, and silica with modifier fraction. This is because $80SiO_2$ was added later on account of its low brittleness [95], as a glass with high crack resistance was wanted to get more reliable data for the residual stress at the load for crack initiation evaluation discussed in section 6.5.

For the soda lime silicate (SLS) series and the KBa composition the appropriate masses for a 25g batch of each reagent was weighed on a Chyo JL-180 (precise to 0.1mg) electric scale. Then melted in a platinum crucible (100%) at 1575°C for two hours in an electrically heated furnace, cast, crushed, and re-melted for another hour at 1575°C to ensure a homogenous glass. At this point the glass was cast into approximately 50 × 20 × 10mm bars in a brass mold on an electrically heated plate, and immediately tranferred to another electric furnace to be annealed for two hours at the glass transition temperature (T_g) indicated in the literature for the respective

Table 4.1.1: The molar compositions and their acronyms as used throughout this work. The first six glasses are the soda lime silicate (SLS) series, the next four the modifier substituted (MS) series.

Series	Acronym	SiO_2	Na_2O	CaO	K_2O	BaO
SLS	$80SiO_2$	80	15	5	-	-
	$75SiO_2$	75	25	-	-	-
	$71SiO_2$	71.4	23.8	4.8	-	-
	$68SiO_2$	68.2	22.7	9.1	-	-
	$65SiO_2$	65.2	21.7	13.0	-	-
	$60SiO_2$	60	20	20	-	-
MS	KBa	75	-	-	15	10
	NaBa	75	15	-	-	10
	KCa	75	-	10	15	-
	NaCa	75	15	10	-	-

composition. If this literature T_g turned out to be more than 10°C from that measured later, then the glass would be re-annealed at this temperature for two hours prior to use.

The modifier substituted (MS) series (excepting the KBa composition) were made as 500g batches, with raw materials weighed on a Mettler Toledo PG500Z-S scale. The melt was charged during 1hr in a platinum-rhodium (90:10) crucible while heating to 1575°C. In place of crushing and re-melting, the melt was stirred after half an hour and one hour with a platinum-rhodium (90:10) rod, homogenised for two hours, and finally cast into approximately 200 × 60 × 10mm slabs in a carbon mold to be immediately annealed at T_g. Other conditions were the same as for the SLS series.

4.2 Glass Transition Temperature

The glass transition temperatures (T_g) of the glasses were measured by thermal mechanical analysis (TMA) in a Seiko Instruments Inc. TMA/SS6000 on rods of approximate dimensions 2 × 2 × 10mm. The instruments recorded the length of the sample as a function of temperature, and T_g was determined by the intersect of two straight lines, one from the approximately linear segment below T_g, the other from the maximum slope in the glass transition range. This method was estimated to be accurate to within 5°C. If the glass transition temperature measured here was significantly different from the annealing temperature employed immediately following casting of the given composition the annealing would be redone at the measured temperature and T_g remeasured. Results are shown in section 5.1.

4.3 Density Determination

An approximately 1g piece was cut from a central portion of the bulk glasses and used for density measurement by the Archimedes' method, and aluminium oxide rods with known density ($\rho_{Al_2O_3} = 3.986\text{g/cm}^3$) used as a standard. A high precision Shimadzu AUW120D (d = 0.01mg) scale was used, calling for a somewhat elaborate procedure to account for delicate factors like baseline drift and buoyancy in air. A computer program would use the average of 30 seconds of data without

the sample loaded onto the scale as zero, then subtract this from the average of 30 seconds of data with the sample loaded. This process would be repeated three times for each sample in air, then the sample immersed in toluene by a stainless steel frame suspended from the scale, the temperature measured, and the above process repeated.

The air buoyuancy corrected mass of the sample would be determined as per,

$$m_{true} = m_{air} \cdot \frac{1 - \rho_{air}/\rho_{sample}}{1 - \rho_{air}/\rho_{steel}} \tag{4.1}$$

where m_{true} and m_{air} are the buoyuancy corrected and measured masses, and ρ the density of the subscripted material. Equation 4.1 has its roots in stainless steel ($\rho_{steel} = 8\text{g/cm}^3$) being used as the internal standard within the scale. The equation is not very sensitive to the exact sample density used, and a rough estimate of $\rho_{glass} = 2.5\text{g/cm}^3$ was used for the glasses, and the above mentioned known density of alumina for this standard. The density is then determined by Archimedes' Principle as,

$$\rho_{sample} = \rho_{Tol.} \cdot \frac{m_{true}}{m_{true} - m_{Tol.}} \tag{4.2}$$

where $\rho_{Tol.}$ is the density of toluene calculated from temperature [112] and $m_{Tol.}$ is the sample mass as measured when immersed in toluene. With this method a standard deviation less than 10^{-3}g/cm^3 could be achieved, however the calculated density of the alumina standard ($\rho_{Al_2O_3} = 3.994\text{g/cm}^3 \pm 9 \cdot 10^{-4}\text{g/cm}^3$) agrees with the literature value ($\rho_{Al_2O_3} = 3.986\text{g/cm}^3$) only to the second decimal, or 10^{-2}g/cm^3. The results are shown in section 5.2.

4.4 Determination of Elastic Moduli

An approximately $10 \times 10 \times 5$mm sample was cut from the bulk sample and progressively dry-polished on silicon nitride paper to a mirror-finish on both faces, as was an amorphous silica standard. The thickness was measured by a digital micrometer, and the coplanarity in all samples was better than a slope of 0.1 degrees. The transverse and longitudinal sound wave velocities were then measured by a Textronix TDS1012B two-channel digital storage oscilloscope equipped with a JSR

Ultrasonics pulser/receiver. Operational frequencies of the transverse and longitudinal piezoelectric transducers were 5MHz and 10MHz, and high and low pass filters of 2.5-7.5Mhz and 7.5-15MHz were employed for the respective transducers. Having selected a clearly distinguished peak (often the largest,) the temporal displacement of each echo was measured and sound velocity calculated as,

$$v = \frac{2L}{\Delta t} \tag{4.3}$$

where v is the velocity of sound, L the sample thickness, and Δt peak separation in time.

Poisson's ratio was then calculated by the classical relations [52, 113],

$$\nu = \frac{1 - 2(v_T/v_L)^2}{2 - 2(v_T/v_L)^2} \tag{4.4}$$

and the Young's modulus by,

$$E = v_L^2 \cdot \rho \cdot \frac{(1+\nu^2)(1-2\nu)}{1-\nu} \tag{4.5}$$

where ν is the Poisson's ratio, E the Young's modulus, and v_T and v_L the respective transverse and longitudinal sound velocities.

The two other major elastic moduli, the bulk and shear modulus, can be calculated by the following well known relations [5],

$$K = \frac{E}{3(1-2\nu)} \tag{4.6}$$

and,

$$G = \frac{E}{2(1+\nu)} \tag{4.7}$$

Where K and G are the bulk and shear modulus, respectively.

The Poisson's ratio and Young's modulus of the amorphous silica standard ($\rho = 2.20\text{g/cm}^3$) is found to be 0.169 ± 0.005 and $73GPa \pm 1GPa$, in excellent agreement with that measured by *Yoshida et al.* [52] also by the velocity of sound. The results are shown in section 5.3.

4.5 Vickers Hardness

Hardness was determined by the use of a Vickers diamond indenter mounted on an Akashi MVK-H2 Hardness Testing Machine. The samples used were the same as for the measurements of Poisson's ratio and Young's modulus in the previous section, i.e. the samples were coplanar and polished to a mirror finish. The samples were stored under vacuum and cleaned in ethanol immediately prior to testing. Hardness was determined at 25gf with a hold time of 15 seconds under ambient conditions with at least ten repeated indentations for the SLS series, and five for the MS series. None of the indents showed signs of radial, lateral, or median cracking. In lieu of the standard optical determination of diagonal length this was determined from the Atomic Force Microscopy (AFM) micrographs measured in the following section (and the conditions described in detail there.) For the 71SiO2 composition at 50gf the validity of the diagonal length as measured by AFM was tested by also measuring the diagonal by optical microscopy. It was found that the hardness as determined by AFM ($4.25 \pm 0.06 GPa$) versus that by light microscopy ($4.1 \pm 0.2 GPa$) exhibited less spread and had similar mean values within experimental error. The data is presented in section 5.4.

4.6 Compositional Dependence of Densification

The indented samples from the previous section would be stored under vacuum for no longer than one day, then the surface cleaned in ethanol and subjected to Atomic Force Microscopy (AFM) measurement. The instrument employed was a SPA400 from Seiko Instruments Inc. fitted with a VeeCo silicon nitride cantilever with a 60nm gold back-coated 0.7-0.9μm tip. An area of approximately 30x30μm would be scanned in contact mode at a resolution of 512x512 pixels and data collected via the NanoNavi software supplied by the manufacturer.

Data analysis was performed with a Scanning Prope Image Processor (SPIP) software by Image Metrology. Initially the base plane would be corrected by fitting to a third order polynomium on the entire area, thereafter repeated only on the area containing the indent and pile-up area. This procedure was necessary to achieve a symmetrical representation of the indent. As per the comparison of optical and

AFM measured diagonal distances in section 4.5, it is believed that this procedure yields a truthful image of the indented area.

Diagonal distances was measured as the peak distance between the pile-up areas, and the average of both diagonals is reported here. Face distances are taken through the middle of the opposite faces and through the center of the indent, and measured as the separation at the level of the base plane. Again, the average of both are reported here. The depth was measured via a by depth histogramic representation of the data, i.e. the frequency of points of the measured surface as a function of depth. The depth was taken as the height from the lowest data point (the absolute bottom of the indent) and the deepest onset of the strongest increase in frequency (the base plane.) The indent volume is determined by the same procedure, only the difference in void volume is measured instead. Unfortunately the pile-up volume is intrinsically a rather arbitrary quantity. It was measured as the volume difference between the highest onset of frequency (the base plane) and the highest data point (the absolute top of pile-up.) However the highest onset of frequency is not well-defined exactly because of the presence of pile-up. Care was taken to ensure a similar shape and area of the pile-up region measured in the micrograph for indents made at the same load.

To recover the densified volume the procedure used by *Yoshida et al.* [52] schematically shown in figure 4.6.1 was employed. Immediately after AFM measurement the sample would be wrapped in aluminium foil to reduce accumulation of dust, with only a single layer covering the indented surface. This was put in an electric furnace with a thermocouple placed a few millimeters above the middle of the indented surface, as the central region would contain the indents. The furnace was preheated to the annealing temperature ($T_a = 0.9 \times T_g$ (K)) and temperature adjusted after putting in the sample. T_a would be reached within 5-10 minutes, and annealing then proceed at this temperature for two hours as per the method employed by *Yoshida et al.* [52,57,59,60,111] and *Kato et al.* [9,33,61]. The samples were cooled in the furnace to room temperature at a rate of approximately 1°C per minute.

Post-annealing AFM measurements were performed analogues to the previous

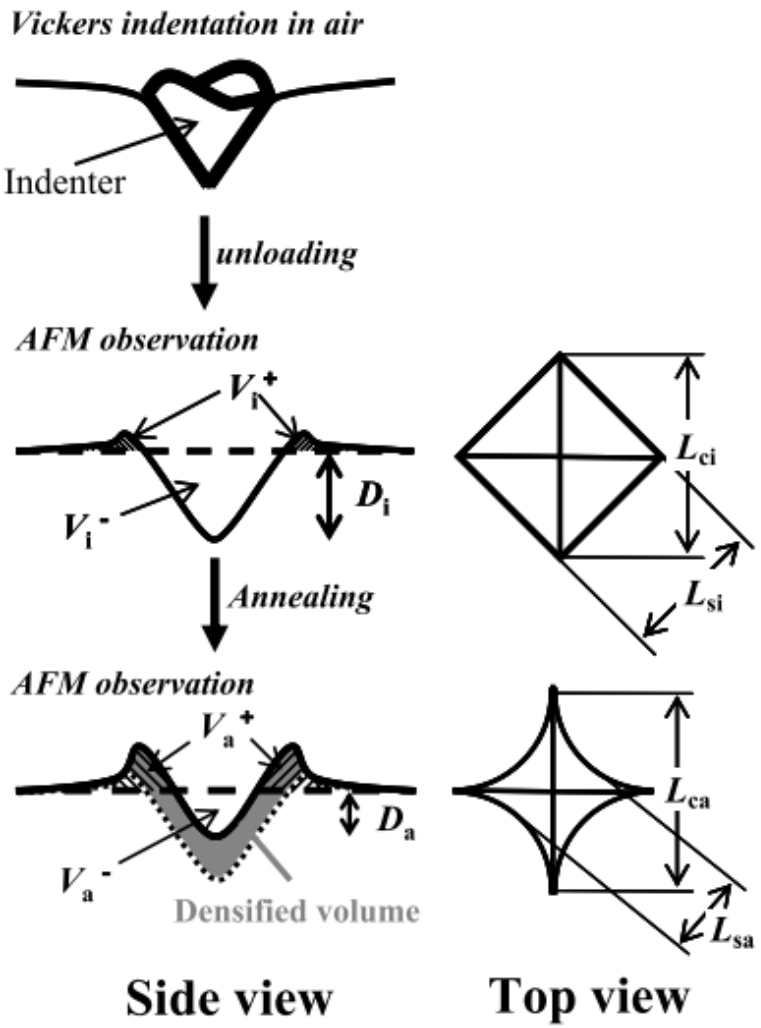

Figure 4.6.1: The method employed in this work for quantification of the densified volume. The annealing conditions employed were $0.9 \times T_g$ (K) for 2 hours.

ones, using the same cantilever and settings. When determining the pile-up volume care was taken to ensure that the pile-up area was similar or slightly larger than that prior to annealing. The surface tends to get somewhat dirty when annealed, and dirt on the surface iwas excluded from measurements of pile-up volume by marking the area to be excluded in the software. If dirt was present in the actual indent, the data point would be discarded. For the SLS series between 10 and 12 good data points were achieved for a given composition and load, while for the MS series, due to the large span of loads measured, only three to five usable data points were obtained at each load.

The volume recovery ratio, V_R, is defined as the densified volume relative to the initial indentation volume, and determined as,

$$V_R = \frac{(V_i^- - V_a^-) + (V_a^+ - V_i^+)}{V_i^-} = \frac{V_d}{V_i^-} \tag{4.8}$$

where superscript + and - indicate above or below the surface level, and subscript i and a initally measured and after annealing respectively, as visualised in figure 4.6.1. V_d is the densified volume, and is related to the plastic flow volume, V_p, as,

$$V_p = V_i^- - V_d \tag{4.9}$$

This definition might seem slightly odd, as the pile-up area before annealing is not involved. This is because the presence edge cracks, present in some compositions at loads in excess of 50gf, will tend to increase V_i^+ dramatically, while the difference in pile-up volumes as measured before and after annealing $(V_a^+ - V_i^+)$ is within experimental error. The pile-up volume before annealing is generally small and error prone, why this minor error is deemed acceptable given that it enables comparison with the data by *Yoshida et al.* [52]. Also, this definition works well with the V_R of equation 4.8, as the corresponding plastic flow ratio will be the remainder to 100%.

The ratio of indentation depth recovery (RID) is determined simply by,

$$RID = \frac{D_a}{D_i} \tag{4.10}$$

D_i being the initial depth and D_a that after annealing. In the same manner the recovery of indentation face distance (RIF) is measured,

$$RIF = \frac{L_{sa}}{L_{si}} \tag{4.11}$$

L_{si} and L_{sa} being the initial and post-annealing average face distances.

4.7 Determination of Crack Resistance

Samples from the MS series of approxiate size 25mm × 30mm and a thickness of 1.1-1.2mm and coplanarity better than 0.1 degrees were lapped with an aluminum oxide slurry, then finished with a cerium oxide to obtain a mirror finish on both sides. These samples were then stored in controlled atmosphere for at least 24 hours at a relative humidity of 30% and a temperature of 25°C before testing. The humidity and temperature was chosen to mimic real world conditions, while keeping the influence of atmospheric conditions constant.

Indentations were made on a Matsuzawa MxT50 High Quality Digital Hardness Tester equipped with a Vickers Diamond indenter placed within the glove box. First a prelimary test was performed with a few indents to find the approximate range in which the number of radial cracks would vary from zero to four. The actual measurement would then be performed with 20 indents at each of seven or eight loads and a 15 second dwell time. The indents were all made in the central region of the sample on the grounds of possible edge defects and poor polishing. Also, they were spaced approximately $200\mu m$ apart as to avoid the influence of indentation induced residual stress of other indents. The number of radial cracks would be counted exactly 15 seconds after the start of unloading, however little time dependence on the crack initiation was observed.

As for the $80SiO_2$ composition, the measurement was done outside of controlled atmosphere (at 26°C and a relative humidy between 50% and 60%.) The indentation setup was the same as used for the hardness measurements, which unfortunately does not yield as good a resolution in load. Other variables were identical to the other crack resistance measurements.

4.8 Helium Solubility in Glass

The glass was processed in an indentical manner as in the previous section, then placed in a helium atmosphere under atmospheric pressure at elevated temperatures until saturation reached; time and temperature given below. Extraction was performed by cutting the saturated sample into cubes with approximate weight 0.15-0.16g, and melted at 1100°C under high vacuum conditions (around $2 \cdot 10^{-7}$

Torr) for 30 minutes, while the extracted helium was measured continuously by quadropole mass spectroscopy. A single data points consists of the average of five cubes cut at regular spacings spanning the width of the sample. Another data point would be measured by the same method, but by cutting at the opposite side of the sample, as shown in figure 4.8.1.

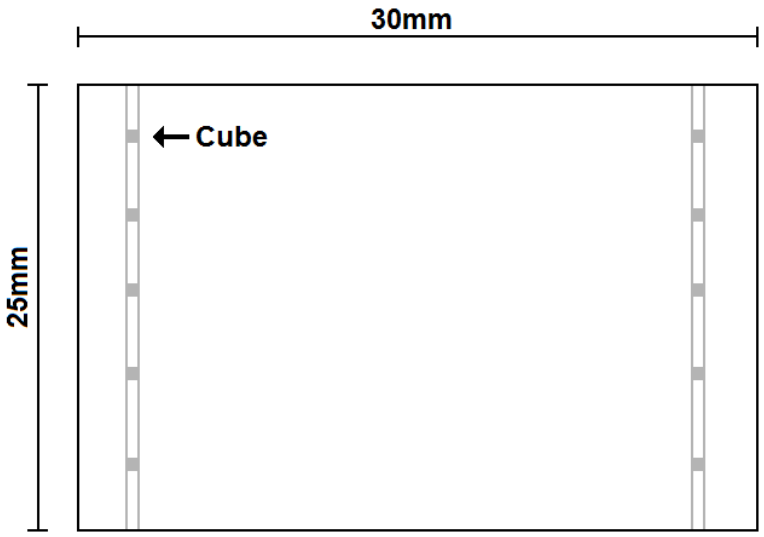

Figure 4.8.1: The extraction of cubes for helium solubility determination of the originally saturated sample. The thickness of the samples was between 1.08mm and 1.22mm.

Preliminary experiments were carried out to determine a temperature at which the time for saturation was within reasonable limits for a standard soda-lime-silicate composition, and found to be so at $0.9 \times T_g$ (K) and three hours. The temperature was chosen as a fraction of T_g since it was believed that the relative effect of temperature of the compositions would be approximately the same. A single data point was obtained at 18 hours of saturation for the MS compositions, as well as two points at three hours, to make sure that saturation had indeed been reached.

5. RESULTS

5.1 Glass Transition Temperature

The results are shown in figure 5.1.1 and tabulated in table 5.4.1 along with other properties of the glasses. As it can be seen in figure 5.1.1 T_g increases approx-

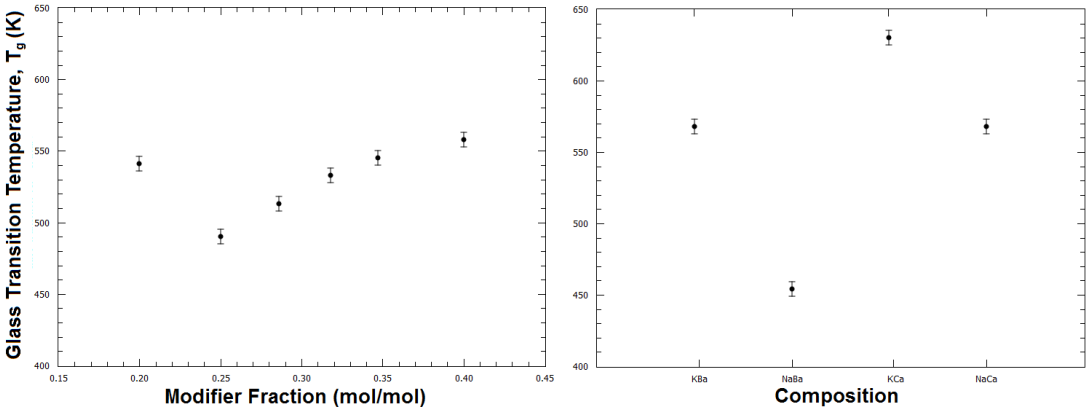

Figure 5.1.1: (a) The glass transition temperature, T_g, of the SLS series plotted against modifier fraction, i.e. the molar fraction of modifying oxides. (b) That of the MS series. The experimental error is $\pm 5°$C.

imately linearly with modifier fraction in the SLS series, excepting $80SiO_2$, while the data for the MS glasses are scrambled.

5.2 Density Determination

The results are shown in figure 5.2.1 and table 5.4.1. Again, an approximately linear relationship with modifier fraction is seen for the SLS series, with no obvious correlations for the MS glasses.

5.3 Elastic Properties

The results are shown in figures 5.3.1 and 5.3.2 and tabulated in table 5.4.1 It is seen that, excepting the $80SiO_2$ composition, E and v vary approximately linearly with modifier fraction in the SLS series. For the MS series, a relationship is seen where the relative contribution to Young's modulus of each component decreases

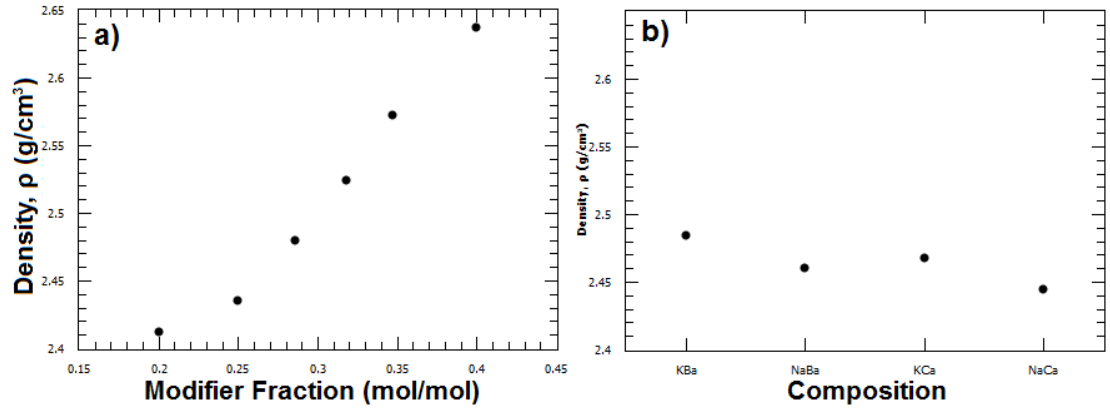

Figure 5.2.1: (a) Density, ρ, of the SLS series plotted against modifier fraction, i.e. the molar fraction of modifying oxides. (b) Density of the MS series. The maximum experimental error is $\pm 0.001 g/mL$.

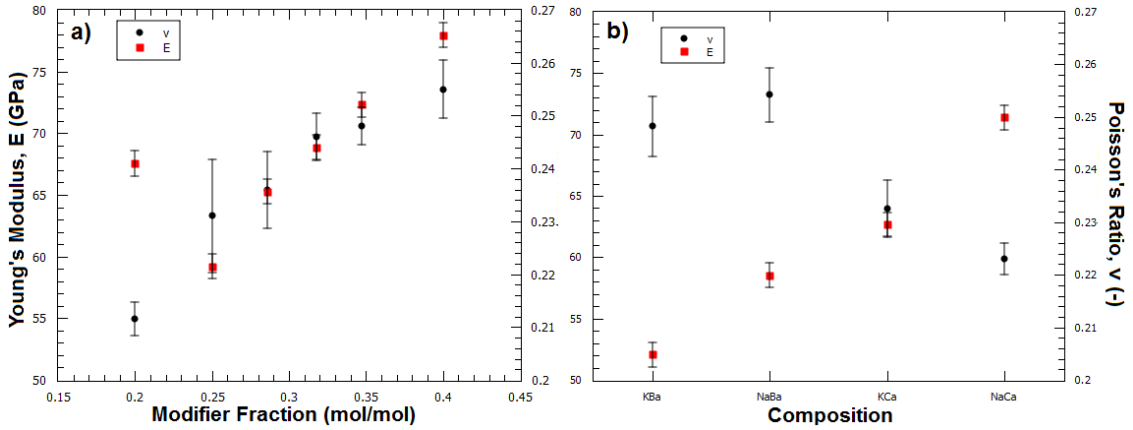

Figure 5.3.1: (a) Young's modulus, E, and Poisson's ratio, ν, of the SLS series plotted against modifier fraction, i.e. the molar fraction of modifying oxides. (b) Those of the MS series. Error bars indicate ± 1 standard deviation.

as Ca >Ba >Na >K (the order of the field strength,) while there is no simple relationship for the Poisson's ratio. In figure 5.3.2 it is seen that also K and G vary approximately linearly with modifier fraction for the SLS series. This is a direct consequence of the relationship witnessed in figure 5.3.1, due to the relationship between elastic moduli, as seen in equations 4.6 and 4.7 used to calculate these values. Again, the relationship for the MS compositions is slightly more complicated, but follow the trend of E fairly well, with K being more sensitive to ν than is G.

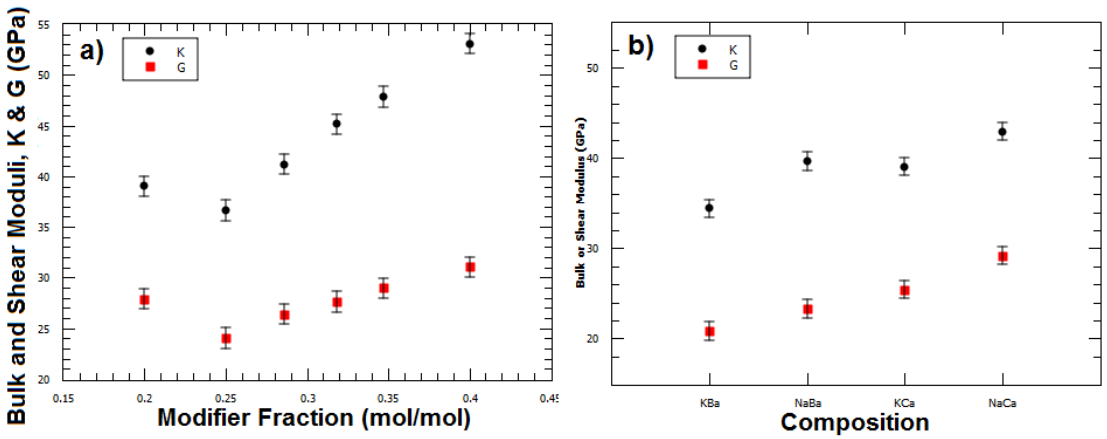

Figure 5.3.2: (a) Bulk modulus, K, and shear modulus, G, of the SLS series plotted against modifier fraction, i.e. the molar fraction of modifying oxides. (a) Those of the MS series. Error bars indicate ± 1 standard deviation.

5.4 Vickers Hardness Determination

Results of the Vickers hardness determination can be seen in figure 5.4.1 and are summarised in table 5.4.1 along with results from the previous sections. The

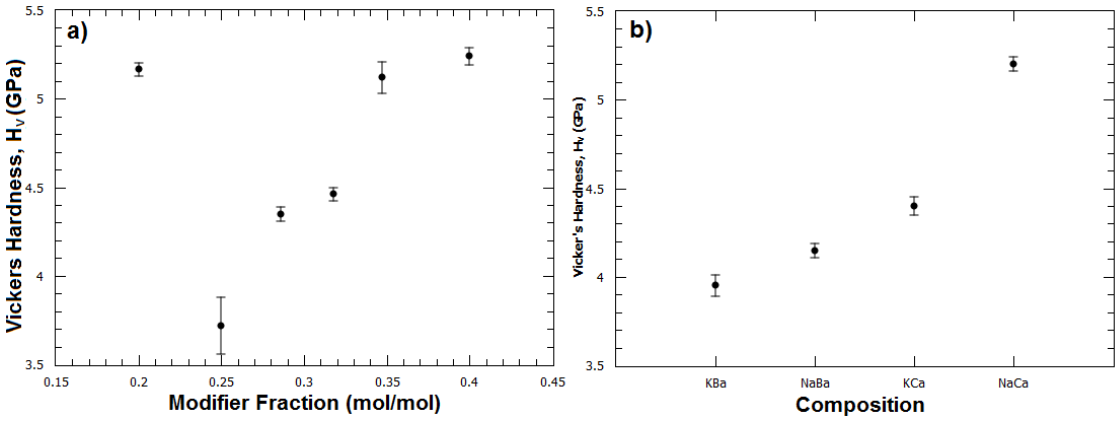

Figure 5.4.1: (a) Vickers hardness, H_V, of the SLS series plotted against modifier fraction, i.e. the molar fraction of modifying oxides. (a) That of the MS series. Error bars indicate ± 1 standard deviation.

linear relationship seen here for the SLS series is not as smooth as that for the previous data, even considering the larger standard deviation. However, the trend for both the SLS and MS glasses is similar to that of the Young's or shear modulus..

Table 5.4.1: Glass transition temperature, T_g, density, ρ, Poisson's ratio, ν, Young's modulus, E, bulk modulus, K, shear modulus, G, and finally Vickers hardness, H_V determined at 25gf for the compositions examined in this work. The error given is the maximum standard deviation among the mean values found in the table.

Composition	T_g [°C]	ρ [g/cm^3]	ν	E [GPa]	K [GPa]	G [GPa]	H_V [GPa]
$80SiO_2$	541	2.412	0.21	68	39	28	5.4
$75SiO_2$	490	2.435	0.23	59	37	24	3.7
$71SiO_2$	513	2.480	0.24	65	41	26	4.4
$68SiO_2$	533	2.524	0.25	69	45	28	4.5
$65SiO_2$	545	2.572	0.25	72	48	29	5.1
$60SiO_2$	558	2.637	0.26	78	53	31	5.2
KBa	568	2.445	0.25	52	34	21	4.4
NaBa	454	2.461	0.25	59	40	23	4.2
KCa	630	2.468	0.23	63	39	25	4.4
NaCa	568	2.484	0.22	71	43	29	5.2
Error	±5	±0.001	±0.01	±1	±1	±1	±0.1

5.5 Volume Recovery of Densification at Constant Load

The compositional variation of the densified and plastic flow volumes are shown in figure 5.5.1, and the relative recovery ratios, V_R, RID, and RIF are shown in figure 5.5.2, and found in tabulated form in table 5.5.1.

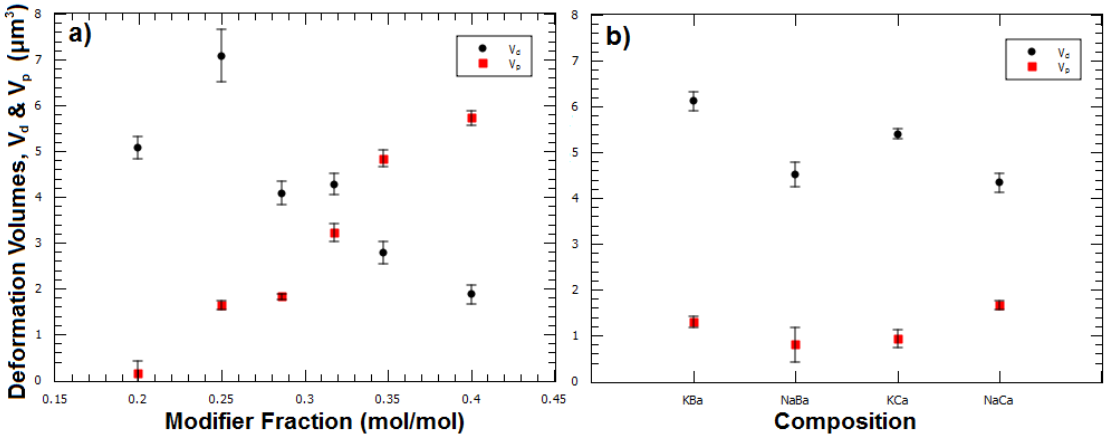

Figure 5.5.1: (a) Densified (V_d) and plastic flow volume (V_p) of the SLS series plotted against modifier fraction, i.e. the molar fraction of modifying oxides. (b) Those of the MS series. Error bars indicate ±1 standard deviation.

For the SLS series the densified and plastic flow volumes seem to have an

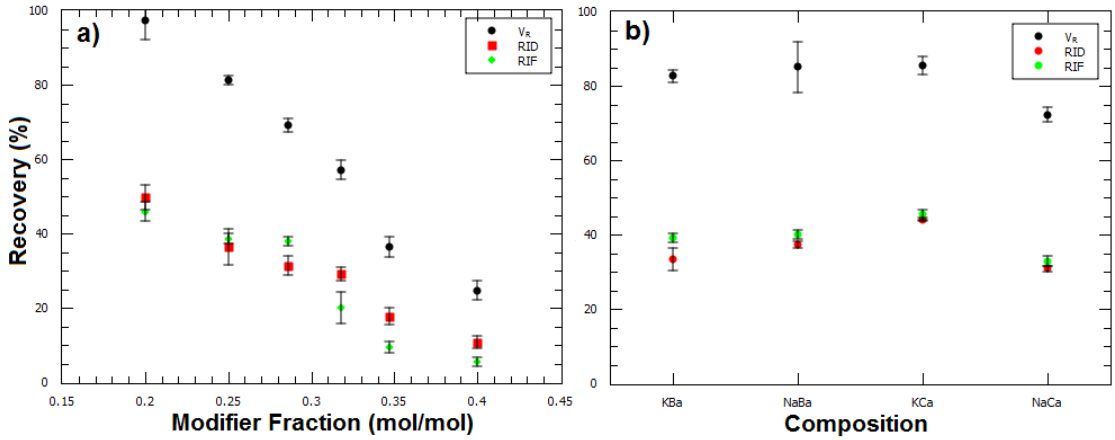

Figure 5.5.2: (a) The volume ratio of recovery, V_R, ratio of indentation depth recovery, RID, and ratio of indentation face recovery, RIF, of the SLS series plotted against modifier fraction, i.e. the molar fraction of modifying oxides. (b) Those of the MS series. Error bars indicate ± 1 standard deviation.

approximate monotonical dependence on modifier fraction, densified volume decreasing and plastic flow volume increasing. The relative recovery ratios, V_R, RID, and RIF are also approximately linear. In the MS series no obvious tendencies are observed. The correlation between these measures of densificative recovery is examined in figure 5.5.3, where V_R is taken as the abscissa, as this is thought to be the most reliable measure of recovery, having the greatest span of values and lowest relative standard deviation, and is immune to any change in the distribution of the densificatied volume with composition. As can be seen, both RID and RIF are well described by a linear fit to the measured volume recovery, however only the RID has an intercept close to origo, and thus differing from V_R by a constant factor. The non-zero intercept of the RIF data may be caused by difficulty in measuring the exact minimum face-to-face distance post-annealing, when the indent is no longer clearly defined. Any skewing of the measured cross-section will cause the measured distance to be larger, and thus the RIF smaller than the true value. Whatever the reason, it is believed that the V_R and RID are the better descriptors of recovery of densification, and the RIF will therefore not be discussed in this work.

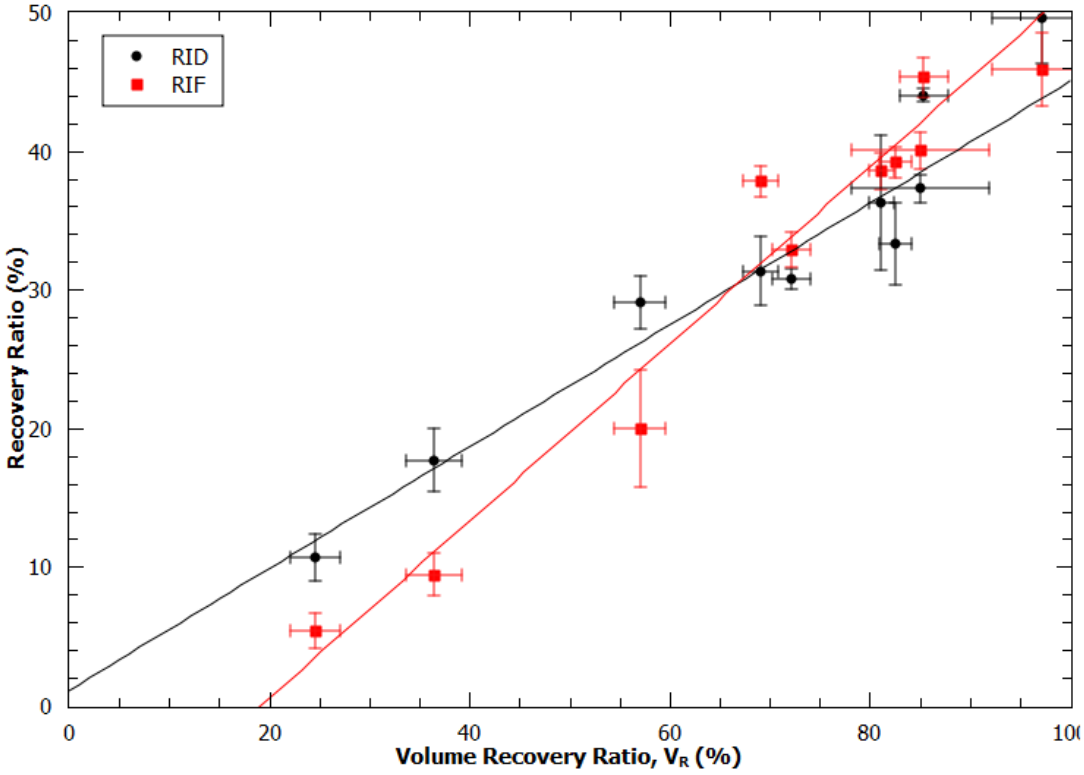

Figure 5.5.3: The ratio of indentation depth recovery, RID, and ratio of indentation face recovery, RIF, plotted against the volume ratio of recovery, V_R. The lines are obtained by linear regression. Error bars indicate ± 1 standard deviation.

5.6 Hardness and Densification with Variable Load

The results from 5gf to 200gf are shown in figures 5.6.1 and 5.6.2, and the entire data range is tabulated in table 5.6.1. Within experimental error the hardness seems to decrease continously with load, apparently reaching a relative constant value around 100gf. This magnitude of the hardness ISE is in the order of: NaCa>80SiO_2 >KBa>KCa>NaBa. Most of the compositions exhibit the classical exponential-like decrease of hardness with load within experimental error, yet the NaBa composition seems to have too low a hardness at the lowest loads.

As for the recovery ratios there generally seems to be a discrepancy at 5gf. Although accompanied by a large experimental error, generally the values lie below that which is expected from the trend in the data, an increase with lower load. Looking past the 5gf data though, there seems to be an approximately linear decrease

Table 5.5.1: The densified volume, V_d, plastic flow volume, V_p, volume ratio of recovery, V_R, ratio of inentation depth recovery, RID, ratio of indentation face recovery, RIF, and Vickers hardness, H_V, at 25gf of the compositions examined in this work. The error given is the maximum standard deviation among the mean values found in the table.

Composition	V_d [μ m^3]	V_p [μ m^3]	V_R	RID	RIF	H_V [GPa]
80SiO_2	5.1	0.1	97%	50%	46%	5.4
75SiO_2	7.1	1.6	81%	36%	39%	3.7
71SiO_2	4.1	1.8	69%	31%	38%	4.4
68SiO_2	4.3	3.2	57%	29%	20%	4.5
65SiO_2	2.8	4.8	36%	18%	9%	5.1
60SiO_2	1.9	5.7	25%	11%	5%	5.2
KBa	4.9	1.3	79%	35%	37%	4.4
NaBa	4.5	0.8	85%	37%	40%	4.2
KCa	5.4	0.9	85%	44%	45%	4.4
NaCa	4.3	1.7	72%	31%	33%	5.2
Error	$\pm$0.6	$\pm$0.4	$\pm$7%	$\pm$5%	$\pm$4%	$\pm$0.1

of the recovery ratios with load for all but the barium containing compositions. For the KBa composition, there seems to be no load dependence of densification, while the trend is very complicated for the NaBa one. Indeed, for the latter the recovery ratios, V_R and RID, do not correspond well to each other. It is thought that high reactivity with water is the origin of this effect. For the indentations at 5 and 10gf two pile-up peaks were found at different distances from the indentation center. This could well be indicative of a softening of the uppermost surface layer by reaction with water vapor in the atmosphere. It was also observed that the KBa composition tarnished rapidly when exposed to atmospheric conditions. Due to these facts, and the few data points available for the KBa composition, the results of both barium containing compositions and all the data taken at 5gf are considered unreliable and will not be discussed.

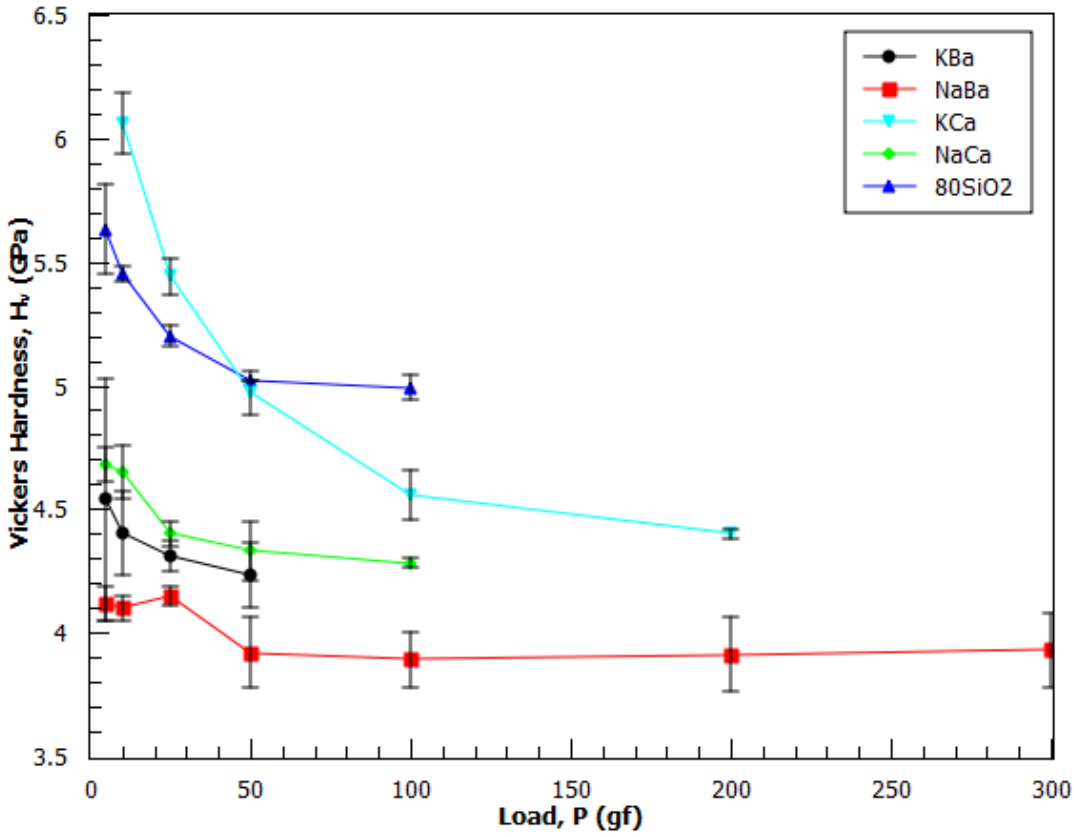

Figure 5.6.1: Vickers hardness, H_V, as a function of load for the MS series and 80SiO_2 composition. Error bars indicate ± 1 standard deviation.

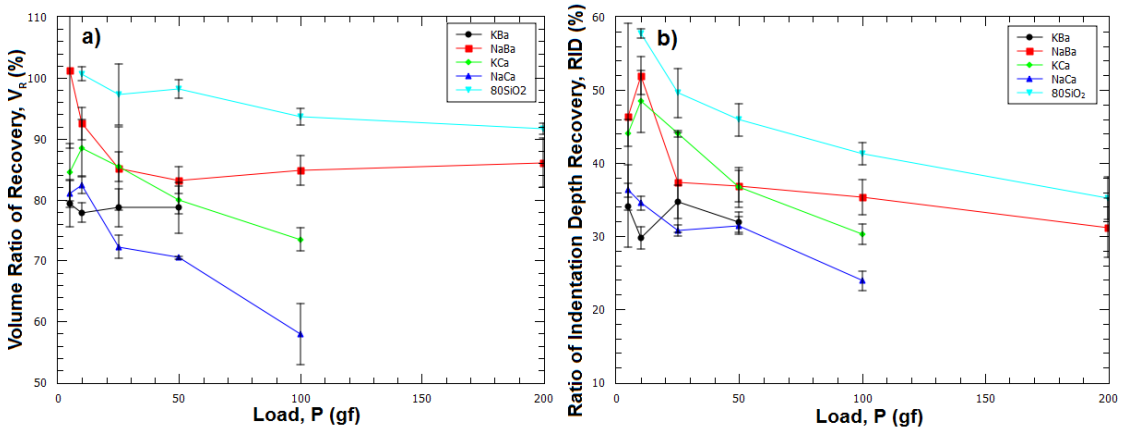

Figure 5.6.2: (a) The volume ratio of recovery, V_R, and (b) ratio of indentation depth recovery, RID, as a function of load, P, for the MS series and 80SiO_2 composition. Error bars indicate ± 1 standard deviation.

5.7 Determination of Crack Resistance

The explicit purpose of the crack resistance measurements was to evaluate the hypothesis of a single value of residual stress at the load for crack initiation in silicate glasses. For this reason, only the NaCa, KCa, and $80SiO_2$ compositions were measured, as the densification data at variable load for the barium containing compositions are thought to be unreliable, as discussed further in section 6.5.

The results where fitted sigmoidally with the Boltzmann function,

$$C_{rad} = \frac{C_i - C_f}{1 + \exp\left[w(P - CR)\right]} + C_f \tag{5.1}$$

where C_{rad} is the number of radial cracks divided by four, subscript i and f are initial and final values (inital guesses 0 and 1,) and w is a constant approximately equal to the width of the high slope region. The results fitted with the Boltzmann function can be seen in figure 5.7.1, while the data and calculated CR is tabulated in table 5.7.1.

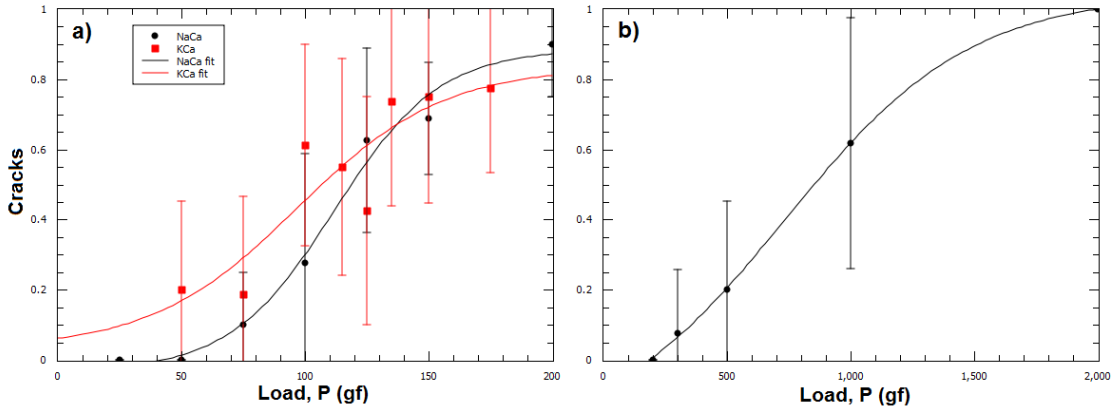

Figure 5.7.1: Number of radial cracks divided by four as a function of Vickers indentation load, P, for (a) the NaCa and KCa, and (b) $80SiO_2$ compositions. Error bars indicate ± 1 standard deviation.

5.8 Helium Solubility

As the helium solubility is only measured at one temperature for each glass within a rather narrow range, the results will be interpreted in terms of the free volume model proposed by *Doremus* [87, 88] assuming that there is no change in

Table 5.6.1: Densified volume, V_d, plastic flow volume, V_p, volume ratio of recovery, V_R, ratio of indentation depth recovery, RID, and Vickers hardness, H_V, as measured by AFM on the MS and 80SiO_2 compositions at various loads. The error is given as the maximum standard deviation among the compositions at a given load.

	Load [gf]	V_d [μ m^3]	V_p [μ m^3]	V_R	RID	H_V [GPa]
KBa	5	0.37	0.04	79%	34%	4.5
	10	1.2	0.34	78%	30%	4.4
	25	4.9	1.3	79%	35%	4.3
	50	14.1	3.8	79%	32%	4.2
NaBa	5	0.40	0.00	101%	46%	4.1
	10	1.2	0.09	92%	52%	4.1
	25	4.5	0.8	85%	37%	4.2
	50	13.3	2.7	85%	37%	3.9
	100	39	7	85%	35%	3.9
	200	106	17	86%	31%	3.9
	300	183	38	83%	20%	3.9
KCa	5	0.40	0.07	84%	44%	4.7
	10	1.2	0.16	88%	48%	4.7
	25	5.4	0.9	85%	44%	4.4
	50	14.5	3.6	80%	37%	4.3
	100	38	14	73%	30%	4.3
NaCa	5	0.39	0.09	81%	36%	5.6
	10	1.2	0.26	82%	35%	5.5
	25	4.3	1.7	72%	31%	5.2
	50	12.3	5.2	70%	31%	5.0
	100	28	20	58%	24%	5.0
80SiO_2	10	1.13	-0.01	101%	58%	6.1
	25	5.1	0.2	0.97%	50%	5.2
	50	16.3	0.3	98%	46%	5.0
	100	47	3.2	94%	41%	4.6
	200	130	12	92%	35%	4.4
Error	5	±0.05	±0.05	±13%	±6%	±0.5
	10	±0.1	±0.06	±5%	±4%	±0.2
	25	±0.3	±0.4	±7%	±2%	±0.1
	50	±0.9	±0.7	±4%	±3%	±0.1
	100	±3	±2	±5%	±4%	±0.1
	200	±3	±5	±4%	±2%	±0.1
	300	±8	±8	±4%	±1%	±0.1

Table 5.7.1: Mean number of radial cracks, the standard deviation at each load, and the crack resistance, CR, as determined by equation 5.1 for the NaCa, KCa, and 80SiO_2 glasses. The CR error is given as the interval of data points between which it is determined to lie.

	NaCa		KCa		80SiO_2	
Load [gf]	Cracks	Error	Cracks	Error	Cracks	Error
25	0.0	0.0	-	-	-	-
50	0.0	0.0	0.8	1.0	-	-
75	0.4	0.6	0.8	1.1	-	-
100	1.1	1.2	2.5	1.2	-	-
115	-	-	2.2	1.2	-	-
125	2.5	1.1	1.7	1.3	-	-
135	-	-	3.0	1.2	-	-
150	2.8	0.6	3.0	1.2	-	-
175	-	-	3.1	1.0	-	-
200	3.6	0.6	-	-	0.0	0.0
300	-	-	-	-	0.3	0.7
500	-	-	-	-	0.8	1.0
1000	-	-	-	-	2.5	1.4
2000	-	-	-	-	4.0	0.0
CR [gf]	112	100-125	97	75-100	736	500-1000

volume of the glass upon gas penetration and no interaction between the matrix and helium gas. Under these assumptions equation 2.17 becomes,

$$\left(\frac{C_d}{C_{atm}}\right) = V_f \tag{5.2}$$

The Ostwald helium solubilities measured on the glasses (equal to the free volume fraction per equation 5.2,) the saturation temperatures, and the other proposed measures of free volume of the glassy network (Poisson's ratio and the space ratio as calculated by equation 2.15) are given in table 5.8.1. As seen in table 5.8.1 in the helium solubility results section the Ostwald solubilities are the same within experimental error for both the 3 hour and 18 hour results, maybe with a slight increase in solubility for NaBa composition. For this reason all the measured values for a single composition will be averaged.

Table 5.8.1: The measured Ostwald helium solubilities, C_d/C_{atm}, measured at the saturation temperature, $T_{sat.}$, along with other proposed measures of free volume; Poisson's ratio, ν, and space ratio, V_{SR}, for the MS series

Composition	$T_{sat.}$ [°C]	C_d/C_{atm} (3hr)	C_d/C_{atm} (18hr)	ν	V_{SR}
KBa	456	0.10%	0.10%	0.25	47.1%
NaBa	381	0.06%	0.08%	0.25	56.2%
KCa	540	0.16%	0.15%	0.23	46.4%
NaCa	484	0.14%	0.14%	0.22	50.1%
Error	±5	±0.01%	±0.01%	±0.01	-

6. DISCUSSION

6.1 Glass Properties

The T_g, density, and mechanical properties given in sections 5.1, 5.2, 5.3, and 5.4 were found to have approximately linear dependency on modifier fraction for the SLS series (excluding the $80SiO_2$ composition,) but having no obvious correlation either with composition nor other properties for the MS series (having the same modifier fraction.) This was expected, as these properties (except hardness) as a first approximation can all be predicted from appropriately weighted linear combination of the fraction that each oxide constitutes in the glass [47–49, 114], although more complex models exist, e.g. for prediction of glass density [115]. As hardness shows correlations to elastic properties like Young's modulus [28], or thermal properties like T_g [37], or the softening point [46], it is not surprising that this also property varies approximately linearly in for most of the SLS series.

For exactly the same reasons, no major correlations were expected nor found in the MS series. Although the alkaline and alkaline earth modifying ions respectively are chemically similar, their effect on glass properties are quite different in magnitude. This series serves as an important check to any model serving to predict hardness or densification from other properties, as it breaks the strong correlations between the properties as found in the SLS series.

6.2 Comparison of Hardness Models

In this section the two models presented in the literature review attempting to account for the compositional variation of hardness, and the general correlation with elastic moduli, will be discussed in relation to the results obtained in section 5.4 and literature data for a variety of silicates (exact compositions and properties given in appendix B.)

6.2.1 Correlation with Elastic Moduli

As have been mentioned before, hardness is roughly proportional to the elastic moduli, with the best correlation found for the shear modulus, as seen in figure 6.2.1. As it can be seen, the correlation is very strong in silicates, and any model to explain

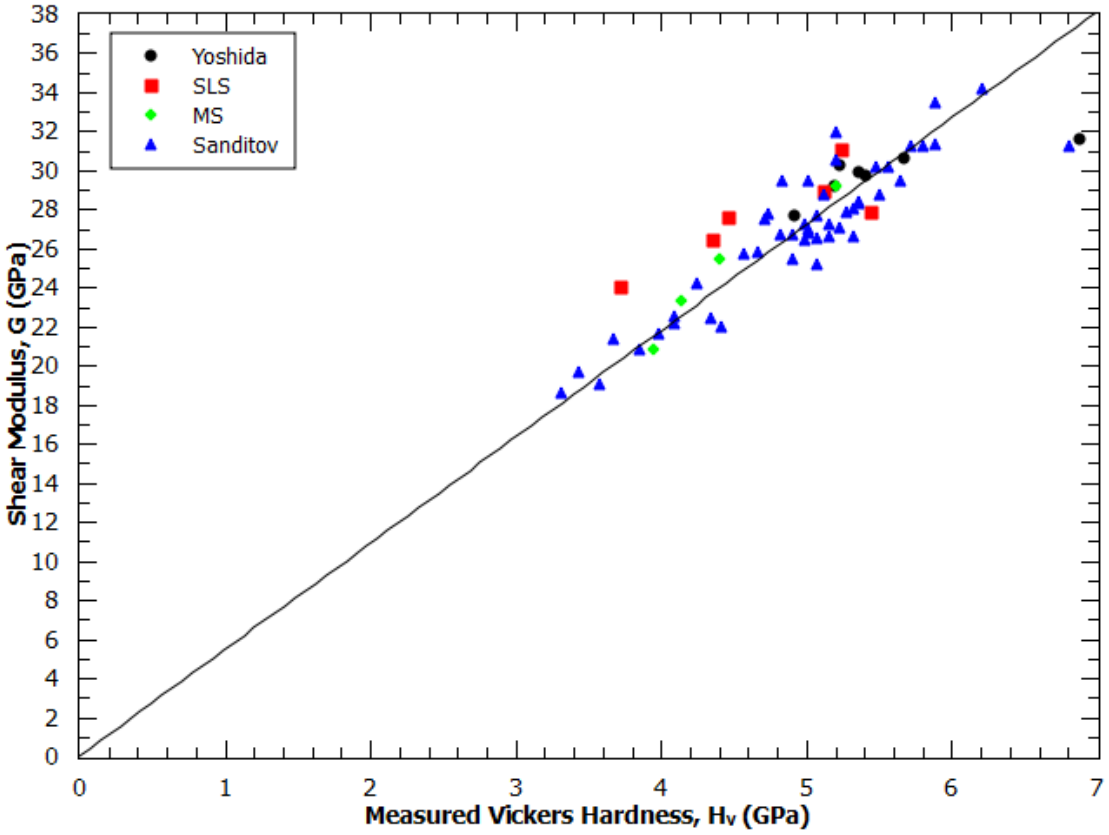

Figure 6.2.1: The measured values of shear modulus, G, against the measured Vickers Hardness, H_V, for a variety of silicate based glasses. The coefficient of determination is $R^2 = 0.748$ with intercept forced through origo.

hardness is expected to include the elastic properties somehow.

6.2.2 The Maximum Internal Pressure Model

As the free volume of a glass is difficult to evaluate, the A term in equation 6.1 will be approximated as a constant as was also done by the original authors [37]. It was seen in section 2.4 that the free volume of silicates varies between some 1% to around 3% for pure silica, giving $0.98 < A < 1.28$, which is why it is taken as

a constant of unity, and some error for high silica glasses accepted. Equation 2.11 then becomes,

$$P_m = \frac{1-2\nu}{6(1+\nu)}E \tag{6.1}$$

This equation is plotted against the measured values of hardness in figure 6.2.2. Considering that there are no empirical fitting parameters involved, and that the

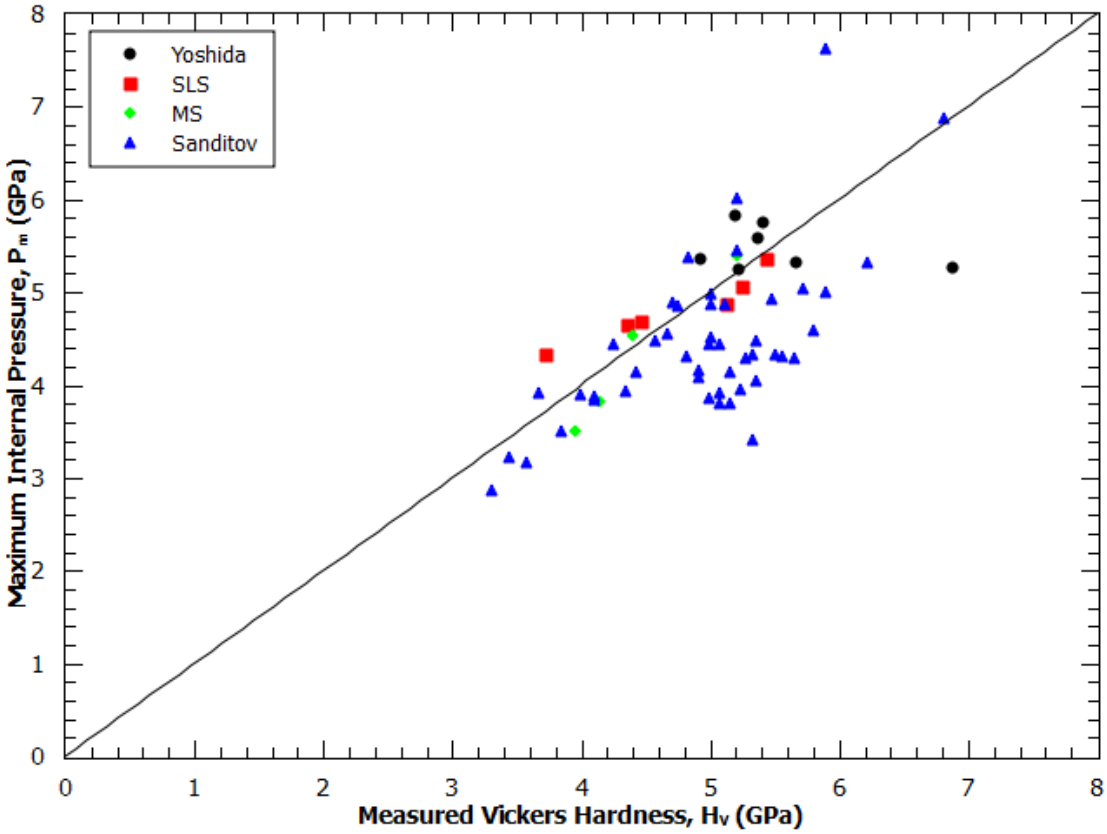

Figure 6.2.2: The calculated maximum internal pressure, P_m, (equation 6.1) using measured elastic properties against the measured values of Vickers hardness, H_V of a variety of silicate based glasses. The coefficient of determination is $R^2 = 0.386$ with intercept forced through origo.

maximum internal pressure of amorphous silica is expected to be underestimated by almost 25%, the fit is quite good with $R^2 = 0.386$, but fades in comparison to that with shear modulus shown in figure 6.2.1.

6.2.3 The Yamane & MacKenzie Model

First the proportionality constant between Vickers hardness and the total resistance, C_{YM} in equation 2.7, is determined from empirical values of elastic constants and hardness of amorphous silica. *Yamane & MacKenzie* [34] utilise $H_V = 6.38GPa$, $G = 31GPa$, $K = 35GPa$, and of course an α of unity (as per the calculation shown in appendix A,) ultimately yielding $C_{YM} = 0.19$. Vickers hardness is then calculated as,

$$H_V = 0.19\sqrt{\alpha GK} \tag{6.2}$$

It is not the aim of this work to evaluate the error introduced from the method of calculating elastic properties from composition, why the measured values are used in this calculation. As seen in figure 6.2.3 the calculated values are slightly overestimated, but generally correspond well to the measured ones with $R^2 = 0.774$. This is excellent agreement considering the inherent error involved in hardness measurement often said to be around 10%, not to mention possible systematic deviations, however the model only does slightly better than the empirical correlation to shear modulus in figure 6.2.1. A plot of the residuals relative to the measured hardness is shown in figure 6.2.4, where it can be seen that the maximum error is below 20%, and that the data by *Sanditov et al.* [37] seems to be overestimated, quite possibly due to a higher testing load (not given in the paper) and the indentation size effect.

Although not shown, the data by *Kato et al.* [9, 33] is not described well by the model, and is generally significantly overestimated. These compositions are the only ones to contain boron and alumina - elements excluded in the compositions used to develop the *Yamane & MacKenzie* model [34]. These elements change their coordination number depending on the amount of modifiying ions present, and thus the calculated average bond strength could well be thought to contain some error. But even if the data by *Kato et al.* [9, 33] is included, the fit is significantly better than the maximum internal pressure model.

Having thus determined that the *Yamame & MacKenzie* model is indeed the best predictor of indentation hardness then let us turn our attention to how well the individual resistances relate to actual measured data of the densified and plastic

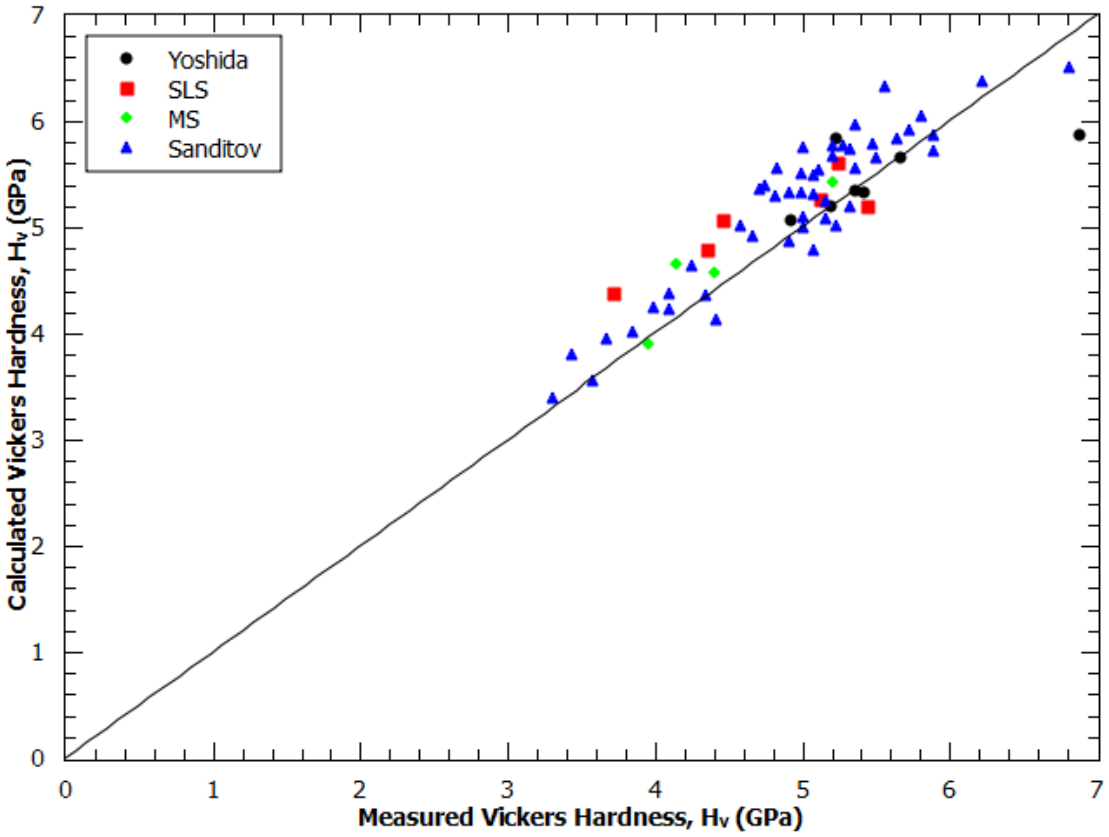

Figure 6.2.3: The calculated values of Vickers Hardness, H_V, by the *Yamane & MacKenzie* method (equation 6.2) using measured elastic properties against the measured ones for a variety of silicate based glasses. The coefficient of determination is $R^2 = 0.774$ with intercept forced through origo.

flow volumes.

6.3 Volume Recovery of Densification at Constant Load

6.3.1 Compositional Variation

In section 5.5 it was seen that the V_R decreased linearly with modifier fraction in the SLS series (from 97% to 25%), and remained relatively constant ($V_R = 80 \pm 6\%$) for the MS glasses. This is an enormous change with relatively small compositional changes for the SLS series, however the change in mechanical properties is modest, and comparable to that of the MS series. It seems that in silicates a property closely related to the modifier fraction is paramount to explaining the

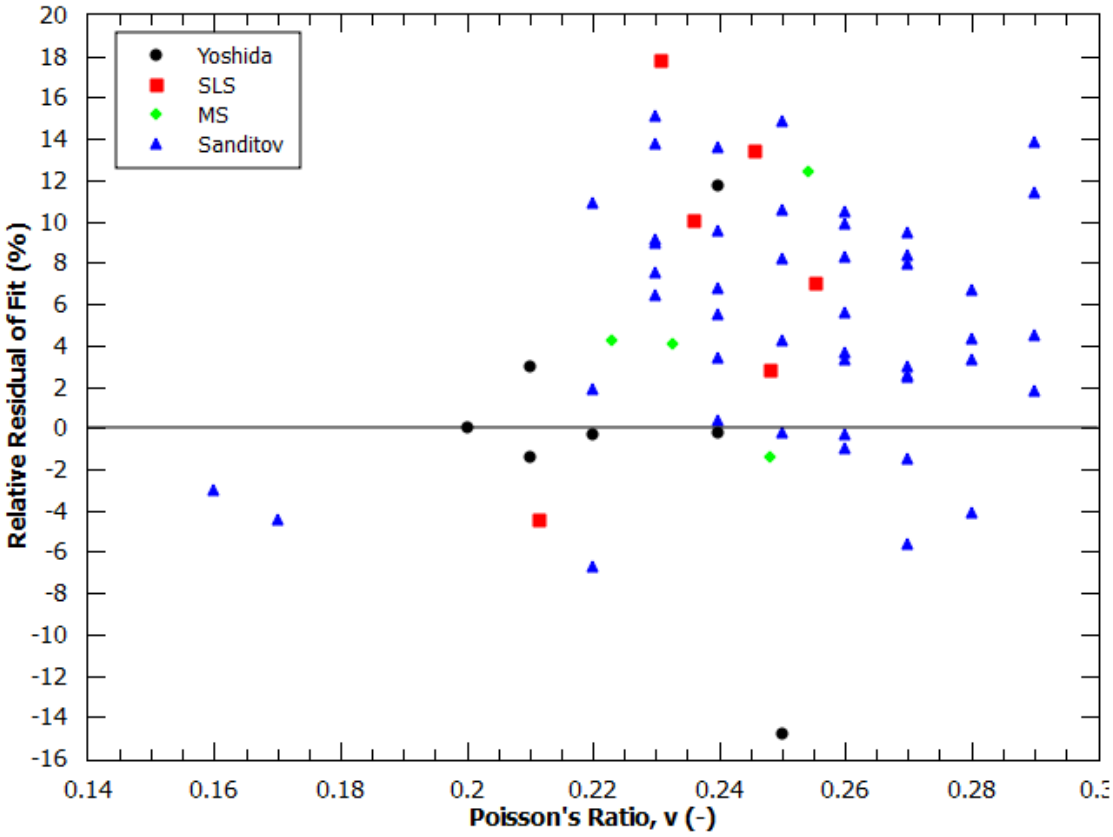

Figure 6.2.4: Residuals relative to the measured value of Vickers hardness, H_V, as a function of Poisson's ratio, ν, for the fit to the *Yamane & MacKenzie* model.

relative contribution of densification.

As for the absolute volumes, a monotonical dependence on modifier fraction is observed.

6.3.2 A Yamane & MacKenzie Approach

Densified and plastic volume are plotted against the R_D in the Yamane & MacKenzie model [34] in figure 6.3.1, Vickers hardness against R_T (mathematically equivalent to R_D) in figure 6.3.2, and finally figure 6.3.3 examines the relationship of both densified volume and hardness to R_E. See appendix A for details of the calculation and a table of the average bond strength values used in calculating R_D and R_P. It is seen that the densified volume and hardness are described well by the R_D (equal to R_T) employed in this approach. However, the plastic flow volume

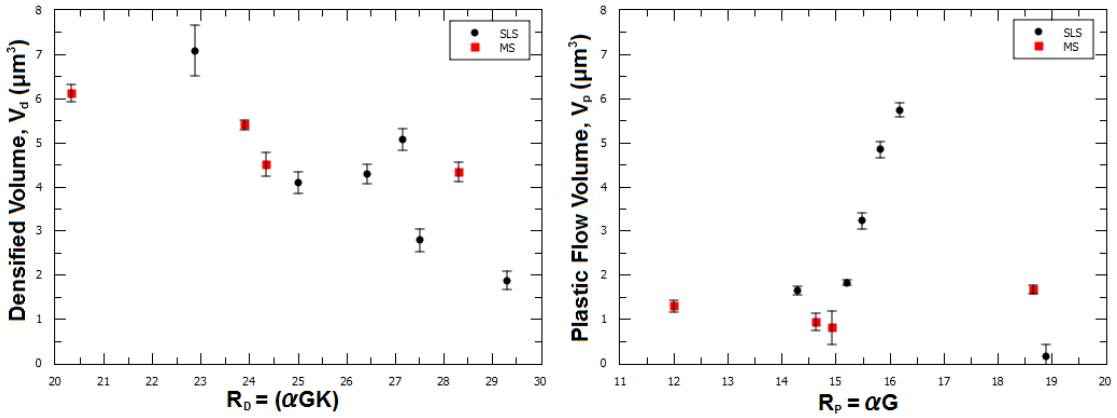

Figure 6.3.1: (a) Densified volume, V_d, as a function of $R_D = (\alpha GK)^{1/2}$ and (b) plastic flow volume, V_p, as a function of $R_P = \alpha G$. Error bars indicate ± 1 standard deviation.

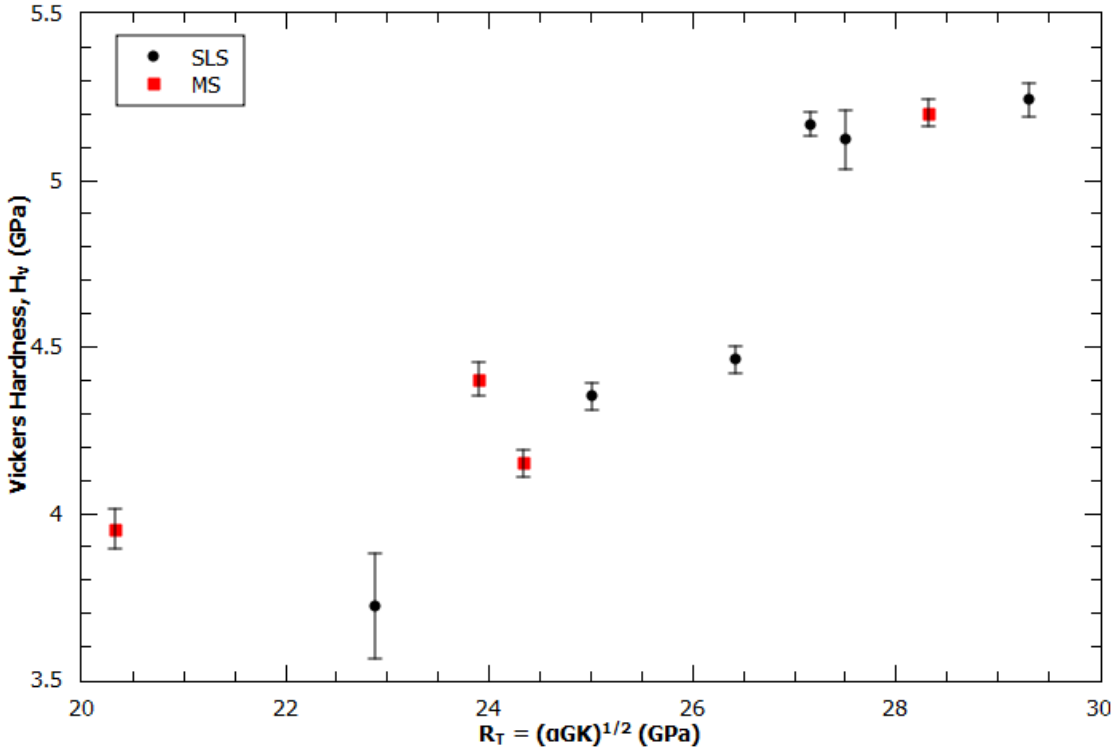

Figure 6.3.2: Vickers hardness, H_V, as a function of $R_T = (\alpha GK)^{1/2}$. Error bars indicate ± 1 standard deviation.

shows very poor correlation with the R_P used. Densified volume shows a strong correlation with R_E, and hardness less so. The applicability of the elastic resistance $R_E = K$ will not be examined in this work, but there seems room for improvement

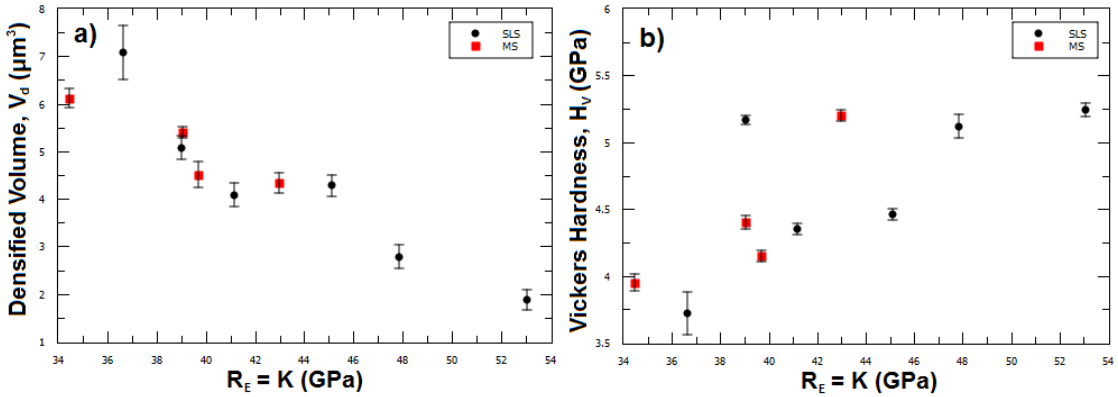

Figure 6.3.3: (a) Densified volume, V_d, and (b) Vickers hardness, H_V, as a function of $R_E = K$. Error bars indicate ± 1 standard deviation.

in regards to the other two resistances; densificative and plastic flow.

6.3.3 New Proposed Resistances

As discussed briefly in the problem statement, the influence of average bond strength on the resistances seems difficult to root in theory. Moreover, judging from figure 6.3.3, there seems to be good agreement between the densified volume and bulk modulus, and there seems no need to invoke this parameter. A non-linear fit of the type $K^{\omega}G^{1-\omega}$ (where $0 \leq \omega \leq 1$) to the densified volume was performed to elucidate if the 50/50 contribution of compression and shear assumed by *Yamane & MacKenzie* is plausible or not, and it was found that $\omega = 0$, meaning that the best descriptor of the densified volume is the bulk modulus alone. It should be noted that under a Vickers indenter approximately two-thirds of the stress distribution is hydrostatic [50]. The fit of densified volume to the proposed $R_D = K$ is shown in 6.3.4.

As for the plastic flow volume, the strongest correlation seems to be that to the modifier fraction, as was seen in figure 5.5.1. Clearly, the volume must decrease with a resistance, which is why it is taken as $R_P = n_{SiO_2}$, that is the molar silica fraction of the glass. This is also plotted in 6.3.4. The linear fit to this new R_D and R_P is significantly better than that of the *Yamane & MacKenzie* model [34] (figure 6.3.1.)

As dealt with in the literature review, the modifying ions are thought to be

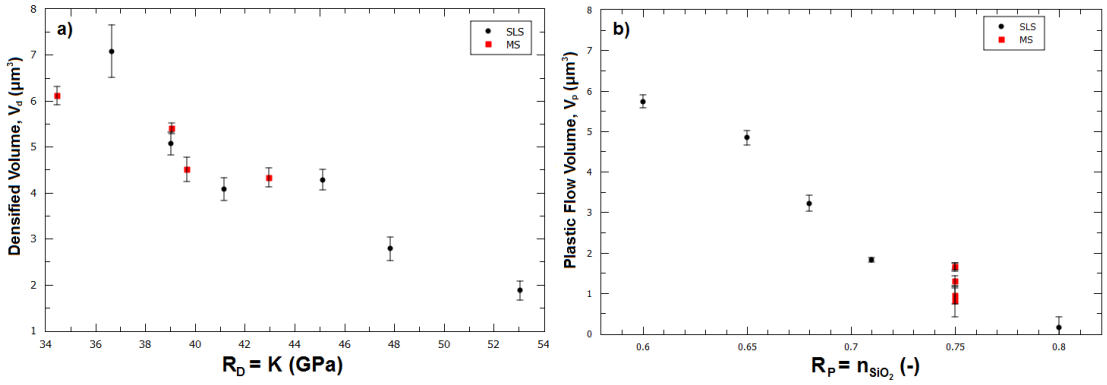

Figure 6.3.4: (a) Densified volume, V_d, plotted as a function of $R_P = K$ and (b) plastic flow volume, V_p, against $R_P = n_{SiO_2}$. The lines are obtained by linear regression on the SLS series. Error bars indicate ± 1 standard deviation.

the cause of slipping of different parts of the network during plastic flow. *Peter* [29] previously reported a threshold modifier fraction for the manifestation of plastic flow in silicate glasses during indentation. This hypothesis apparently agrees with the results here; the threshold at 25gf occuring around 20% modifier content by moles.

6.3.4 Interpretation of Proposed Resistances

The new parameter found to best describe the densificative resistance is the bulk modulus, a quantity firmly rooted in thermodynamics. It is the elastic resistance to reduction of the volume by a factor $1/e$ under uniform compression, and formally defined as,

$$K = -V\frac{\partial P}{\partial V} \tag{6.3}$$

The densified volume under indentation is obviously not elastically compressed, but has been stressed beyond some yield pressure [62], yet as elastic compression must take place before this yield pressure, as a first approximation it is thought that K does well to describe the total resistance to densification. K times V_d in theory yields the work of densification, which is interesting as an energetic interpretation of hardness has won favour since the advent of high-sensitivity load-displacement indentation equipment [38, 116, 117]. Unfortunately, it is beyond the scope of this work to evaluate whether there is a relation between this work of densification and

the work of plastic deformation seen in figure 2.3.2.

As for the resistance to plastic flow it was realised that n_{SiO2} is proportional to the average coordination number, C_{av}, in the simple silicates measured here. Using $R_P = C_{av}$ allows for use of the plastic flow resistance also for other glass forming families. A comparison of both the proposed $R_D = K$ and $R_P = C_{av}$ is shown with sodium borates as measured by *Yoshida et al.* [59] in figure 6.3.5, where coordination numbers of boron were calculated using the random-pair model of *Gupta* [118]. It is observed that the resistances describe the densified and plastic flow volume of both silicate and borate glasses well.

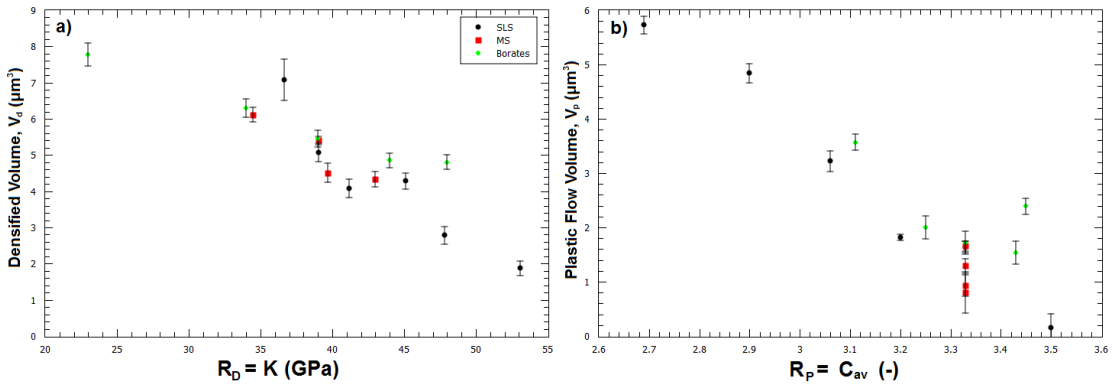

Figure 6.3.5: (a) The densified volume, V_d, plotted against $R_D = K$ and (b) the plastic flow volume, V_p, plotted against $R_P = C_{av}$ for the SLS and MS series measured under 25gf Vickers indentation in this work, and that of sodium borates glasses by *Yoshida et al.* under identical conditions. Error bars indicate ± 1 standard deviation.

It is not thought that this dependence of average coordination number is a general truth, as evidenced by metallic glasses having very large plastic flow volumes [52], but it does open for speculation into whether or not an energetic interpretation is possible. Perhaps it is the bond strength per volume of the glass forming network that is paramount, where it should be noted that the single bond strength of silica and boron is similar ($\epsilon_{Si} = 106$kcal/mol versus $\epsilon_B = 119$kcal/mol) [63]. Such an interpretation would lend itself well to the theory of hardness in crystalline solids proposed by *Gilman* [67, 68] briefly described in section 2.3.3, where hardness is found to be proportional to the so-called bond modulus, a measure of bond energy per dislocation volume.

6.3.5 Volume Ratio of Recovery

6.3.5.1 Correlation with Poisson's Ratio

The volume ratio of recovery, V_R, is calculated as the ratio of densified volume over total permanent deformation volume, as seen in equation 4.8. For this reason, it is thought to be determined by ratio of plastic flow to densificative resistance, and has previously been shown by *Yoshida et al.* [52] to decrease monotonically with Poisson's ratio in a variety of glasses, as was seen in figure 2.3.3. Thus the relationship can be described as,

$$V_R \propto \frac{R_P}{R_D} \propto \frac{1}{\nu} \tag{6.4}$$

To examine applicability of this relationship with Poisson's ratio, the measured data is plotted with that of *Yoshida et al.* [52] in figure 6.3.6. With the exception of a few outliers, an almost linear relationship emerges for the silicate compositions measured by *Yoshida et al.* [52], and indeed also for the SLS series, but their slopes are very different. Because there is relatively little change in Poisson's ratio across the SLS series, yet a large difference in V_R, the slope necessarily becomes very large. Conversely, for the MS series there is relatively little change in V_R, but rather large differences in ν (as compared to the SLS series,) and these glasses do not have a linear trend in the plot. The relation seems to capture some truth of the much more varied compositions measured by *Yoshida et al.* [52], but does little in explaining the large differences found in the simple silicates measured in this work.

6.3.5.2 Correlation with Free Volume by Helium Solubility

The relation found by *Yoshida et al.* [52] with Poisson's ratio which was examined in the previous section is thought to be due to differences in free volume of the glasses. For this reason a more direct measure of the free volume, namely the helium solubility, was employed to see how this parameter correlates with Poisson's ratio and space ratio, and also if it has any explanatory power over the volume recovery of densification. Poisson's ratio and ionic volume fraction as a function of the measured Ostwald solubility are shown in figure 6.3.7.

As low values of Poisson's ratio means an open structure of the material, free

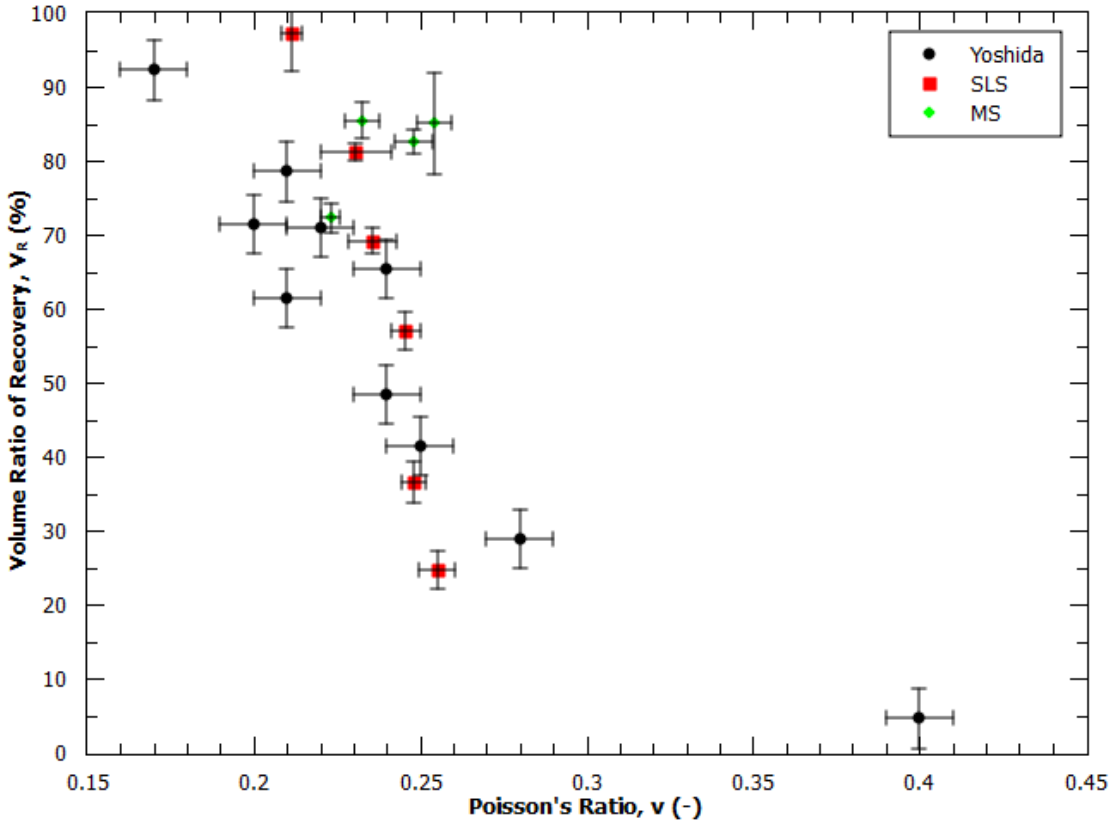

Figure 6.3.6: The volume ratio of recovery, V_R, as a function of inverse Poisson's ratio, $1/\nu$, of 25gf Vickers indents on the SLS and MS series of this work, and 50gf indents on various silicates and a oxy-nitride glass, 10gf on amorphous silica, and finally 20gf on a bulk metallic glass measured by *Yoshida et al.* (data found in appendix B.) Error bars indicate ± 1 standard deviation.

volume should be inversely related to it, which fits quite well with the data in figure 6.3.7a. Although the trend is not quite monotonic, these two measures of free volume seem to be strongly correlated. However, this cannot be said for the space ratio show in figure 6.3.7b. This should have a positive correlation with free volume, yet no such thing is found. Moreover, comparing the space ratios in table 5.8.1 to that of amorphous silica ($C_{av} = 54.4\%$ [52,86]) that of the NaBa composition ($C_{av} = 56.2\%$) is higher. It is indeed difficult to imagine a silicate glass with higher free volume than pure amorphous silica [86], which is why the space ratio calculation of the free volume is not thought to be accurate, as previously suspected by *Doremus* [87].

It was seen in figure 6.3.7 that the measured Ostwald solubility of helium

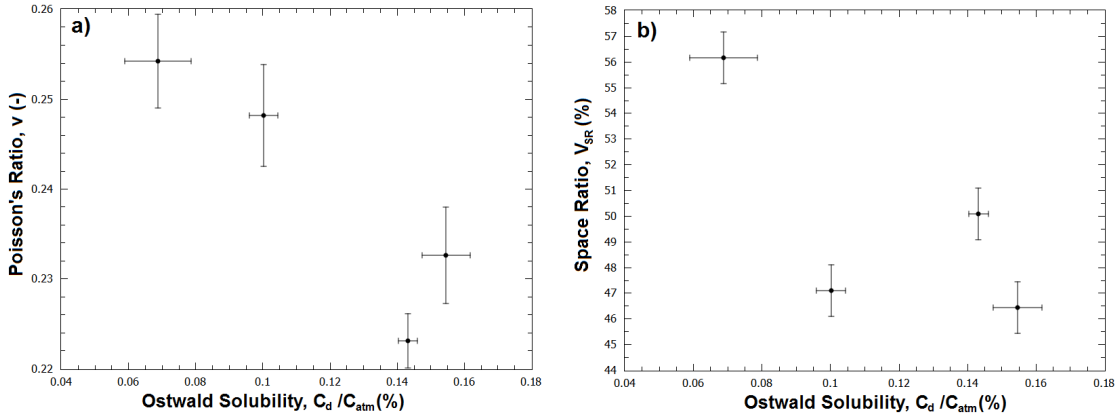

Figure 6.3.7: (a) Poisson's ratio, ν, and (b) space ratio, V_{SR}, as a function of the measured Ostwald helium solubilities. Error bars indicate ± 1 standard deviation. The error in space ratio is taken to be 1%.

decreased almost monotonically with Poisson's ratio within the MS series. Given that this is the case, equation 6.4 can be modified to become,

$$V_R \propto \frac{1}{\nu} \propto \frac{C_d}{C_{atm}} \tag{6.5}$$

This implies that the relation with Poisson's ratio is fundamentally caused by a difference in free volume. If the helium solubility is a more correct measure of the free volume than Poisson's ratio, it would be expected that the V_R values of the MS series increase monotonically with the measured Ostwald solubilities. As seen in figure 6.3.8, this is hardly the case. The NaBa and KCa compositions have similar V_R's around 85%, yet very different Ostwald helium solubilities, while KCa and NaCa have similar solubilities, but very different values of V_R. Even accepting a possible outlier, the slope should be positive, not negative. Clearly, there is no correlation between the measured helium solubilities and volume recovery of densification.

6.3.5.3 Relative Resistances

If the ratio of resistances as in equation 6.4 - $R_D = K$ and $R_P = n_{SiO_2}$ - is plotted (figure 6.3.9,) the data points almost collapse onto a single line within the standard deviation. This is as expected if the individual resistances describe the measured deformation volumes well.

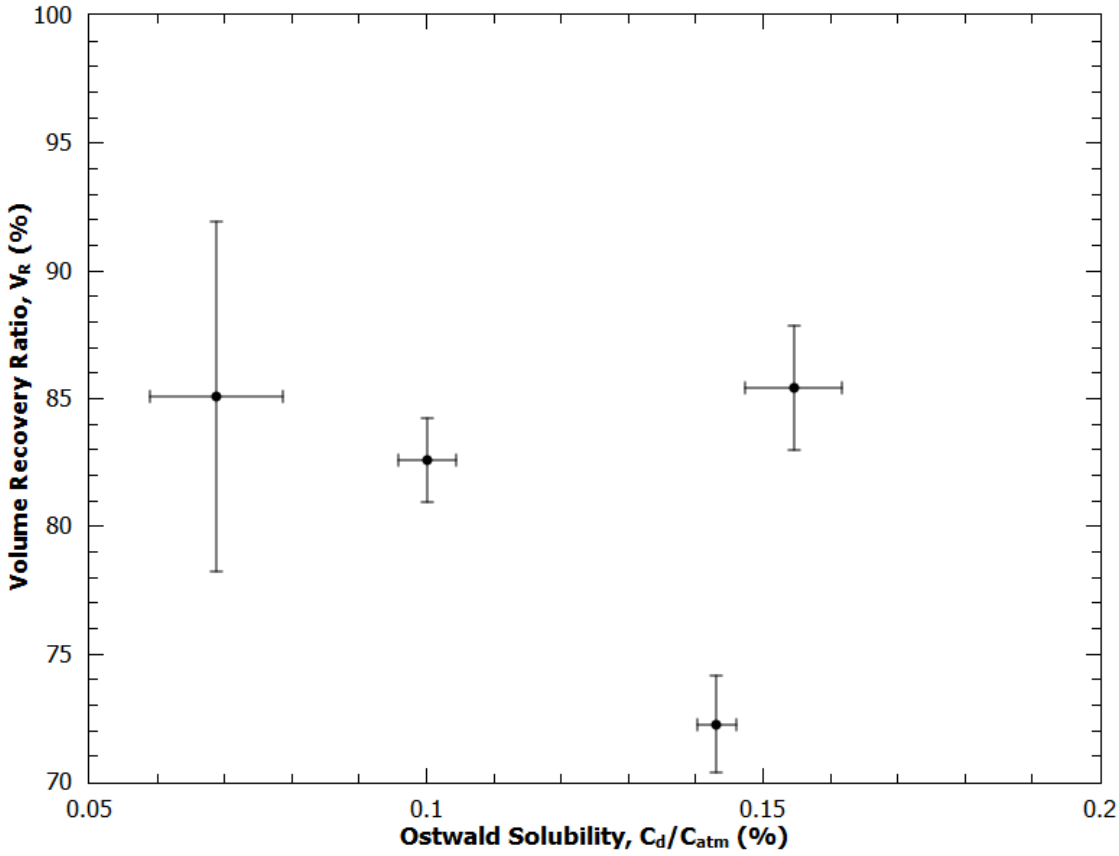

Figure 6.3.8: The volume ratio of recovery, V_R, plotted against the Ostwald helium solubility, C_d/C_{atm}. Error bars indicate ± 1 standard deviation.

6.4 An Improved Hardness Model

It immediately seems that the success of the *Yamane & MacKenzie* model is due to it capturing both the strong relation between hardness and shear modulus, and also that of densified volume and bulk modulus. However, it seems to fail to account very well for the plastic deformation, as seen in figure 6.3.1. The compositions used to develop the model generally contain rather low amounts of modifying ions, thought to correspond to high values of V_R, as per figure 5.5.2. Although the calculated hardness corresponds well to the measured one for a wide variety of glasses (and modifier fractions) as was seen in figure 6.2.4, it is thought that there is room for improvement given the much better fits obtained for densified and plastic flow volumes to the new resistances.

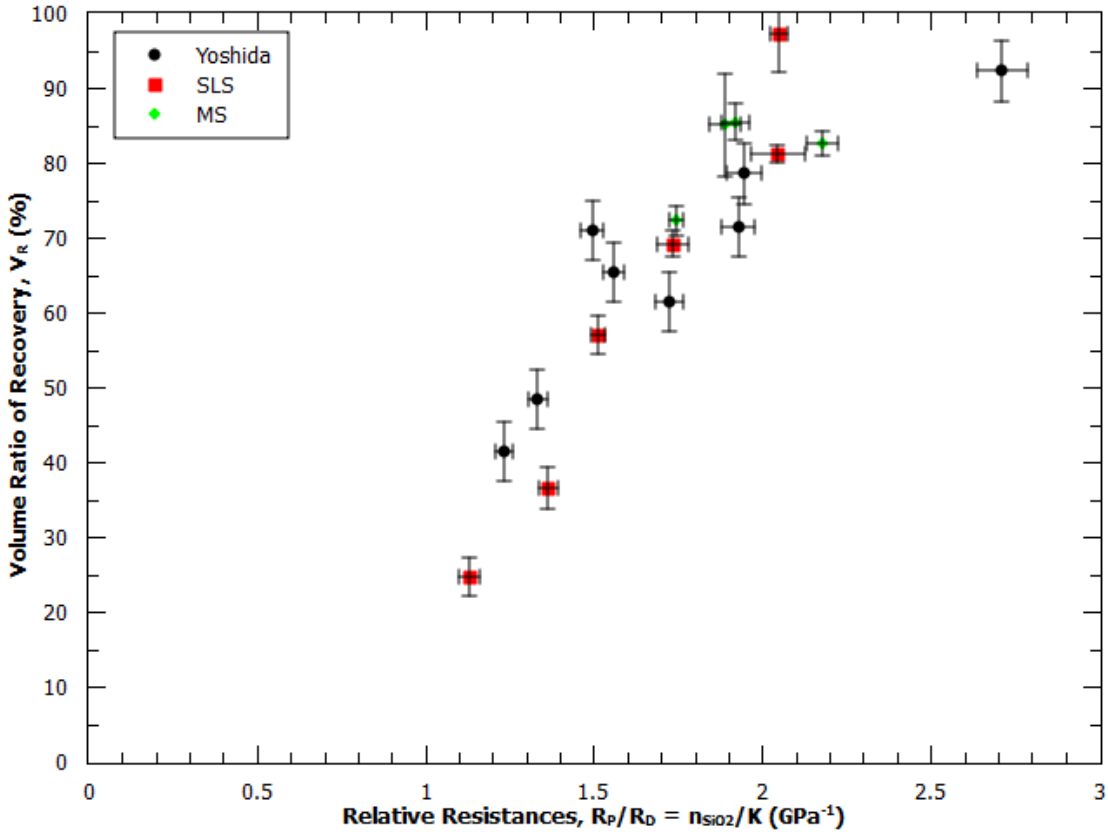

Figure 6.3.9: The volume ratio of recovery, V_R, as a function of the ratio of resistance to plastic flow ($R_P = n_{SiO_2}$) and densification ($R_D = K$) of 25gf Vickers indents on the SLS and MS series of this work, and 50gf indents on various silicates and a oxy-nitride glass, 10gf on amorphous silica, and finally 20gf on a bulk metallic glass measured by *Yoshida et al.* (data found in appendix B.) Error bars indicate ± 1 standard deviation.

Relating hardness to the resistances has been carried out through evaluation of a total resistance proportional to hardness;

$$H_V = C_P \cdot R_T \tag{6.6}$$

where C_P is a proportionality constant. Using the resistances, $R_D = K$, and $R_P = n_{SiO_2}$, found by measuring deformation volumes in section 6.3.3, and the assumption of $R_E = K$, a variety of combinations of the resistances have been attempted, such as given in table 6.4.1.

By far the best of these models is the square root of the three resistances

Table 6.4.1: The models attempted to predict the total resistance, R_T, which should be proportional to hardness.

Connection	Total resistance, R_T
Parallel	$1/R_D + 1/R_P$
Serial	$R_E + R_D + R_P$
Serial-parallel	$R_E/R_D + R_E/R_P$
Weighted contribution	$R_D^{\omega} R_P^{1-\omega}$
Geometrical mean	$(R_E R_D R_P)^{1/3}$
Square root	$\sqrt{R_E R_D R_P}$

multiplied, giving $R_T = \sqrt{n_{SiO_2} K^2}$, which resembles that of *Yamane & MacKenzie* [34] ($R_T = \sqrt{\alpha G K}$.). The proportionality constant in equation 6.6 is found by linear regression, and the new model then becomes,

$$H_V = C_P \cdot R_T = 7.42 \cdot \sqrt{R_E R_D R_P} \tag{6.7}$$

This relation has a coefficient of determination is $R^2 = 0.482$ and is plotted in figure 6.4.1.

It can be seen in figure 6.4.1 that the hardnesses of a few compositions are underpredicted rather severely. This is examined further in the plot of relative residuals in figure 6.4.2, where an apparent systematic error with Poisson's ratio is seen.

Despite having excellent correlation between the resistances and measured deformation volumes the new model performs poorly both in regards to the *Yamane & MacKenzie* model [34], and the empirical correlation to shear modulus. Two possible reasons are considered: Possibly the assumed elastic resistance of $R_E = K$ is incorrect, and effects the total resistance appreciably. In this case further studies with load-displacement indentation equipment and measurement of the work of elastic deformation may yield the true elastic resistance. On the other hand, the hypothesis that deformation volumes determine hardness might be incorrect, in which case it is thought that an energy-based approach could provide a route to better prediction of hardness from composition.

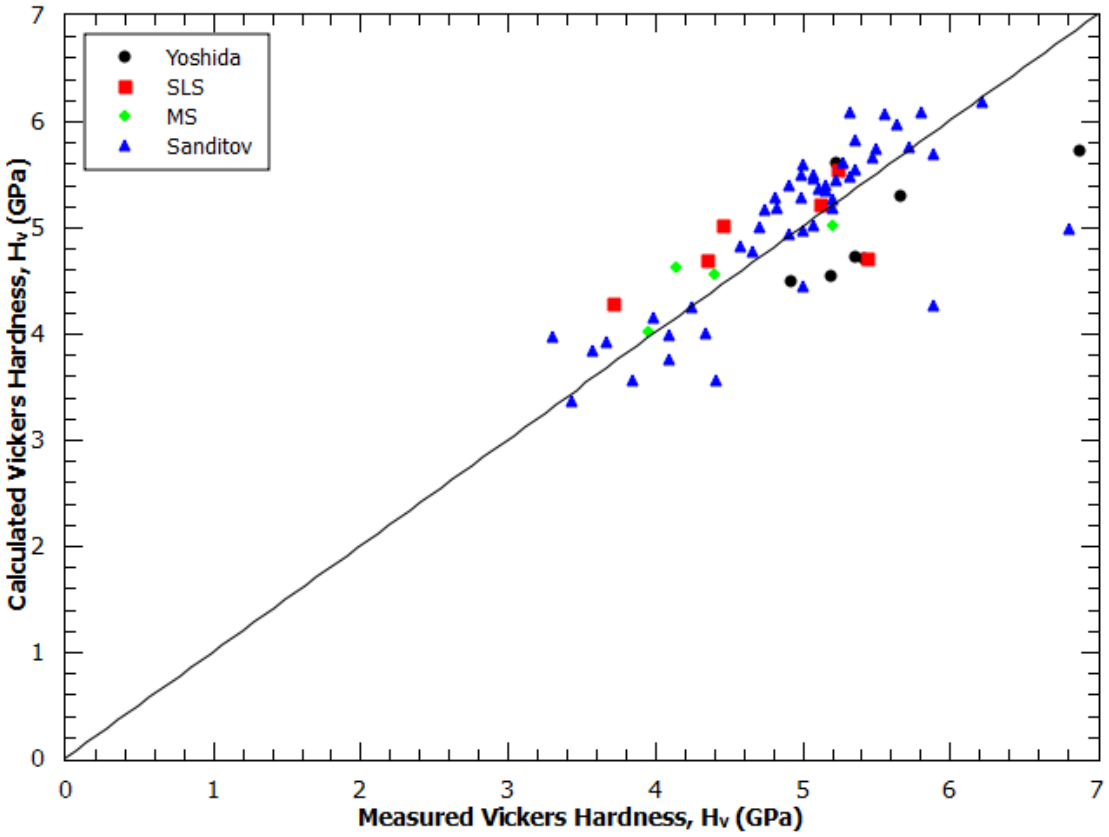

Figure 6.4.1: Calculated Vickers hardness, H_V, using the new model (equation 6.7) plotted against the measured values for a variety of silicate-based glasses.

6.5 Crack Resistance and Load Dependence of Densification

As mentioned in the results section only the data for KCa, NaCa, and the $80SiO_2$ compositions will be discussed. The volume recovery ratio data that will be used are replotted in figure 6.5.1 for clarity.

The residual stress at the load for crack initiation will be calculated from equation 2.19. *Kato et al.* calculates the change in plastic flow volume as the post-annealing volume of the indentation, approximated by the post-annealing depth and assuming a pyramidal shape,

$$\Delta V_{pz,d} = \frac{1}{3} \cdot S \cdot D_a = \frac{1}{6} L_{ci}^2 \cdot D_a \tag{6.8}$$

where $\Delta V_{pz,d}$ is the plastic deformation volume as determined by depth, and S

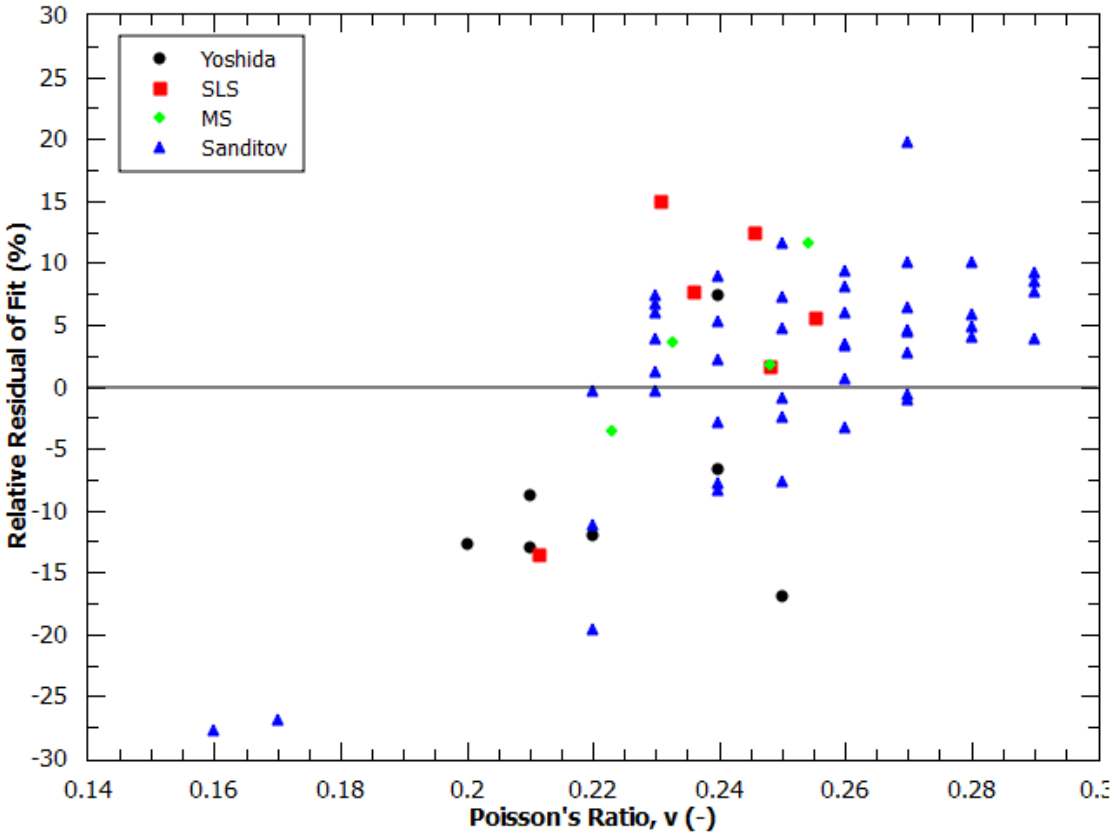

Figure 6.4.2: Residuals relative to the measured value of Vickers hardness, H_V, as a function of Poisson's ratio, ν, for the fit to the new model. The coefficient of determination is $R^2 = 0.482$ with the intercept forced through origo.

the projected area of the Vickers indentation. A more accurate method would be to merely use the plastic flow volume, V_p, as determined directly by AFM as the change in plastic zone volume. It turns out that the volumes, and hence the calculated residual stresses by using equations 2.19, 2.20, and 6.8 or $\Delta V_{pz} = V_p$ are very different. Although containing larger error, and not enabling comparison with previous data, it is thought to be more correct to use the plastic flow volumes to calculate the residual stress at the load for crack initiation. *Lawn et al.* [104] and *Kato et al.* [33,61] both attempt to estimate this quantity indirectly, but in this work it is measured exactly, given only that the densified volume is completely recovered in the method employed, as proven previously by *Yoshida et al.* [57].

Kato et al. [33] argue that the residual stress increases logarithmically with

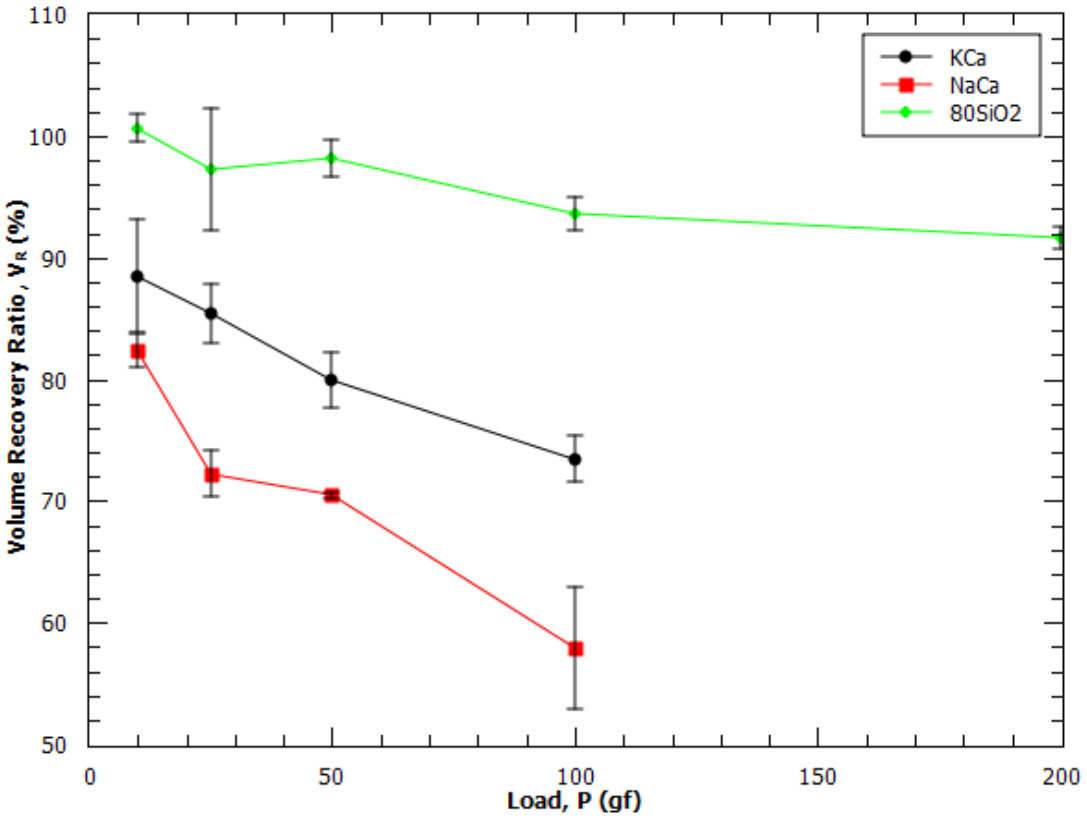

Figure 6.5.1: The volume ratio of recovery, V_R, as a function of indentation load, P, of the NaCa, KCa, and 80SiO$_2$ compositions. Error bars indicate ± 1 standard deviation.

load. Despite the relatively few data points (*Kato et al.* tested six loads spanning from 5gf to 200gf [33]) and error involved this seems reasonable judging from figure 6.5.2a. The data is fitted as,

$$\sigma_{rs} = a \log P + b \tag{6.9}$$

where a is the slope and b the intercept. This logarithmic fit is shown in figure 6.5.2b. Regression parameters and calculated residual stresses at the load for crack initiation determined in section 5.7, σ_{CR}, can be found in table 6.5.1.

As seen in table 6.5.1, the calculated values of the residual stress at the load for crack initiation, σ_{CR}, fall in the range of 110MPa to 470MPa, a rather large relative difference, even considering the considerable error involved.

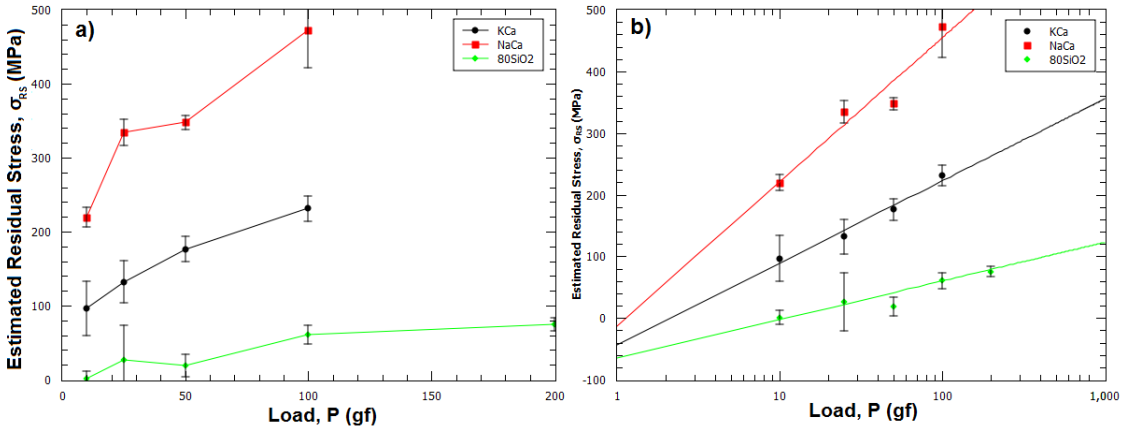

Figure 6.5.2: Calculated residual stress, σ_{rs}, by using the plastic flow volume, V_p.

Table 6.5.1: Regression parameters from application of equation 6.9, the measured crack resistance, CR, and the predicted residual stress at the load for crack initiation, σ_{CR}. Errors are given as the standard deviations of the data.

Composition	Slope, A	Intercept, B	R^2	CR [gf]	σ_{CR} [MPa]
KCa	130 ± 20	-40 ± 30	0.838	97 ± 22	220 ± 50
NaCa	230 ± 30	-10 ± 40	0.874	112 ± 13	470 ± 70
$80SiO_2$	60 ± 10	-70 ± 20	0.567	736 ± 264	110 ± 40

The scale of the values calculated are approximately a factor of 5 smaller than those calculated by *Kato et al.* [33, 61] using the post-annealing indentation depth and equation 6.8. If this method is employed values in the range of 1.3GPa to 1.7GPa (±0.1GPa) are found, which are rather close to those of 1.7GPa to 1.9GPa given by these authors, yet not similar enough to conclude a single value with this method either. The results presented in this section challenges the hypothesis stated by *Kato et al.* [33] that the residual stress at the load for crack initiation is a constant within the silicate system. Given this state of affair, it seems necessary to undertake further studies into the meaning of these residual stress values, e.g. the compositional variation or evaluation of the stress distribution.

7. CONCLUSION & PROSPECTS

It was shown that the method of measuring indentation and pile-up volumes before and after annealing at $0.9 \times T_g$ (K) can accurately determine the densified and plastic flow volumes occuring under sharp indentation of glass. The densified volume decreases linearly with the bulk modulus, the elastic resistance to isotropic compression, both in silicates and sodium borates. The plastic flow volume however has no relation to elastic properties, instead being determined by the modifier fraction in the silicate composition, and is insensitive to the specific modifying ions within the sodium, potassium, calcium, and barium containing compositions tested. For indentations made at 25gf the threshold modifier fraction for the emergence of plastic flow is close to 20% by moles. It is possible that the plastic flow volume is related to the average coordination number of the glass forming species, as the data for silicates and borates appear very similar in this interpretation. The hypothesis of free volume determining the relative densification magnitude by *Yoshida et al.* [52, 62] was disproven, instead the ratio of the above mentioned densificative and plastic flow resistances can explain these results.

Despite the success in explaining the compositional dependence of the densified and plastic flow volumes, it has not been possible to develop an improved model for prediction on hardness based on these relations. It is thought that hardness is determined mainly from the elastic properties, as most of the work of indentation occurs as elastic deformation, and that also the densificative part of the permanent deformation depends strongly on the bulk modulus. To accurately predict hardness from composition it will be necessary to investigate the elastic deformation in detail.

It was concluded that a single stress for crack initiation for silicate glasses does not exist. The values found span from 110-470MPa ($\pm$70MPa,) however given the limited amount of data it is not known what extent of spread can be expected. More research is needed to find the origin of this difference, which could originate in actual differences in intrinsic strength or the stress distribution under the indent.

Some predictions can be made given the results obtained for the compositional

dependence of densification and plastic flow. In the brittleness proposed by *Lawn & Marshall* [99] the ratio of hardness to fracture toughness determines when fracture occurs, yet *Kato et al.* [9, 33, 61] instead concludes that the plastic flow induced residual stress is paramount. These requirements - low hardness and plastic flow - transcribe into low elastic constants and high glass former content as per the results in this work. Indeed the most crack resistant glasses developed so far fit these criteria. These are based on amorphous silica (which is highly crack resistant under moisture-free conditions [7].) Small amounts of modifiers which reduce elastic properties are added (up to around 20%, the threshold for emergence of plastic flow mentioned above,) and in some cases with alumina to negate their depolymerising effect [8, 95].

BIBLIOGRAPHY

[1] W. E. Taylor, "Plastic Deformation of Optical Glass," *Nature*, vol. 163, p. 323, 1949.

[2] J. E. Neely and J. D. Mackenzie, "Hardness and low-temperature deformation of silica glass," *Journal of Materials Science*, vol. 3, pp. 603–609, Nov. 1968.

[3] V. Lehouerou, "Surface damage of soda-lime-silica glasses: indentation scratch behavior," *Journal of Non-Crystalline Solids*, vol. 316, pp. 54–63, Feb. 2003.

[4] T. E. Wilantewicz and J. Varner, "A recording microindentation instrument for in situ study of crack initiation in glass," *Journal of Materials Science*, vol. 42, no. 20, pp. 8529–8536, 2007.

[5] P. Sellappan, A. Sharafat, V. Keryvin, P. Houizot, T. Rouxel, J. Grins, and S. Esmaeilzadeh, "Elastic properties and surface damage resistance of nitrogen-rich (Ca,Sr)SiON glasses," *Journal of Non-Crystalline Solids*, vol. 356, pp. 2120–2126, Sept. 2010.

[6] J. Sehgal and S. Ito, "Brittleness of glass," *Journal of Non-Crystalline Solids*, vol. 253, pp. 126–132, 1999.

[7] T. M. Gross and M. Tomozawa, "Crack-free high load Vickers indentation of silica glass," *Journal of Non-Crystalline Solids*, vol. 354, pp. 5567–5569, Dec. 2008.

[8] T. M. Gross, M. Tomozawa, and A. Koike, "A glass with high crack initiation load: Role of fictive temperature-independent mechanical properties," *Journal of Non-Crystalline Solids*, vol. 355, no. 9, pp. 563–568, 2009.

[9] Y. Kato, H. Yamazaki, Y. Kubo, and S. Yoshida, "Effect of B2O3 content on crack initiation under Vickers indentation test," *Journal Of The Ceramic Society Of Japan*, vol. 118, no. 9, pp. 792–798, 2010.

[10] S. Deriano, A. Jarry, T. Rouxel, J. Sangleboeuf, and S. Hampshire, "The indentation fracture toughness (K_C) and its parameters: the case of silica-rich glasses," *Journal of Non-Crystalline Solids*, vol. 344, pp. 44–50, Sept. 2004.

[11] J. Sehgal, Y. Nakao, H. Takahashi, and S. Ito, "Brittleness of glasses by indentation," *Journal of Materials Science Letters*, vol. 14, no. 3, pp. 167–169, 1995.

[12] R. J. Hand and D. R. Tadjiev, "Mechanical properties of silicate glasses as a function of composition," *Journal of Non-Crystalline Solids*, vol. 356, no. 44-49, pp. 2417–2423, 2010.

[13] S. Yoshida, A. Hidaka, and J. Matsuoka, "Crack initiation behavior of sodium aluminosilicate glasses," *Journal of Non-Crystalline Solids*, vol. 344, no. 1-2, pp. 37–43, 2004.

[14] F. Cleymand and S. Testu, "Statistical investigation of the influence of maximum shear stresses induced by thermal treatments on fracture toughness of soda-lime silica glasses: Comparison between Hertzian and Vickers indentations," *Glass Physics and Chemistry*, vol. 35, pp. 369–377, Sept. 2009.

[15] R. J. Anton and G. Subhash, "Dynamic Vickers indentation of brittle materials," *Wear*, vol. 239, pp. 27–35, Apr. 2000.

[16] E. Le Bourhis, "Indentation response of glass with temperature," *Journal of Non-Crystalline Solids*, vol. 316, pp. 153–159, Feb. 2003.

[17] A. Arora, D. B. Marshall, B. R. Lawn, and M. V. Swain, "Indentation Deformation/Fracture of Normal and Anomalous Glasses," *Journal of Non-Crystalline Solids*, vol. 31, pp. 415–428, June 1979.

[18] W. C. Oliver and G. M. Pharr, "An improved technique for determining hardness and elastic modulus using load and displacement sensing indentation experiments," *Journal of Materials Research*, vol. 7, no. 6, pp. 1564–1583, 1992.

[19] G. Pharr, W. C. Oliver, and F. Brotzen, "On the generality of the relationship among contact stiffness, contact area, and elastic modulus during indentation," *Journal of Materials Research*, vol. 7, pp. 613–617, Jan. 1992.

[20] G. Pharr, "Measurement of mechanical properties by ultra-low load indentation," *Materials Science and Engineering A*, vol. 253, pp. 151–159, Sept. 1998.

[21] J. A. Howell, J. R. Hellmann, and C. L. Muhlstein, "Nanomechanical properties of commercial float glass," *Journal of Non-Crystalline Solids*, vol. 354, pp. 1891–1899, 2008.

[22] J. A. Howell, J. R. Hellmann, and C. L. Muhlstein, "Correlations between free volume and pile-up behavior in nanoindentation reference glasses," *Materials Letters*, vol. 62, pp. 2140 – 2142, 2008.

[23] A. K. Varshneya and D. J. Mauro, "Microhardness, indentation toughness, elasticity, plasticity, and brittleness of Ge-Sb-Se chalcogenide glasses," *Journal of Non-Crystalline Solids*, vol. 353, pp. 1291–1297, 2007.

[24] F. Lofaj and P. Hvizdos, "Indentation moduli and microhardness of RE-Si-Mg-O-N glasses (RE = Sc, Y, La, Sm, Yb and Lu) with different nitrogen content," *Materials Science*, vol. 357, pp. 181–187, 2003.

[25] A. Chorfa, M. A. Madjoubi, M. Hamidouche, N. Bouras, J. Rubio, and F. Rubio, "Glass Hardness and Elastic Modulus Determination by Nanoindentation Using Displacement and Energy Methods," *Ceramics - Silikáty*, vol. 54, no. 3, pp. 225–234, 2010.

[26] W. H. Li, K. Shin, C. G. Lee, B. C. Wei, and T. H. Zhang, "Simple phenomenological determination of contact stiffness and elastic modulus of Ce-based bulk metallic glasses through nanoindentation," *Applied Physics Letters*, vol. 90, no. 17, p. 171928, 2007.

[27] K. Kese, M. Tehler, and B. Bergman, "Contact residual stress relaxation in soda-lime glass Part I. Measurement using nanoindentation," *Journal of the European Ceramic Society*, vol. 26, no. 6, pp. 1003–1011, 2006.

[28] F. M. Ernsberger, "Mechanical Properties of Glass," *Journal of Non-Crystalline Solids*, vol. 25, pp. 293–321, 1977.

[29] K. Peter, "Densification and flow phenomena of glass in indentation experiments," *Journal of Non-Crystalline Solids*, vol. 5, pp. 103–115, Nov. 1970.

[30] R. H. Doremus, *Glass Science*. New York: Wiley, 1973.

[31] D. M. Marsh, "Plastic Flow and Fracture of Glass," *Proceedings of the Royal Society A: Mathematical, Physical and Engineering Sciences*, vol. 282, pp. 33–43, Oct. 1964.

[32] J. E. Shelby, *Introduction To Glass Science and Technology*. Cambridge: The Royal Society of Chemistry, 2nd ed., 2005.

[33] Y. Kato, H. Yamazaki, S. Yoshida, and J. Matsuoka, "Effect of densification on crack initiation under Vickers indentation test," *Journal of Non-Crystalline Solids*, vol. 356, pp. 1768–1773, Aug. 2010.

[34] M. Yamane and J. D. Mackenzie, "Vicker's Hardness of Glass," *Journal of Non-Crystalline Solids*, vol. 15, pp. 153–164, 1974.

[35] K. Park, "Master Thesis, University of California, Los Angeles, California," 1973.

[36] K. Sangwal, "Review: Indentation size effect, indentation cracks and microhardness measurement of brittle crystalline solids - some basic concepts and trends," *Crystal Research and Technology*, vol. 44, no. 10, pp. 1019 – 1037, 2009.

[37] D. S. Sanditov, F. J. Baltá Calleja, and V. P. Privalko, "Review: the microhardness of non-crystalline materials," *Journal of Materials Science*, vol. 7, pp. 4507 – 4516, 2002.

[38] S. Yoshida, H. Sawasato, M. Yoshikawa, and J. Matsuoka, "Energy-based hardness of soda-lime silicate glass," *International Journal of Materials Research*, vol. 99, no. 08, pp. 865–870, 2008.

[39] H. Ji, V. Keryvin, T. Rouxel, and T. Hammouda, "Densification of window glass under very high pressure and its relevance to Vickers indentation," *Scripta Materialia*, vol. 55, pp. 1159–1162, Dec. 2006.

[40] Y. Cheng, "Scaling, dimensional analysis, and indentation measurements," *Materials Science and Engineering: R: Reports*, vol. 44, pp. 91–149, Aug. 2004.

[41] S. J. Bull, T. F. Page, and E. H. Yoffe, "An explanation of the indentation size effect in ceramics," *Philosophical Magazine Letters*, vol. 59, no. 6, pp. 281–288, 1989.

[42] J. Quinn and G. Quinn, "Indentation brittleness of ceramics: a fresh approach," *Journal of Materials Science*, vol. 32, p. 4331, 1997.

[43] H. Li and R. C. Bradt, "The indentation load/size effect and the measurement of the hardness of vitreous silica," *Journal of Non-Crystalline Solids*, vol. 146, pp. 197–212, 1992.

[44] J. Antunes, L. Menezes, and J. Fernandes, "Influence of Vickers tip imperfection on depth sensing indentation tests," *International Journal of Solids and Structures*, vol. 44, pp. 2732–2747, May 2007.

[45] C. Pelletier, E. Dekkers, L. Govaert, J. Dentoonder, and H. Meijer, "The influence of indenter-surface misalignment on the results of instrumented indentation tests," *Polymer Testing*, vol. 26, pp. 949–959, Oct. 2007.

[46] H. A. El-Batal and N. A. Gnoheim, "Microindentation Hardness of Cabal Glasses: Part 1 - Cabal Glasses," *Glass and Ceramic Bulletin*, vol. 24, no. 2, pp. 48–59, 1977.

[47] A. Makishima and J. D. Mackenzie, "Direct Calculation of Young's Modulus of Glass," *Journal of Non-Crystalline Solids*, vol. 12, pp. 35–45, 1973.

[48] A. Makishima and J. D. Mackenzie, "Calculation of Bulk Modulus, Shear Modulus and Poisson's Ratio of Glass," *Journal of Non-Crystalline Solids*, vol. 17, pp. 147–157, 1975.

[49] S. Inaba, S. Fujino, and K. Morinaga, "Youngs Modulus and Compositional Parameters of Oxide Glasses," *Journal of the American Ceramic Society*, vol. 82, no. 12, pp. 3501–3507, 1999.

[50] D. Tabor, *The Hardness of Metals*. New York: Oxford C. Press, 1951.

[51] R. Hill, *Mathematical Theory of Plasticity*. London: Clarendon Press, 1950.

[52] S. Yoshida, J. Sangleboeuf, and T. Rouxel, "Quantitative evaluation of indentation-induced densification in glass," *Journal of Materials Research*, vol. 20, no. 12, pp. 3404–3412, 2005.

[53] T. Rouxel, H. Ji, J. P. Guin, F. Augereau, and B. Ruffle, "Indentation deformation mechanism in glass: Densification versus shear flow," *Journal of Applied Physics*, vol. 107, no. 9, p. 094903, 2010.

[54] F. Gao, "Hardness estimation of complex oxide materials," *Physical Review B*, vol. 69, pp. 1–6, Mar. 2004.

[55] K. Suzuki, Y. Benino, T. Fujiwara, and T. Komatsu, "Densification Energy during Nanoindentation of Silica Glass," *Journal of the American Ceramic Society*, vol. 85, p. 3102, 2002.

[56] J. D. Mackenzie, "High-Pressure Effects on Oxide Glasses: I, Densification in Rigid State," *Journal of the American Ceramic Society*, vol. 46, no. 10, pp. 461–470, 1963.

[57] S. Yoshida, S. Isono, J. Matsuoka, and N. Soga, "Shrinkage Behaviour of Knoop Indentations in Silica and Soda-Lime-Silica Glasses," *Journal of the American Ceramic Society*, vol. 84, no. 9, p. 2141, 2001.

[58] J. D. Mackenzie, "High-pressure effects on oxide glass: II. Subsequent heat treatment.," *Journal of the American Ceramic Society*, vol. 46, p. 470, 1963.

[59] S. Yoshida, Y. Hayashi, A. Konno, T. Sugawara, Y. Miura, and J. Matsuoka, "Indentation induced densification of sodium borate glasses," *Physical Chemistry of Glasses: European Journal of Glass Science and Technolology B*, vol. 50, no. 1, pp. 63–70, 2009.

[60] H. Sawasato, S. Yoshida, T. Sugawara, Y. Miura, and J. Matsuoka, "Relaxation behaviors of Vickers indentations in soda-lime glass," *Journal of the Ceramic Society of Japan*, vol. 116, no. 1356, pp. 864–868, 2008.

[61] Y. Kato, H. Yamazaki, S. Itakura, S. Yoshida, and J. Matsuoka, "Load dependence of densification in glass during Vickers indentation test," *Journal of the Ceramic Society of Japan*, vol. 119, no. 2, pp. 110–115, 2011.

[62] T. Rouxel, H. Ji, T. Hammouda, and a. Moréac, "Poissons Ratio and the Densification of Glass under High Pressure," *Physical Review Letters*, vol. 100, pp. 1–4, June 2008.

[63] K. H. Sun, "Fundamental Condition of Glass Formation," *Journal of the American Ceramic Society*, vol. 30, pp. 277–281, Sept. 1947.

[64] R. D. Shannon, "Revised Effective Ionic Radii and Systematic Studies of Interatomic Distances in Halides and Chalcogenides," *Acta Crystallographica Section A*, vol. 32, pp. 751–767, 1976.

[65] J. C. Mauro, P. Gupta, and R. J. Loucks, "Composition dependence of glass transition temperature and fragility. II. A topological model of alkali borate liquids.," *The Journal of chemical physics*, vol. 130, p. 234503, June 2009.

[66] J. S. Tse, "Intrinsic hardness of crystalline solids," *Journal of Superhard Materials*, vol. 32, pp. 177–191, July 2010.

[67] J. J. Gilman, "Bond modulus and stability of covalent solids," *Philosophical Magazine Letters*, vol. 87, no. 2, pp. 121–124, 2007.

[68] J. J. Gilman, "Electronic basis of hardness and phase transformations (covalent crystals)," *Journal of Physics D: Applied Physics*, vol. 41, p. 074020, 2008.

[69] A. Puthucode, R. Banerjee, S. Vadlakonda, R. Mirshams, and M. J. Kaufman, "Incipient Plasticity and Shear Band Formation in Bulk Metallic Glass Studied Using Indentation," *Metallurgical and Materials Transactions A*, vol. 39, pp. 1552–1559, Dec. 2007.

[70] T. Burgess, K. Laws, and M. Ferry, "Effect of loading rate on the serrated flow of a bulk metallic glass during nanoindentation," *Acta Materialia*, vol. 56, pp. 4829–4835, Oct. 2008.

[71] J. Fornell, A. Concustell, S. Suriñach, W. H. Li, N. Cuadrado, A. Gebert, M. Baró, and J. Sort, "Yielding and intrinsic plasticity of Ti-Zr-Ni-Cu-Be bulk metallic glass," *International Journal of Plasticity*, vol. 25, pp. 1540–1559, Aug. 2009.

[72] R. Chakraborty, A. Dey, and A. K. Mukhopadhyay, "Loading Rate Effect on Nanohardness of Soda-Lime-Silica Glass," *Metallurgical and Materials Transactions A*, vol. 41, pp. 1301–1312, Feb. 2010.

[73] A. Faivre, F. Despetis, F. Guillaume, P. Solignac, and M. Ramonda, "Role of Mobile Cations on Microplasticity in Alumino-Phosphate Glasses," *Journal of the American Ceramic Society*, vol. 93, pp. 2986–2989, Oct. 2010.

[74] J. H. Simmons, R. Ochoa, K. D. Simmons, and J. J. Mills, "Non-Newtonian Flow in Soda-Lime-Silicate Glass at Forming and Annealing Temperatures," *Journal of Non-Crystalline Solids*, vol. 105, pp. 313–322, 1988.

[75] J. H. Li and D. R. Uhlmann, "The Flow of Glass at High Stress Levels," *Journal of Non-Crystalline Solids*, vol. 3, pp. 127–147, 1970.

[76] D. M. Heyes, J. J. Kim, C. J. Montrose, and T. A. Litovitz, "Time dependent nonlinear shear stress effects in simple liquids: A molecular dynamics study," *The Journal of Chemical Physics*, vol. 73, no. 8, p. 3987, 1980.

[77] R. F. Landel, M. L. Williams, and J. D. Ferry, "The Temperature Dependence of Relaxation Mechanisms in Amorphous Polymers and Other Glass-forming Liquids," *Journal of the American Chemical Society*, vol. 77, pp. 3701–3707, 1955.

[78] J. D. Ferry, *Viscoelastic Properties of Polymers*. New York: John Wiley & Sons, Inc., 1961.

[79] M. H. Cohen and G. S. Grest, "Liquid-glass transition, a free-volume approach," *Physical Review B*, vol. 20, no. 3, pp. 1077–1098, 1979.

[80] G. Adam and J. H. Gibbs, "On the Temperature Dependence of Cooperative Relaxation Properties in Glass-Forming Liquids," *The Journal of Chemical Physics*, vol. 43, no. 1, pp. 139–146, 1965.

[81] I. M. Hodge, "Adam-Gibbs Formulation of Enthalpy Relaxation Near the Glass Transition," *Journal of Research of the National Institute of Standards and Technology*, vol. 102, no. 2, pp. 195–205, 1997.

[82] M. Goldstein, "Viscous Liquids and the Glass Transition: A Potential Energy Barrier Picture," *The Journal of Chemical Physics*, vol. 51, no. 9, pp. 3728–3739, 1969.

[83] F. H. Stillinger and T. A. Weber, "Packing Structures and Transitions in Liquids and Solids," *Science*, vol. 225, no. 4666, pp. 983–989, 1984.

[84] F. H. Stillinger, "A Topographic View of Supercooled Liquids and Glass Formation," *Science*, vol. 267, no. 5206, pp. 1935–1939, 1995.

[85] S. Sastry, P. G. Debenedetti, and F. H. Stillinger, "Signatures of distinct dynamical regimes in the energy landscape of a glass-forming liquid," *Nature*, vol. 393, pp. 554–557, 1998.

[86] J. E. Shelby, *Handbook of Gas Diffusion in Solids and Melts*. Materials Park, OH: ASM International, 1996.

[87] R. H. Doremus, "Physical Solubility of Gases in Fused Silica," *Journal of the American Ceramic Society*, vol. 49, no. 9, pp. 461–462, 1966.

[88] R. H. Doremus, *Glass Science*. New York: John Wiley, 1973.

[89] J. E. Shelby, "Pressure dependence of helium and neon solubility in vitreous silica," *Journal of Applied Physics*, vol. 47, no. 1, pp. 135–139, 1976.

[90] C. M. Hartwig, "Raman Scattering from Hydrogen and Deuterium Dissolved in Silica as a Function of Pressure," *Journal of Applied Physics*, vol. 47, no. 3, pp. 956–959, 1976.

[91] J. E. Shelby, S. C. Keeton, and J. J. Iannucci, "Effect of Gas Composition on the Pressure Dependence of Helium Solubility in Vitreous Silica," *Journal of Applied Physics*, vol. 47, no. 9, pp. 3952–3955, 1976.

[92] J. E. Shelby, "Molecular Diffusion and Solubility of Hydrogen Isotopes in Vitreous Silica," *Journal of Applied Physics*, vol. 48, no. 8, pp. 3387–3394, 1977.

[93] J. E. Shelby, "Effect of Temperature on the Pressure Dependence of Helium Solubility in Vitreous Silica," *Journal of Applied Physics*, vol. 49, no. 9, pp. 4958–4960, 1978.

[94] R. M. Barrer and D. E. W. Vaughan, "Solution and diffusion of helium and neon in tridymite and cristobalite," *Transactions of the Faraday Society*, vol. 63, p. 2275, 1967.

[95] J. Sehgal and S. Ito, "A new low-brittleness glass in the soda-lime-silica class family," *Journal of the American Ceramic Society*, vol. 81, no. 9, pp. 2485–2488, 1998.

[96] Varner, W. JR;, S. CJ;, and R, "Evaluating effects of processing and surface finishing on crack-initiation behavior using recording microindentation," *Finishing of Advanced Ceramics and Glasses*, vol. 102, pp. 321–329, 1999.

[97] N. M. Keulen and N. Dissel, "Temperature Dependence of Indentation Cracking in Soda Lime Silicate Glass," *Glass Technology*, vol. 34, no. 5, pp. 200–205, 1993.

[98] M. Wada, H. Furukawa, and K. Fujita, "Crack Resistance of Glasses on Knoop Scratch Test," in *Proc. of X International Congress on Glass*, pp. 39–169, 1974.

[99] B. R. Lawn and D. B. Marshall, "Hardness, Toughness, and Brittleness: An Indentation Analysis," *Journal of the American Ceramic Society*, vol. 62, p. 347, 1979.

[100] A. G. Evans and E. A. Charles, "Fracture Toughness Determinations by Indentation," *Journal of the American Ceramic Society*, vol. 59, p. 371, 1976.

[101] T. M. Gross and M. Tomozawa, "Indentation-induced microhardness changes in glasses: Possible fictive temperature increase caused by plastic deformation," *Journal of Non-Crystalline Solids*, vol. 354, pp. 4056–4062, Sept. 2008.

[102] A. Koike and M. Tomozawa, "IR investigation of density changes of silica glass and soda-lime silicate glass caused by microhardness indentation," *Journal of Non-Crystalline Solids*, vol. 353, pp. 2318–2327, July 2007.

[103] T. M. Gross and M. Tomozawa, "Fictive temperature-independent density and minimum indentation size effect in calcium aluminosilicate glass," *Journal of Applied Physics*, vol. 104, no. 6, p. 063529, 2008.

[104] B. R. Lawn, A. G. Evans, and D. B. Marshall, "Elastic/Plastic Indentation Damage in Ceramics: the Median/Radial Crack System," *Journal of the Ceramic Society*, vol. 63, pp. 574–581, 1980.

[105] E. H. Yoffe, "Elastic stress fields caused by indenting brittle materials," *Philosophical Magazine A*, vol. 46, no. 4, pp. 617–628, 1982.

[106] S. Chiang, D. B. Marshall, A. G. Evans, and I. Introduction, "The response of solids to elastic/plastic indentation. I. Stresses and residual stresses," *Journal of Applied Physics*, vol. 53, no. 1, p. 298, 1982.

[107] K. Zeng, A. E. Giannakopoulos, and D. J. Rowcliffe, "Vickers Indentations in Glass II. Comparison of Finite Element Analysis and Experiments," *Acta Metallurgica et Materialia*, vol. 43, no. 5, pp. 1945–1954, 1995.

[108] J. T. Hagan and S. Van Der Zwaag, "Plastic Processes in a Range of Soda-Lime-Silica Glasses," *Journal of Non-Crystalline Solids*, vol. 64, pp. 249–268, 1984.

[109] R. Chakraborty, A. Dey, and A. K. Mukhopadhyay, "Role of the energy of plastic deformation and the effect of loading rate on nanohardness of soda lime silica glass," *Physical Chemistry of Glasses: European Journal of Glass Science and Technolology B*, vol. 51, no. 6, pp. 293–303, 2010.

[110] F. M. Ernsberger, "Role of Densification in Deformation of Glasses under Point Loading," *Journal of the American Ceramic Society*, vol. 51, p. 545, 1968.

[111] S. Yoshida, S. S, R. J-C, and T, "Indentation-induced densification of soda-lime silicate glass," *International Journal of Materials Research*, vol. 98, no. 5, pp. 360–364, 2007.

[112] M. Mclinden and J. Splett, "A Liquid Density Standard Over Wide Ranges of Temperature and Pressure Based on Toluene," *Journal of Research of the National Institute of Standards and Technology*, vol. 113, no. 1, pp. 29–67, 2008.

[113] K. S. Kim, K. I. Lee, H. Y. Kim, S. W. Yoon, and S. H. Hong, "Dependence of particle volume fraction on sound velocity and attenuation of EPDM composites," *Ferroelectrics*, vol. 46, pp. 177–183, 2007.

[114] K. H. Sun and M. L. Huggins, "Energy Additivity in Oxygen-Containing Crystals and Glasses II," *Journal of Physical and Colloid Chemistry*, vol. 51, no. 2, pp. 438–443, 1947.

[115] A. Fluegel, "Global Model for Calculating Room-Temperature Glass Density from the Composition," *Journal of the American Ceramic Society*, vol. 90, pp. 2622–2625, Aug. 2007.

[116] M. Sakai, "Energy principle of the indentation-induced inelastic surface deformation and hardness of brittle materials," *Acta Metallurgica et Materialia*, vol. 41, pp. 1751–1758, June 1993.

[117] M. Sakai, "The Meyer hardness: A measure for plasticity?," *Journal of Materials Research*, vol. 14, pp. 3630–3639, Jan. 2011.

[118] P. Gupta, "The Random-Pair Model of Four-Coordinatied Borons in Alkali-Borate Glasses," in *International Congress on Glass*, (New Delhi, India), pp. 1–10, Unpublished, 1986.

APPENDIX A
Average Bond Strength

A.1 Calculation

The average bond strength is calculated as:

$$\alpha = \frac{\sum (n_i c_i \epsilon_i)}{\epsilon_{Si} \sum (n_i c_i)} \tag{A.1}$$

where α is the relative bond strength relative to amorphous silica, n, c, and ϵ respectively the molar fraction, coordination number, and single bond strength to oxygen of the subscripted cation. The single bond strengths are calculated from the dissociation energy of oxides as,

$$\epsilon = \frac{E_{dis.}}{c} \tag{A.2}$$

where $E_{dis.}$ is the dissociation energy. *Yamane & MacKenzie* [34] used the dissociation energies published by *Sun & Huggins* [114], while this work utilises the newer values given by *Morinaga et al.* [49] and the coordination numbers given by *Sun* [63]. The calculated values are given in table A.1.1.

Table A.1.1: The average bond strength relative to amorphous silica, α, of the compositions used in this work.

Series	Composition	α
SLS	$80SiO_2$	0.678
	$75SiO_2$	0.594
	$71SiO_2$	0.585
	$68SiO_2$	0.577
	$65SiO_2$	0.570
	$60SiO_2$	0.556
MS	KBa	0.576
	NaBa	0.640
	KCa	0.595
	NaCa	0.663

APPENDIX B
Literature Data

B.1 Vickers Hardness and Densification

The primary data source for comparison is that by *Yoshida et al.* [52] having measured the elastic properties, Vickers hardness, and volume recovery of densification by the same method used in this work on simple silicates, an oxy-nitride glass, and a bulk metallic glass. Another important contributor is the work of *Kato et al.* [9, 33] giving also elastic properties, Vickers hardness, and the ratio of indentation depth recovery, though not the volumes, again by the same method. The data concerning densification is shown in table B.1.1, and that related to elastic properties and Vickers hardness in B.1.2. Some additional data by *Sanditov et al.* [37] has been used in the modelling of Vickers hardness alone, which are not duplicated here.

Table B.1.1: Glass transition temperature, T_g, densified volume, V_d, plastic flow volume, V_p, volume ratio of recovery, V_R, and ratio of indentation depth recovery, RID, from *Yoshida et al.* measured identically to the method used in this work. The RID data by *Kato et al.* given is for a Knoop indenter. Experimental error is given as the maximum among the series of glasses measured. *The second largest error in V_p. The largest error is for amorphous silica at 70%.

Composition	T_g [°C]	V_d [μm^3]	V_p [μm^3]	V_R	RID	Ref
10CaO 15Na_2O 75SiO_2	568	10.81	5.72	65%	34%	[52]
20CaO 15Na_2O 65SiO_2	594	7.47	10.56	41%	22%	[52]
10CaO 6MgO 13Na_2O 71SiO_2	562	10.28	6.46	61%	32%	[52]
100SiO_2	1100	0.95	0.08	92%	45%	[52]
10MgO 15Na_2O 75SiO_2	542	13.57	3.71	79%	31%	[52]
20MgO 15Na_2O 65SiO_2	588	10.36	4.26	71%	38%	[52]
5CaO 5MgO 15Na_2O 75SiO_2	543	11.17	4.47	71%	32%	[52]
10CaO 10MgO 15Na_2O 65SiO_2	560	8.08	8.61	48%	30%	[52]
1.2Y 1.6Mg 41S 3.0Al 14O 1.5N	863	2.96	7.28	29%	19%	[52]
40Pd 40Ni 20P	317	0.40	8.39	5%	2%	[52]
Error	±5	±5%	±23%*	±4%	±5%	[52]
80SiO_2 20Na_2O	483	-	-	-	-	[9]
75SiO_2 5B_2O_3 20Na_2O	522	-	-	-	28%	[9]
70SiO_2 10B_2O_3 20Na_2O	553	-	-	-	25%	[9]
60SiO_2 20B_2O_3 20Na_2O	571	-	-	-	13%	[9]
50SiO_2 30B_2O_3 20Na_2O	554	-	-	-	21%	[9]
40SiO_2 40B_2O_3 20Na_2O	527	-	-	-	27%	[9]
80SiO_2 5B_2O_3 15Na_2O	549	-	-	-	32%	[9]
80SiO_2 10B_2O_3 10Na_2O	598	-	-	-	34%	[9]
70SiO_2 10B_2O_3 10Al_2O_3	709	-	-	-	39%	[9]
67.5SiO_2 12.5B_2O_3 10Al_2O_3	692	-	-	-	42%	[9]
65SiO_2 15B_2O_3 10Al_2O_3	676	-	-	-	42%	[9]
70SiO_2 20B_2O_3 5K_2O	500	-	-	-	32%	[33]
75SiO_2 10B_2O_3 5Na_2O	570	-	-	-	34%	[33]
70SiO_2 10Al_2O_3 10B_2O_3	710	-	-	-	34%	[33]
70SiO_2 10Na_2O 10CaO	540	-	-	-	24%	[33]
70SiO_2 10Na_2O 5SrO	520	-	-	-	18%	[33]
70SiO_2 5SrO 5K_2O	630	-	-	-	16%	[33]
60SiO_2 25PbO 5B_2O_3	470	-	-	-	4%	[33]
70SiO_2 15Al_2O_3 10Li_2O	710	-	-	-	38%	[33]
Error	±2	-	-	-	±3%	[9, 33]

Table B.1.2: Average bond strength, α, density, ρ, Poisson's ratio, ν, Young's modulus, E, bulk modulus, K, shear modulus, G, and Vickers hardness, H_V, of the silicate compositions used for measurement of densificative recovery by *Yoshida et al.* and *Kato et al.*

Composition	α	ρ [g/cm^3]	ν	E [GPa]	K [GPa]	G [GPa]	Load [gf]	H_V [GPa]	Ref
10CaO 15Na_2O 75SiO_2	0.64	2.481	0.24	75	48	30	50	5.2	[52]
20CaO 15Na_2O 65SiO_2	0.56	2.613	0.25	79	53	32	50	6.9	[52]
10CaO 6MgO 13Na_2O 71SiO_2	0.63	2.550	0.21	72	41	30	50	5.4	[52]
100SiO_2	1.00	2.20	0.17	73	37	31	10	7.0	[52]
10MgO 15Na_2O 75SiO_2	0.66	2.397	0.21	67	39	28	50	4.9	[52]
20MgO 15Na_2O 65SiO_2	0.66	2.491	0.22	73	43	30	50	5.4	[52]
5CaO 5MgO 15Na_2O 75SiO_2	0.60	2.449	0.20	70	39	29	50	5.2	[52]
10CaO 10MgO 15Na_2O 65SiO_2	0.65	2.559	0.24	76	49	31	50	5.7	[52]
1.2Y 1.6Mg 41S 3.0Al 14O 1.5N	-	3.18	0.28	134	102	52	50	9.7	[52]
40Pd 40Ni 20P	-	9.405	0.40	108	80	39	20	5.3	[52]
Error	-	$\pm$0.005	$\pm$0.01	$\pm$1	$\pm$1	$\pm$1	-	$\pm$0.1	[52]
80SiO_2 20Na_2O	0.65	2.39	0.22	60	36	25	100	3.7	[9]
75SiO_2 5B_2O_3 20Na_2O	0.65	2.45	0.24	69	43	28	100	4.5	[9]
70SiO_2 10B_2O_3 20Na_2O	0.63	2.49	0.21	77	45	32	100	4.9	[9]
60SiO_2 20B_2O_3 20Na_2O	0.66	2.52	0.23	82	51	33	100	5.4	[9]
50SiO_2 30B_2O_3 20Na_2O	0.68	2.49	0.22	79	47	33	100	5.1	[9]
40SiO_2 40B_2O_3 20Na_2O	0.70	2.44	0.23	75	46	30	100	4.9	[9]
80SiO_2 5B_2O_3 15Na_2O	0.72	2.42	0.21	72	42	30	100	4.2	[9]
80SiO_2 10B_2O_3 10Na_2O	0.79	2.40	0.20	77	43	32	100	5.1	[9]
70SiO_2 10B_2O_3 10Al_2O_3	0.86	2.49	0.24	71	47	29	100	5.6	[9]
67.5SiO_2 12.5B_2O_3 10Al_2O_3	0.86	2.49	0.25	70	46	28	100	5.6	[9]
65SiO_2 15B_2O_3 10Al_2O_3	0.87	2.48	0.25	68	46	27	100	5.6	[9]
70SiO_2 20B_2O_3 5K_2O	0.79	2.28	0.23	64	40	26	100	5.7	[33]
75SiO_2 10B_2O_3 5Na_2O	0.80	2.36	0.18	71	37	30	100	6.1	[33]
70SiO_2 10Al_2O_3 10B_2O_3	0.83	2.48	0.21	70	40	29	100	5.8	[33]
70SiO_2 10Na_2O 10CaO	0.63	2.49	0.24	72	47	29	100	5.6	[33]
70SiO_2 10Na_2O 5SrO	0.60	2.76	0.22	68	40	28	100	5.6	[33]
70SiO_2 15Al_2O_3 10Li_2O	2.43	0.84	0.15	81	39	35	100	6.2	[33]
70SiO_2 5SrO 5K_2O	0.62	2.81	0.20	77	43	32	100	5.7	[33]
60SiO_2 25PbO 5B_2O_3	0.79	4.44	0.26	63	44	25	100	4.5	[33]
Error	-	$\pm$0.01	$\pm$0.01	$\pm$1	$\pm$1	$\pm$1	-	$\pm$0.1	[9, 33]